LA-13620-MS

Issued: October 1999

An Empirical Study of Infrasonic Propagation

J. Paul Mutschlecner
Rodney W. Whitaker
Lawrence H. Auer

Los Alamos
NATIONAL LABORATORY
Los Alamos, New Mexico 87545

DISCLAIMER

AN EMPIRICAL STUDY OF INFRASONIC PROPAGATION

by

J. Paul Mutschlecner, Rodney W. Whitaker,
and Lawrence H. Auer

ABSTRACT

Observations of atmospheric nuclear tests carried out at the Nevada Test Site from 1951 to 1958 provided data for an empirical investigation of how infrasonic signals are propagated to distances of about 250 km. Those observations and the analysis documented in this report involved signal amplitudes and average velocities and included three classes of signals: stratospheric, thermospheric, and tropospheric/surface. The authors' analysis showed that stratospheric winds have a dominant effect upon stratospheric signal amplitudes. The report outlines a method for normalizing stratospheric signal amplitudes for the effects of upper atmospheric winds and presents equations for predicting or normalizing amplitude and average velocity for the three types of signals.

I. BACKGROUND AND PURPOSE

Infrasonic signals propagate through the atmosphere in several possible modes. These include tropospheric, stratospheric, and thermospheric signals, which are produced by refraction in the atmosphere and return to the surface from the regions indicated by the three designations. Lamb waves and "creeping" waves transmit infrasound through the lowest layers of the atmosphere. Another mode of propagation is by acoustic-gravity waves. Donn et al. (1963) and Donn and Shaw (1967) discuss acoustic-gravity waves from atmospheric nuclear explosions. We consider here tropospheric/surface, stratospheric, and thermospheric signals at intermediate propagation distances, that is, about 100 to 300 km. It is in this range that waves return to earth from the

appropriate "reflection" heights under the proper conditions. The waves then are reflected from the earth's surface and return to the atmosphere for possible multiple bounces and hence long-range propagation of hundreds to thousands of kilometers. A study of the signals in the first-bounce region is useful and important, both for understanding detections in this region and because this region contains the physics that also determines many aspects of much-longer-distance propagation. We also provide some tests of the applicability of results to greater distances. Gossard and Hooke (1975) and Pierce (1981) have given general reviews of infrasonic signals and propagation.

Stratospheric signals are affected by the character of the atmosphere, primarily the temperature and wind variation with height. Strong amplitude modifications are seen that are dependent upon season and receiver location. Figure 1 contains an example of the seasonal variability of signals from atmospheric nuclear explosions measured at St. George, Utah, over several years. The measurements were taken at a distance of about 220 km. Note that in this and all subsequent figures, amplitudes are in μb peak to peak. The variation in the signal amplitudes scaled to 1 kt is about 1 μb to 1000 μb (μb = microbar = 0.1 pascal). The strong seasonal dependence is obvious; without suitable correction of signals, interpretation will be impossible. This effect has been noted by other researchers, including Reed (1969A), from whom these data are taken. In addition to its effect on amplitude modification, the atmospheric variation also affects the average velocity of propagation of the signal *V*, which is the great circle distance on the surface from source to receiver divided by the transit time of the signal. It is very useful to have knowledge of the character of *V* in the intermediate, or first-bounce, region.

Our purpose in this report is to analyze a comprehensive data set for an empirical determination of how the atmosphere affects, in intermediate ranges, signal amplitude and average velocity. As a product of this study, we present (1) formulations for normalizing the signals for these atmospheric effects and (2) indications of their potential application to signals at longer ranges. This report provides a discussion of the data for stratospheric, thermospheric, and tropospheric/surface signals; it does not provide a corresponding theoretical discussion. However, we do provide commentary on possible interpretations of some aspects of the data. A useful by-product of the results may be empirical tests of future modeling results. An important part of the motivation for the report is its utility for the infrasonic data to be collected by a global network of about 60 infrasonic arrays planned as one of four monitoring technologies under the Comprehensive Nuclear Test Ban Treaty that has been formulated under the auspices of the United Nations. Brief earlier versions of this work were given by Mutschlecner and Whitaker (1990) and by Mutschlecner et al. (1998).

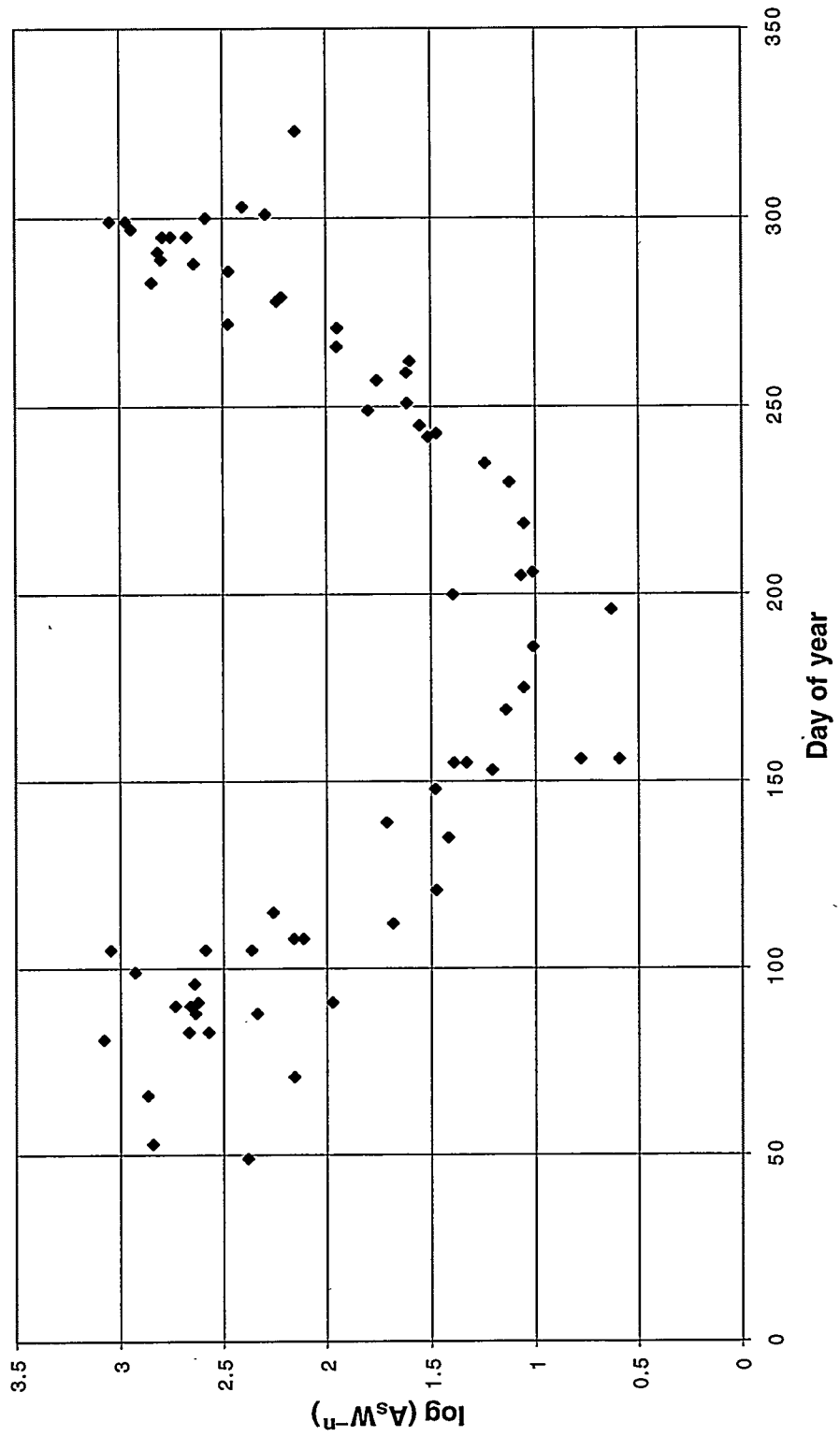

Figure 1. Seasonal variation of yield-scaled amplitude for St. George.

II. THE DATA USED

The data used for this study were taken during a program conducted by Sandia Laboratories (now Sandia National Laboratories). In the Sandia program, microbarograpic observations were made of atmospheric nuclear tests conducted at the Nevada Test Site (NTS). The observations were made primarily to provide data with which to assess and predict potential blast damage at ranges up to a few hundred kilometers. A summary and assessment of the resulting data were presented by Jack Reed (1969A). The observations were made at a set of stations surrounding NTS at roughly the first-bounce point for stratospheric propagation and closer (see Table I). Figure 2 indicates the locations of the stations. On occasion, temporary stations were operated at more-distant locations (for example, San Diego, California, or Albuquerque, New Mexico) and at close-in locations. Table I provides details of the primary stations used in this study. Note that the designation China Lake is used here rather than Inyokern.

Table I. Station Information

Station	Station ID	Azimuth (deg)	Distance (km)
St. George	SG	90	217
Bishop	BI	278	211
Boulder City	BC	139	164
Caliente	CA	64	157
Cedar City	CC	74	282
China Lake	CL	223	212
Las Vegas	LV	142	128
Lund	LU	25	219
Tonopah	TO	317	144
Gold Field	GF	304	128
Pasadena	PS	212	354
Albuquerque	AQ	110	890

The station observations were made with microbarographs produced for Sandia Laboratories. The instruments were broad band, covering frequencies from about 0.05 to 1000 Hz, and had a very wide dynamic range. During the early portion of the observational period (about 1951 to 1952), noise reducers (ported hoses) were attached to the instruments; recording was done on strip chart recorders. Signal levels were generally very large for the nuclear events. Because normal operation included only a single microphone per station, array results such as azimuth cannot now be determined. In a few instances, two instruments were operated a few kilometers apart at a station.

The observations on which we based our study spanned 1951 to 1958, covering nearly every atmospheric nuclear test conducted at NTS during the period: 77 events. However, not all stations operated for every event, and some operated for only a portion of the entire period. Because of the overall coverage of events, observations exist for most of the calendar year except from about December to mid-February. NTS test activity was largely curtailed during that period.

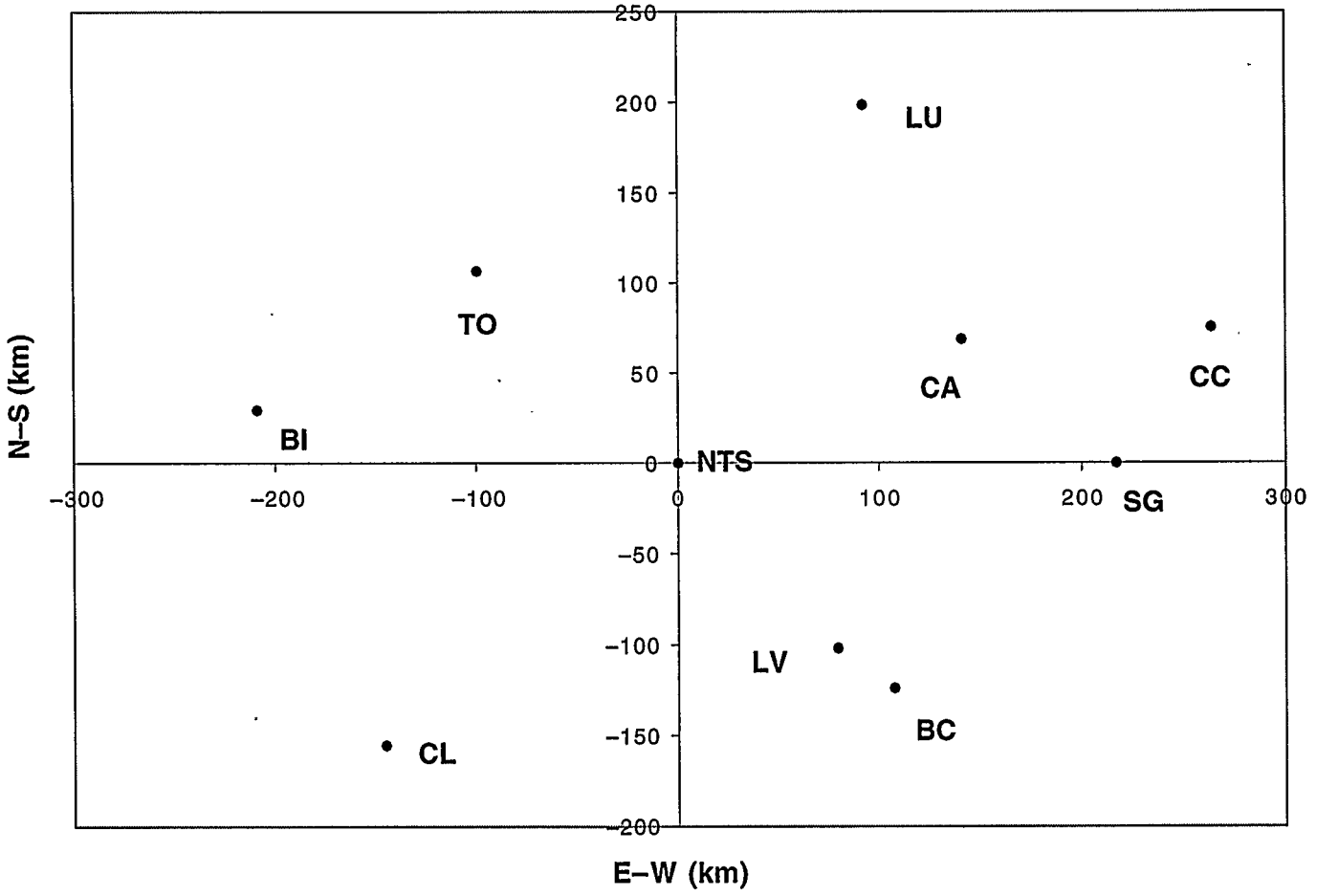

Figure 2. Location of stations surrounding NTS. Identifier labels are given in Table I.

The data resulting from those observations include the peak-to-peak amplitudes of stratospheric, thermospheric, and tropospheric/surface signals. Reed refers to the stratospheric and thermospheric signals as ozonospheric and ionospheric signals, respectively. A database separate from Reed (1969A) provided us with arrival times for most of the signals. High-explosive (HE) calibration shots preceded most of the nuclear test events by a few hours, and Jack Reed made the data from those shots available to us.

Reed based the classifications of signal type upon arrival times. The chart recordings are not currently available to us, and we rely upon Reed's classifications. However, the arrival time data for most of the events allow us to determine values for the average velocities, and those values generally substantiate Reed's classifications. We present the signal statistics for St. George and Bishop, California, in Figs. 3 and 4, respectively. The signals are shown in each of the three categories over a sequence of time intervals. Although the stratospheric signals generally predominate, the thermospheric signals can be about as frequent during parts of the year. St. George provided many tropospheric/surface signals, but Bishop provided very few. It would be interesting to know whether this east-west asymmetry persists at larger distances. For each event Reed also provides values of the nuclear yield in kilotons (kt) and height of burst (HOB).

This data set, although about 40 years old, is both very valuable for our purposes and probably unique. It possesses the following characteristics, which were critical for our study: (1) data coverage of most of the calendar year, (2) observations at or near the first-bounce location, (3) observations distributed in azimuth about the sources, (4) sources covering a very wide range of well-documented yield, (5) consistency in the observational procedures, and (6) generally very high signal-to-noise values. If other data sets of this type exist, the authors would appreciate the opportunity to learn of them.

III. EVENT CHARACTERISTICS

The 1951-to-1958 nuclear tests that provided our data covered a wide range of yields—about 0.6 t to 74 kt, determined by standard scaling of fireball diameter versus time and radiochemistry. The determined yields probably have about 10% accuracy. Figure 5 shows yield versus sequential day of the year (day number). It provides a look at the uniformity of tests over calendar year and distribution in yield. The explosions were carried out at a variety of heights, and Fig. 6 presents the HOB measured from the surface versus yield. We discuss a possible correction for HOB in a later section. The events occurred at NTS's Yucca Flats area. Distances to a given observation station varied by only a small percentage. We took the correct distances into account when determining V. Generally, tests were carried out in the early morning hours, and the "zero" times ranged from about 12:00 to 17:00 UTC, although a few tests occurred later. Reasonable conformity in the zero times was important for some aspects in our analysis, for example, for the assumed meridional winds at high altitude.

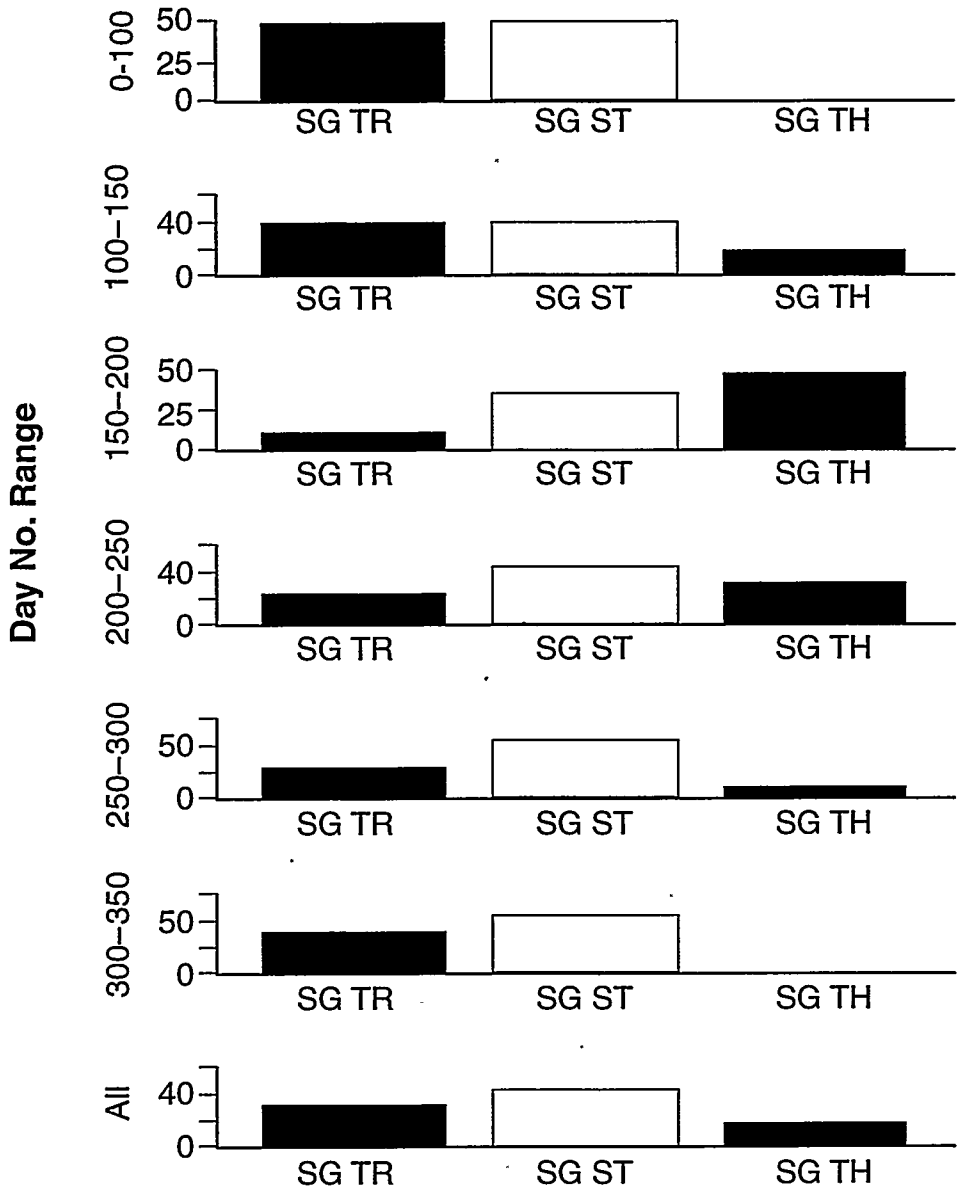

Figure 3. Distribution of three signal types for St. George—(TR) tropospheric/surface, (ST) stratospheric, and (TH) thermospheric. Percentage of types is given for 50-day intervals.

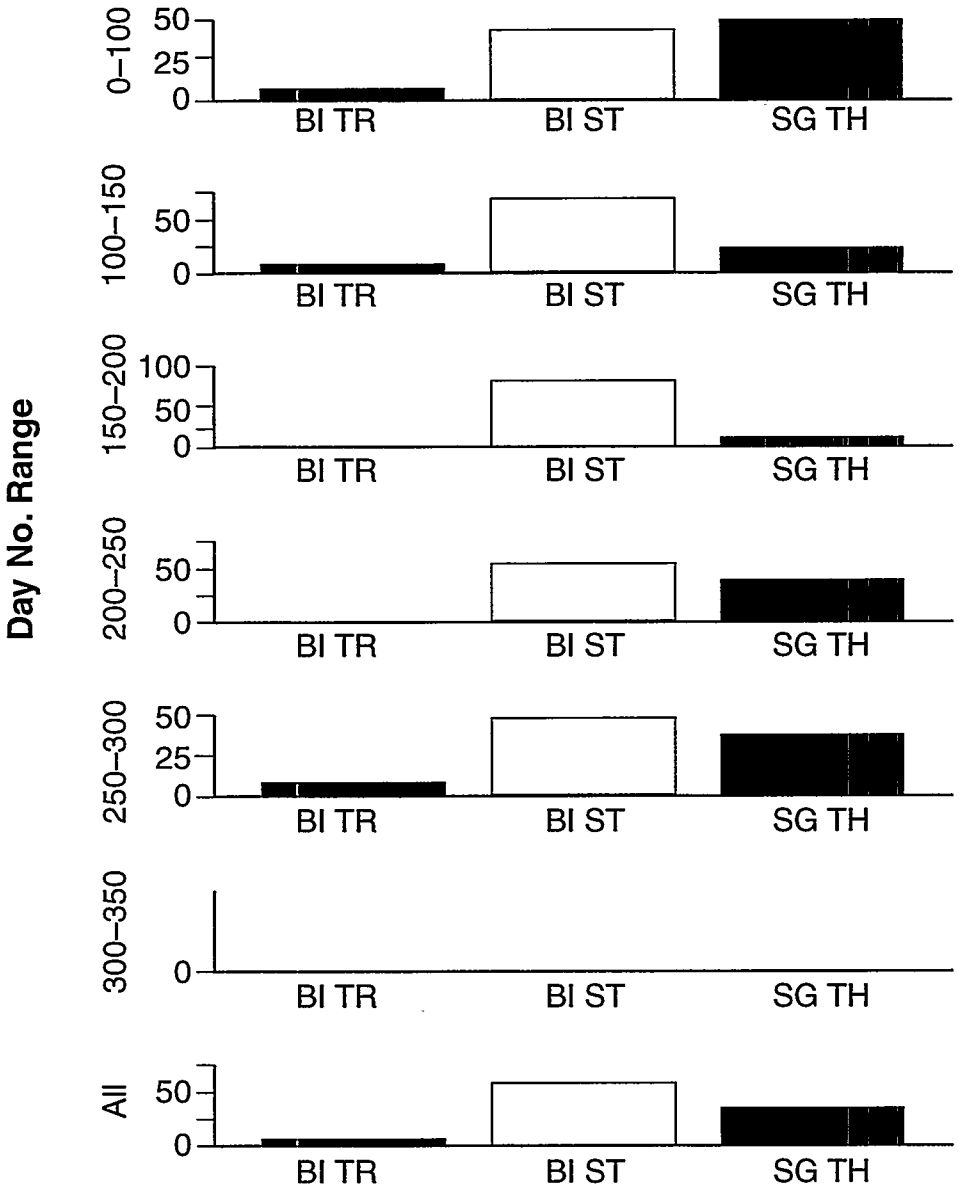

Figure 4. Distribution of three signal types for Bishop—(TR) tropospheric/surface, (ST) stratospheric, and (TH) thermospheric. Percentage of types is given for 50-day intervals.

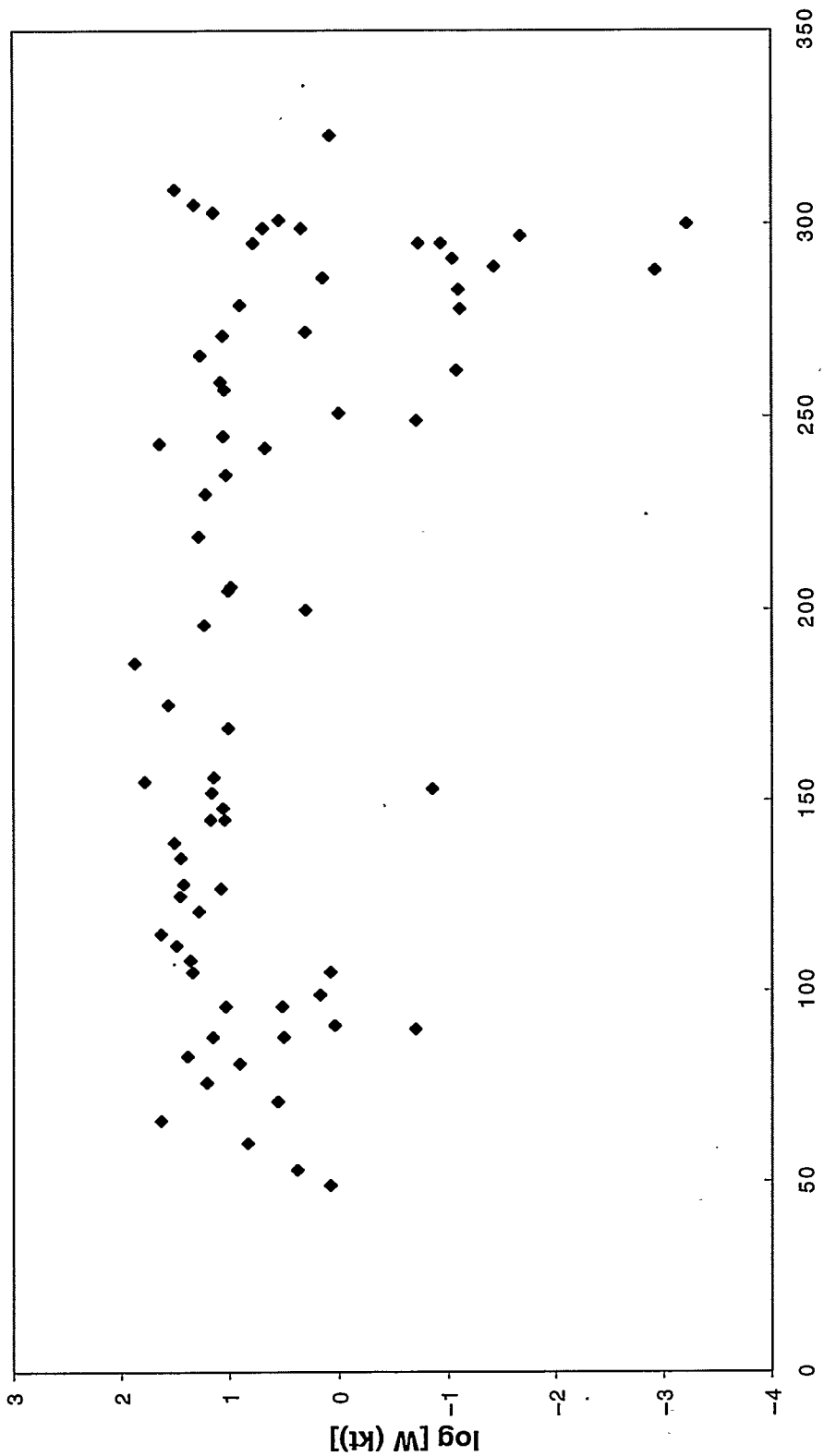

Figure 5. Distribution of events' day of year and yield (W) for St. George.

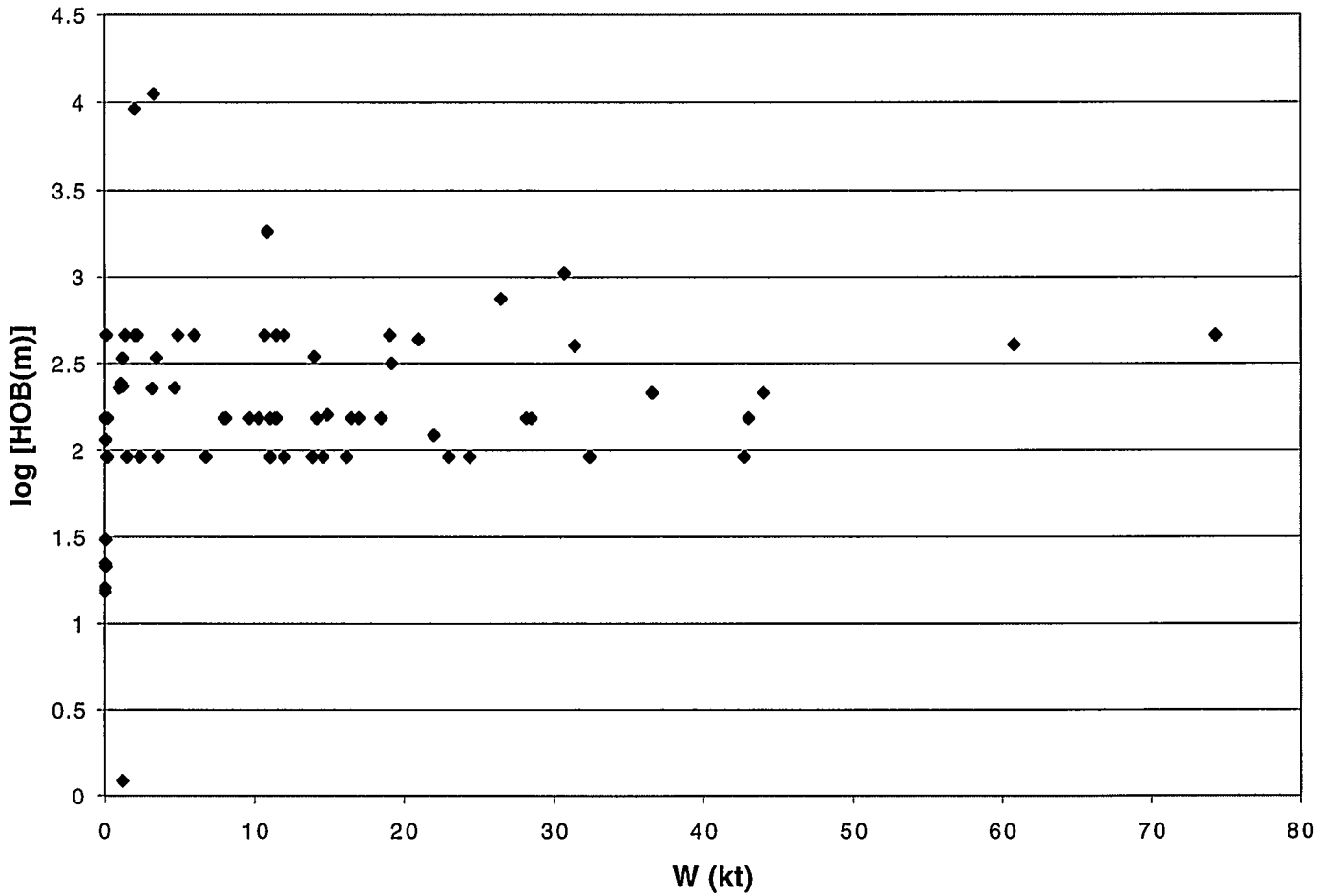

Figure 6. Distribution of HOB and yield for St. George.

IV. DISTANCE, YIELD, AND HEIGHT-OF-BURST SCALING

The yield of a source and its distance must be taken into account when analyzing the observed amplitudes by an appropriate scaling law. The form usually employed—given by the American National Standards Institute (ANSI) (1983)—is as follows:

$$A_o = C(\frac{R}{W^m})^p \ , \tag{1}$$

where A_O is the observed amplitude, C a proportionality constant, R the distance, m a yield-scaling exponent, and p a distance-scaling exponent. In this formulation, range is the quantity scaled by yield. The exponent m theoretically is expected to have a value of 1/3 in the near field and 1/2 in the far field, corresponding respectively to spherical and cylindrical spreading of acoustic waves. In the present analysis, where R is nearly constant for a given station, we can rewrite Eq. (1) as

$$A_o = (CR^p)W^{-pm} \tag{2}$$

or

$$A_o = A_c W^n, \tag{3}$$

where

$$A_c = CR^p \tag{4}$$

is the amplitude at the station for unit yield and

$$n = -pm. \tag{5}$$

The distance-scaling constant p is typically in the range of –1.2 to –1.5. An alternative scaling approach adopted by some authors is to scale the amplitude by yield:

$$\frac{A_o}{W^q} = CR^p. \tag{6}$$

Note that the parameters are interconnected with q identical to $-pm$.

We determined a self-consistent value of the exponent n from the data set. Our procedure was to select, from individual station data, subsets with a reasonably small range in date so that the effects of the seasonal wind change were very small. This permitted us to isolate the effect upon amplitude of yield alone. Using a total of 12 subsets, we performed a statistical analysis on the dependence of amplitude upon yield. The result was

$$n = 0.456 \pm 0.05. \tag{7}$$

Reed used an empirical value of –1.2 for p, and a value of 1/3 for m; this results in a value of 0.4 for n from Eq. (5) and is the value used by Reed. We believe that our larger value for n reflects the fact that at the ranges of these data, the spreading of the wave front is in an intermediate state between spherical and cylindrical.

A correction that might be applied to the yields results from the variation in the HOB of the explosions as depicted in Fig. 6. The concept for this correction is the enhanced close-in blast wave that occurs when the direct pressure wave combines with a ground-reflected shock. This can be accounted for in terms of an adjustment to the yield as described by ANSI (1983). Reed (1969A) accordingly corrected the yields in his analysis; the correction is carried out with a factor C_h:

$$C_h = W_A / W, \tag{8}$$

where W_A is the equivalent free air burst yield (i.e., very high altitude burst yield) and W is the radiochemical yield. The factor C_h is a function of the HOB scaled by $W^{1/3}$ and is presented by Reed in his Fig. 1 (1969A); its value ranges from about 1.5 at the surface to over 5 at intermediate yield-scaled HOBs.

The HOB correction is based upon theoretical calculations and empirical data at close-in distances. An examination of the possibility of the effect at longer distances (i.e., first bounce and longer) was made observationally by Church (1962). Mutschlecner and Whitaker (1998) reexamined this evidence and concluded that the existence of the HOB effect at longer distances is unclear. Hence, it is presently uncertain whether the values W or W_A should be used in the analysis. In fact, we find that there is a relatively small effect on some results, whether the HOB correction is included or not. As we show later, the statistical errors in the results are changed very little. We present examples of the results with and without the HOB correction. The use of W_A gives a value for n of 0.429 in comparison with the value 0.456 from the use of W.

V. SEASONAL EFFECTS ON AMPLITUDE

Figure 1 illustrates the variation in yield-scaled amplitude of stratospheric signals versus day number for the St. George station. Here the peak-to-peak amplitudes are scaled by the factor W^{-n}. The figure shows the strong increase in scaled amplitude during the winter and a corresponding decrease during the summer. Figure 7 provides the same information for the station at Bishop. Here the scaled amplitude peaks in the summer and reaches minimum values during the winter. The Bishop data essentially invert the trend of the data for St. George.

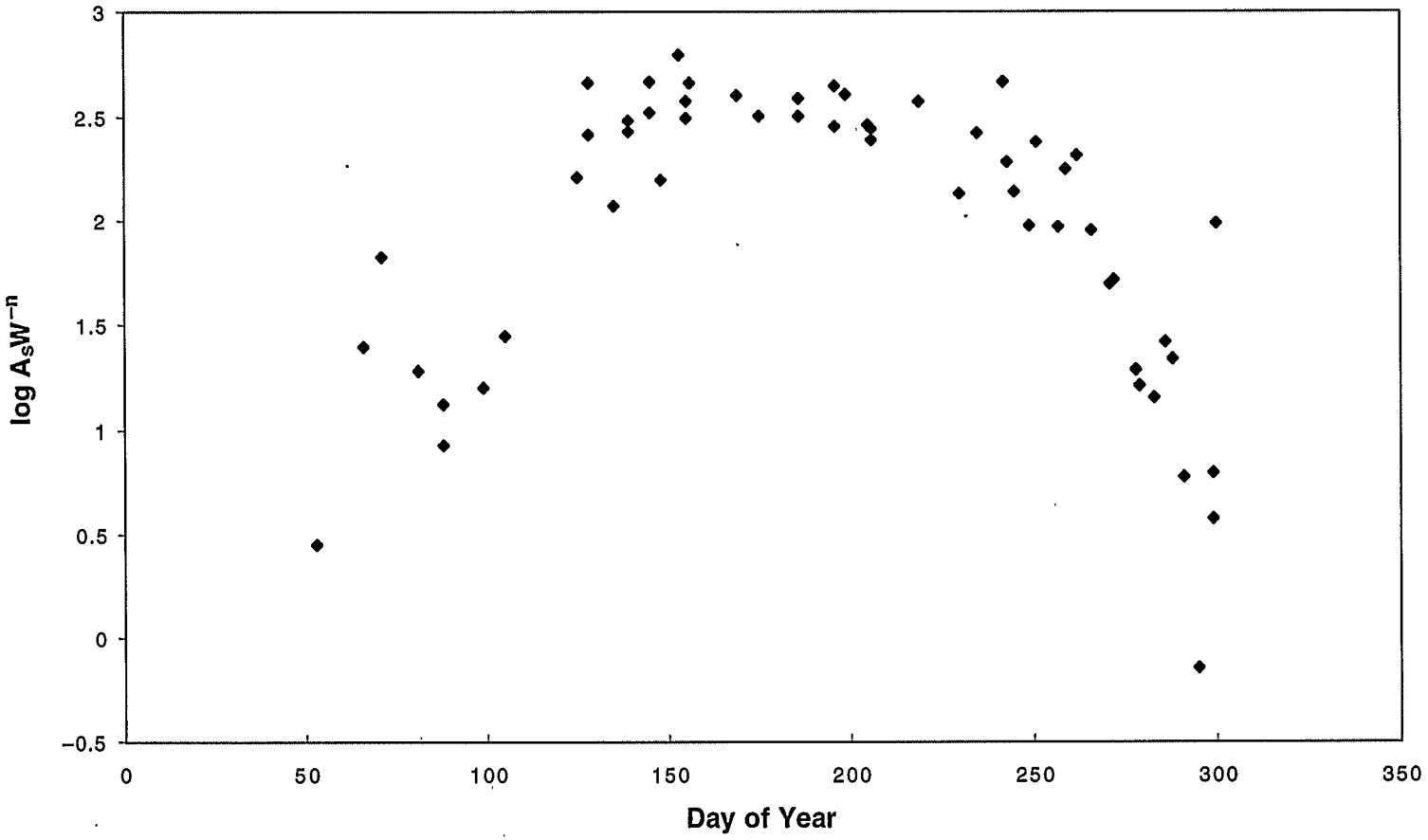

Figure 7. Seasonal variation of yield-scaled amplitude for Bishop.

St. George is at an azimuth of 90° and Bishop at 278° from NTS; thus, the data were taken to the east and west of the sources, respectively. Figure 8 shows the seasonal variation for all of the stations arranged by azimuth from the source and reveals a reasonably smooth variation of the seasonal effect with azimuth. These data provide evidence of two effects: (1) seasonal variation in the scaled amplitude and (2) azimuthal dependence of this variation. Reed (1969A) also notes these effects. These empirical results indicate that *the role of date and azimuth must be incorporated in any process to correct, or normalize, signal amplitudes.* Failure to correct amplitudes taken for the distances considered here will result in substantial errors in an analysis.

In looking at these results in 1983, one of us (JPM) considered that the seasonal variation in the high-altitude winds might be the major cause and made efforts to correlate the amplitude variations with high-altitude wind variations. The parameter chosen to test this concept was the stratospheric circulation index (SCI) described by Webb (1966). The SCI is an average of the wind velocity over the altitude interval 45–55 km. Webb presents statistical evaluations of the annual variation of the SCI for various latitudes and stations. The SCI was chosen as a parameter partly for its accessibility and partly for its usefulness in accurately characterizing wind conditions near the atmospheric "reflection" level for stratospheric signals. To illustrate this connection, Fig. 9 compares the yield-scaled amplitudes of St. George with the zonal SCI (i.e., longitudinal component) over the year. Figure 10 shows the same comparison for Bishop, with the component of the SCI directed towards the station from NTS. Both examples show the similarity between seasonal variations of amplitude and stratospheric wind speed.

Figure 11 presents the log of the yield-scaled amplitudes for St. George versus the zonal SCI. The figure shows a linear relation between the two variables, although there is considerable scatter. A rough analysis using ray-trace results shows the expectation of a linear relationship of this kind. At the time of the initial work on this topic, Los Alamos National Laboratory personnel were making observations at St. George of acoustic signals from underground nuclear tests at NTS; thus, it made sense to use the zonal SCI as the putative parameter with which to determine corrections to the raw amplitudes. Given the observed azimuthal dependence, it seems likely that the vector component of the SCI from NTS to each station should be used. That is the procedure we used in this study. Thus, using Eq. (3), we can write the following for stratospheric signal amplitudes:

$$A_s = A_{cs} W^n 10^{kV_d} , \qquad (9)$$

where A_{CS} represents the amplitude for unit yield and zero wind, k is an empirical constant to be determined, and V_d is the SCI wind vector from source to receiver given by

$$V_d = V_z \sin\theta + V_M \cos\theta , \qquad (10)$$

where V_Z and V_M are the zonal and meridional components of the SCI, respectively, and θ is the azimuth of the receiver as seen from the source. We adopted Eq. (9) as a putative empirical expression in the analysis.

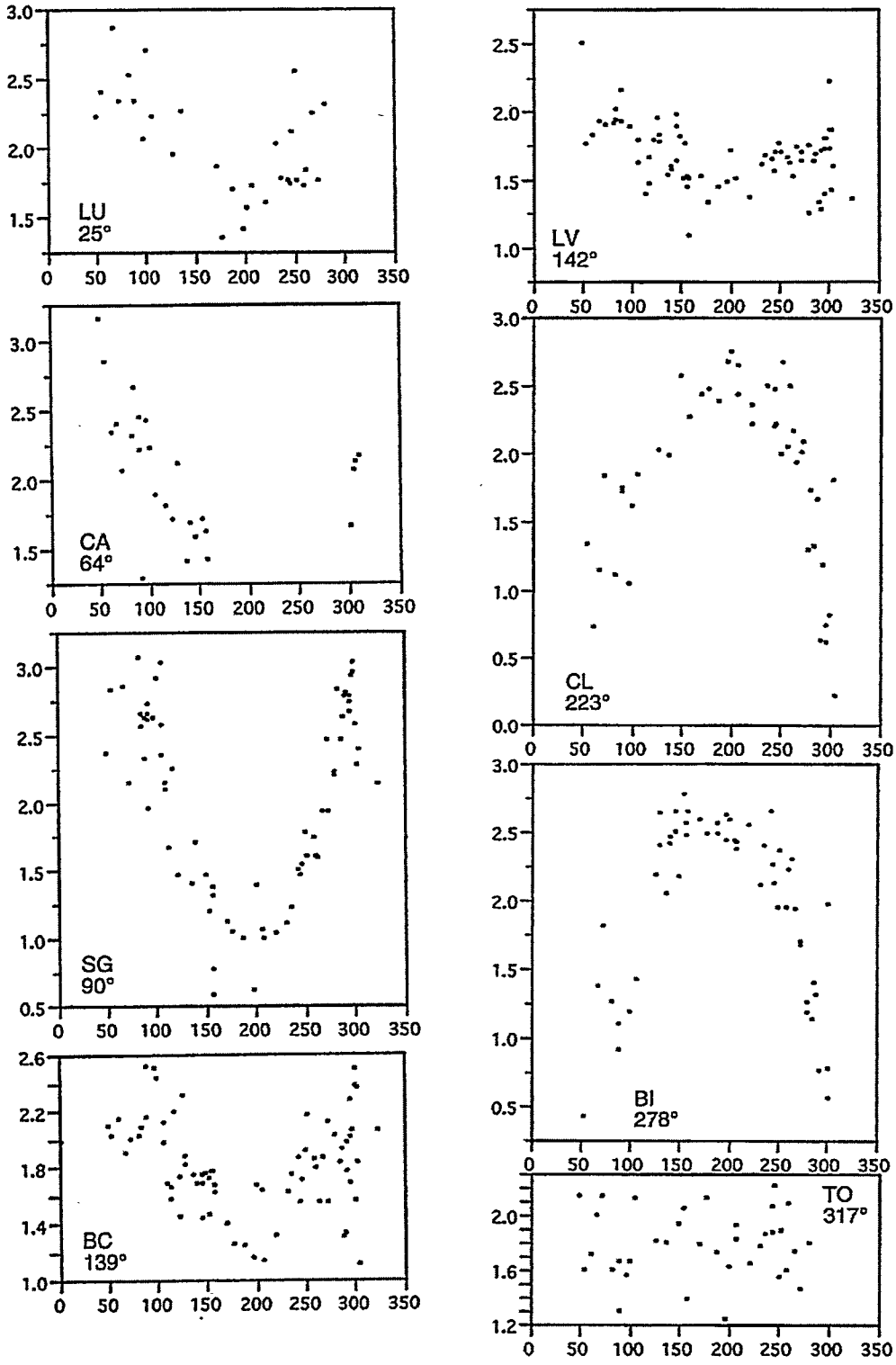

Figure 8. Seasonal variation of amplitude for all stations. Abscissas are day of year, and ordinates are log of yield-scaled amplitudes in μb. Azimuths to stations from NTS are given. Note the systematic variation of the seasonal effect with azimuth.

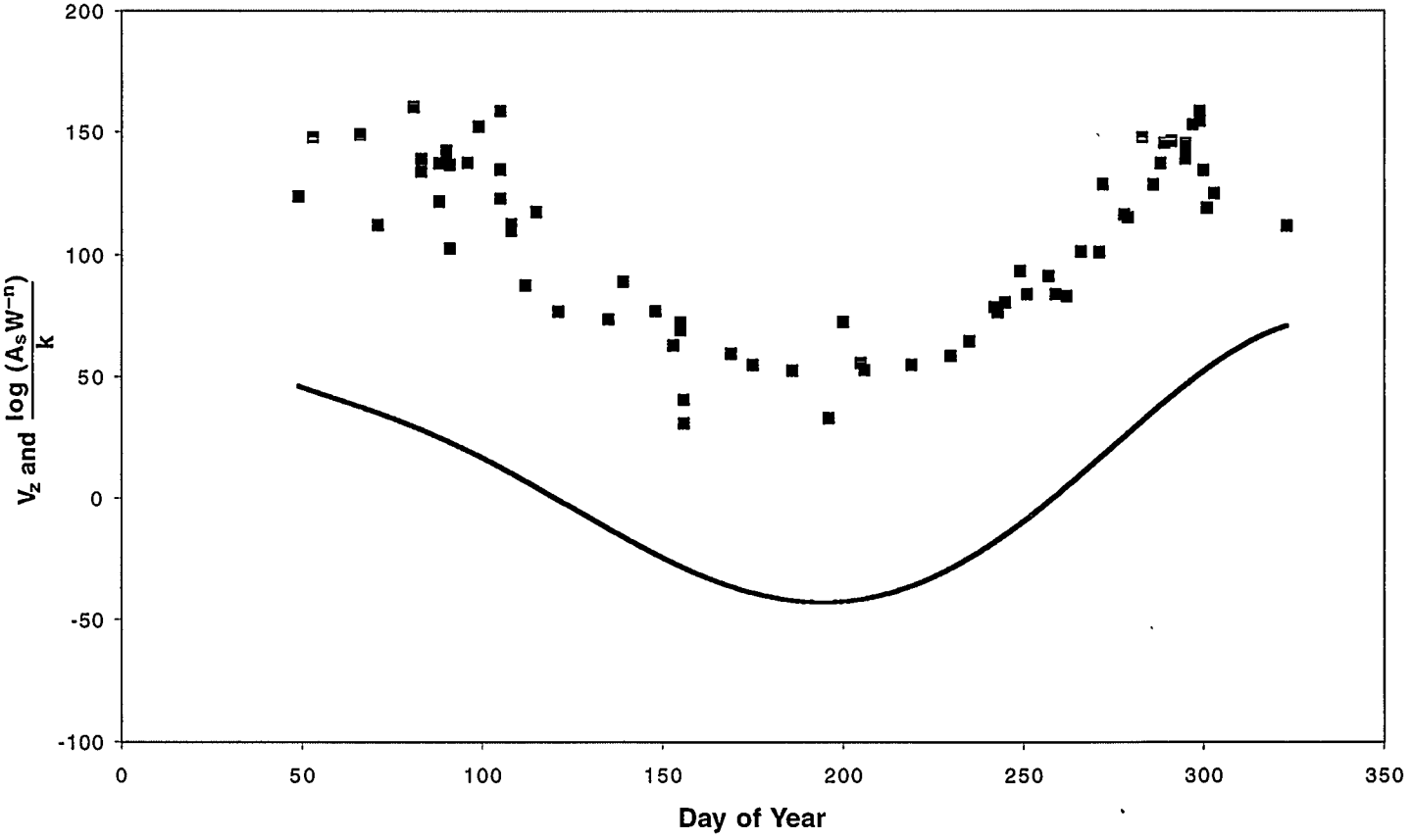

Figure 9. The seasonal variation of the zonal SCI (line) compared with the seasonal variation of the yield-scaled amplitude for St. George. The latter quantity is scaled by a constant ($1/k$).

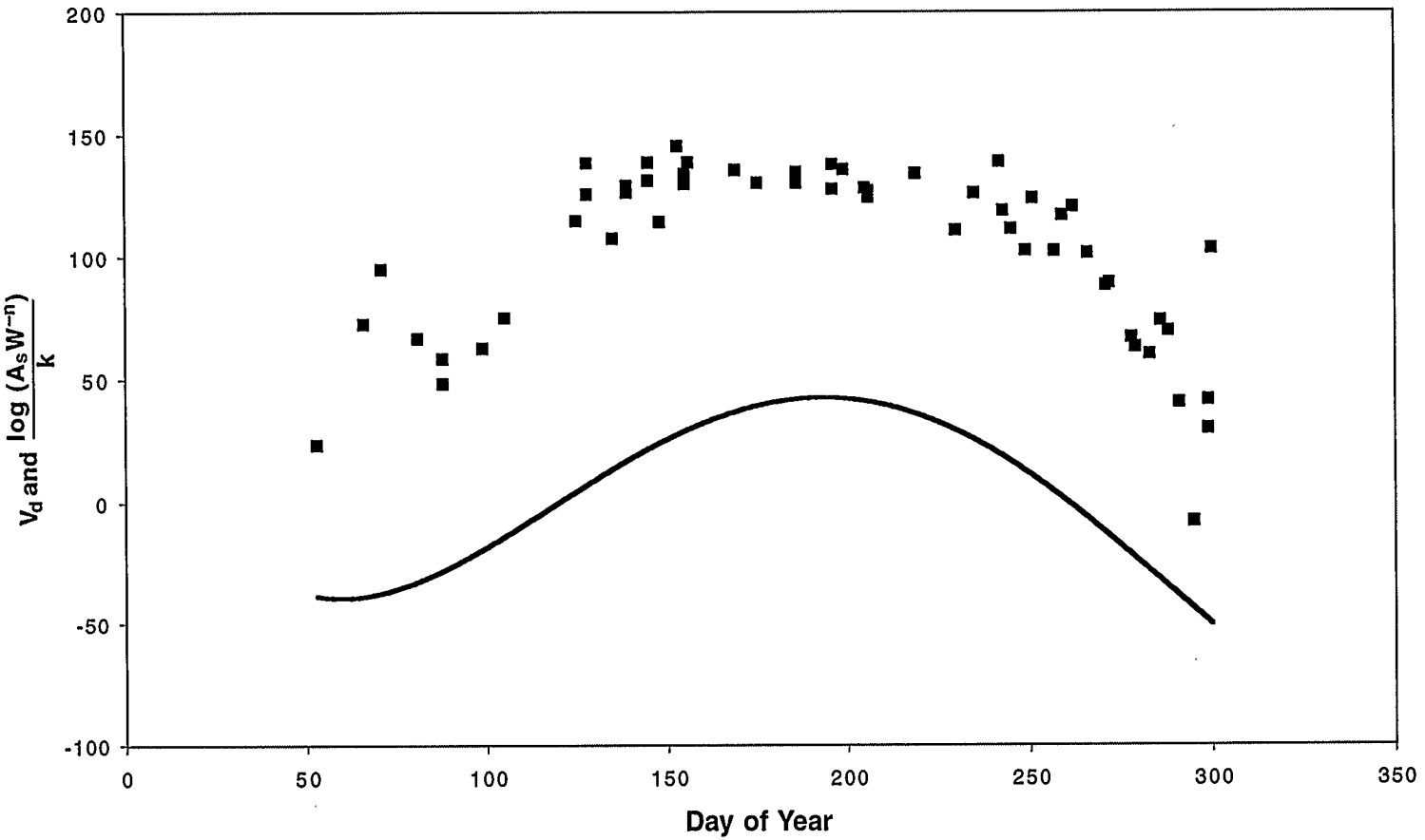

Figure 10. The seasonal variation of the directed SCI (line) compared with the seasonal variation of the yield-scaled amplitude for Bishop. The latter quantity is scaled by a constant ($1/k$).

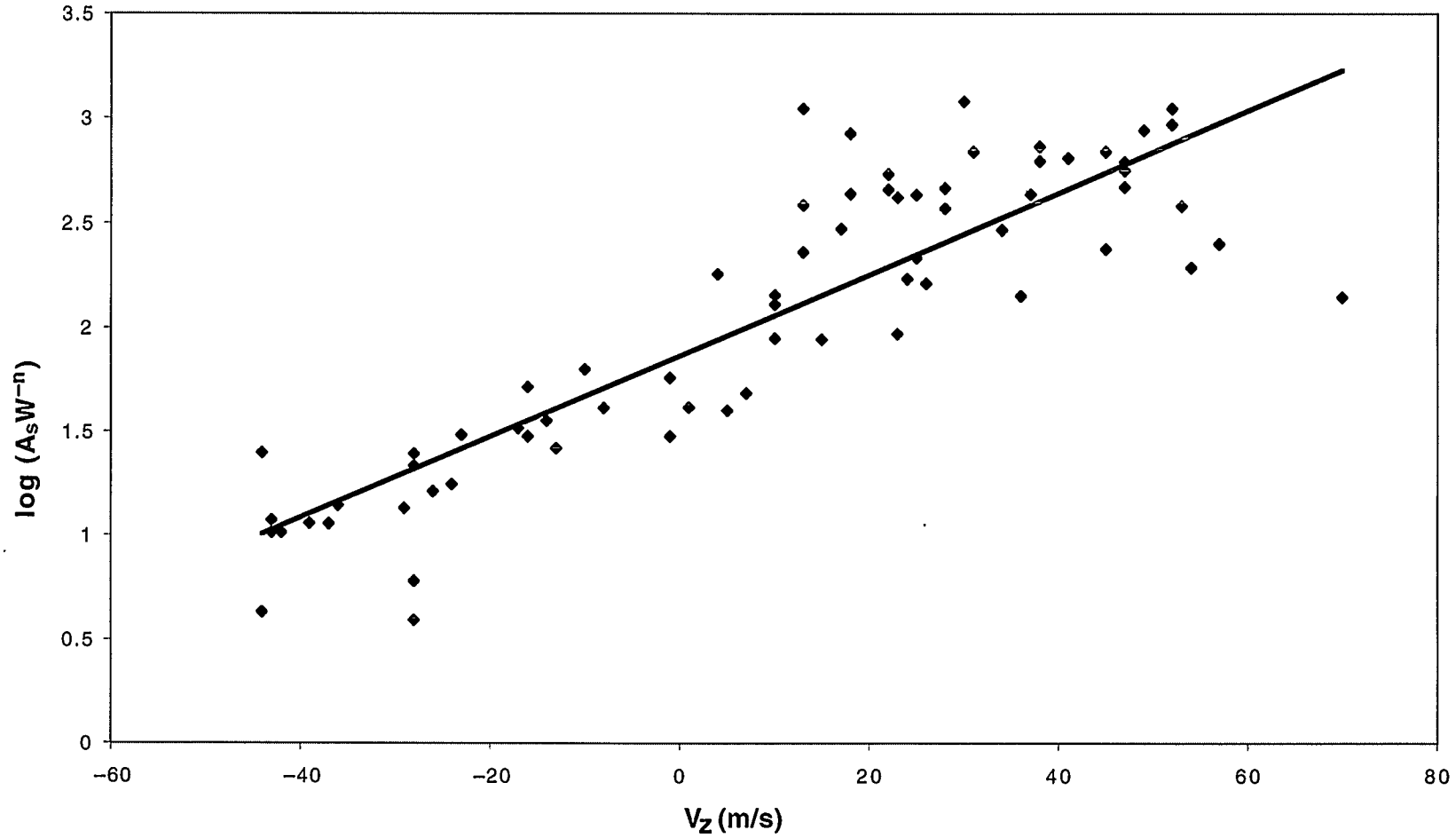

Figure 11. Example of the relation between yield-scaled amplitude and the SCI zonal wind V_Z for St. George. A least-squares fit is shown.

VI. STATISTICAL WIND MODEL

In order to proceed with an analysis of the data for the effect of wind, it is necessary to have the values of V_Z and V_M for the time of each event at the latitude of NTS. The traditional source of stratospheric wind profiles has been rocketsonde observations, which can provide data up to about 80 km. From about 1959 to 1964 or later, the global Meteorological Rocket Network (MRN) provided many observations by rocketsondes. More recently, stratospheric wind data have been provided by satellite, radar, and lidar, although not generally with the overall height coverage given by rocketsondes. Unfortunately, for the period covered by the NTS nuclear events, few if any rocketsonde observations were available. Consequently, it was necessary for us to adopt a statistical description of the SCI values for our analysis.

We used four sources of seasonal wind profiles to develop a statistical model for V_Z. The sources were data sets given by Randel (1987), Hamilton (1982), and McCullough and Novlan (1977), and the COSPAR model given by Fleming et al. (1990). We interpolated the data sets as necessary for the approximate latitude of NTS and for the standard SCI altitude of 50 km. The variations among the four data sets are reasonably small in general. We placed a mean curve through these values as a function of day number, giving particular weight to the data of McCullough and Novlan because their data were taken at a latitude and longitude close to those of NTS. Figure 12 gives the adopted statistical V_Z as a function of day number. As is well known, there are strong east-directed winds during the winter months in the northern hemisphere and strong west-directed winds during the midsummer months, but the variation is far from sinusoidal.

Obviously, the disadvantage of using this statistical model for the analysis is that year-to-year variations will cause the adopted statistical values to be in error. The greatest variance in the winds tends to occur from November to January, but few of the nuclear tests occurred during that period. Later in this report we provide a discussion of how the SCI's yearly variance affected our analysis.

Our determination of a statistical model for V_M was based upon three data sets: McCullough and Novlan (1977) for White Sands Missile Range; a summary for the Wallops Island Missile Range by the Meteorological Group, Range Commander's Council (1983); and Webb (1966). We determined a mean curve, and the result is shown in Fig. 13. The meridional component is generally much smaller than the zonal component, typically only 5 m/s to 10 m/s.

The meridional component has a diurnal tidal variation. Typically, this variation has a range of about 10 m/s. This effect has been described by researchers, for example, by Nastrom and Belmont (1976). The phase of the meridional tide is a complicated function of height, latitude, and date. It is not possible to properly correct for the tidal variation without more observations. However, the observations of the nuclear events used here were usually in the early morning hours. Thus, any tidal effect bias in the meridional values may be reasonably constant. Since the meridional component is generally much smaller than the zonal component, the effect of uncertainty in V_M upon our results should be small.

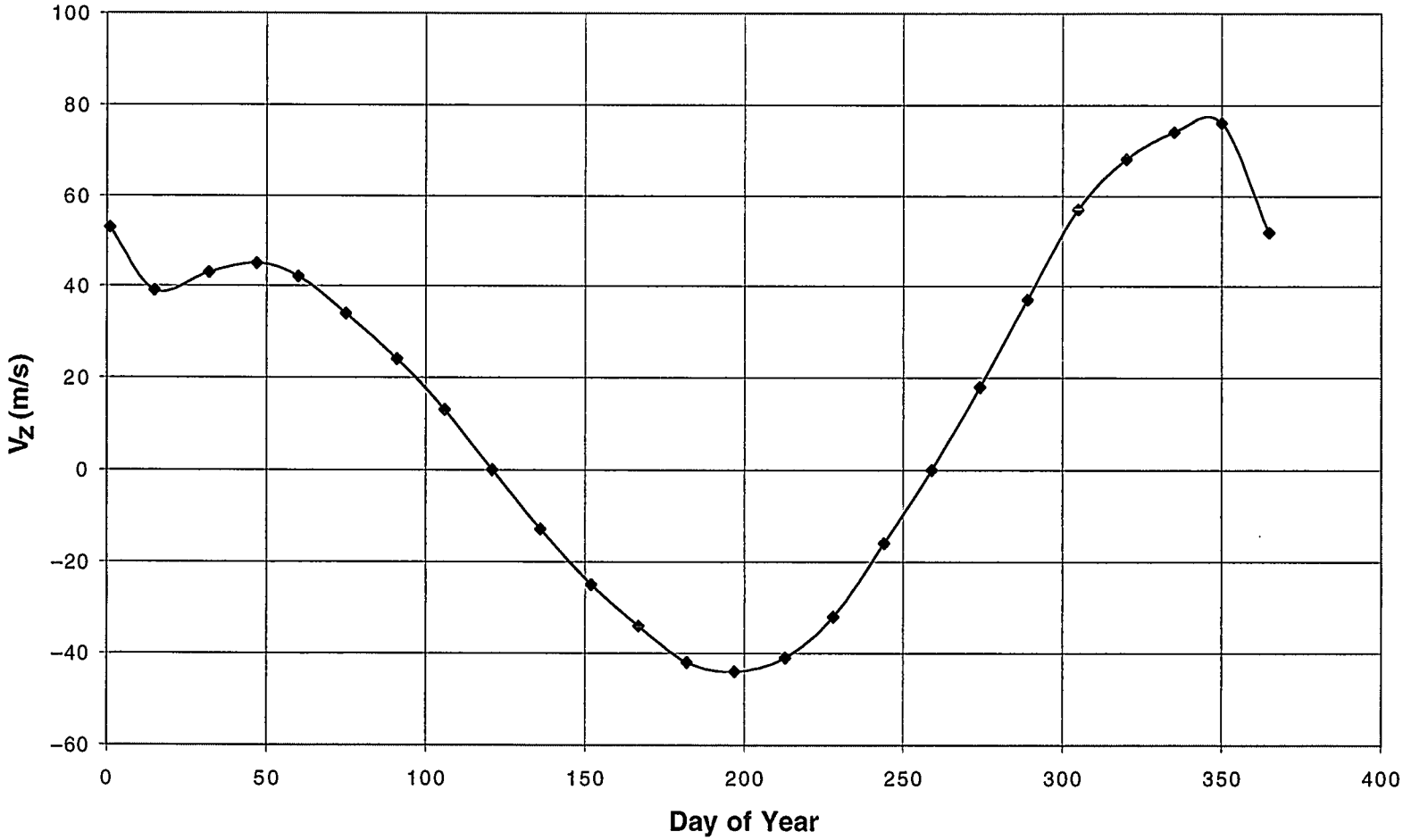

Figure 12. Statistical model for the SCI zonal wind V_z used in the analysis. See text for details.

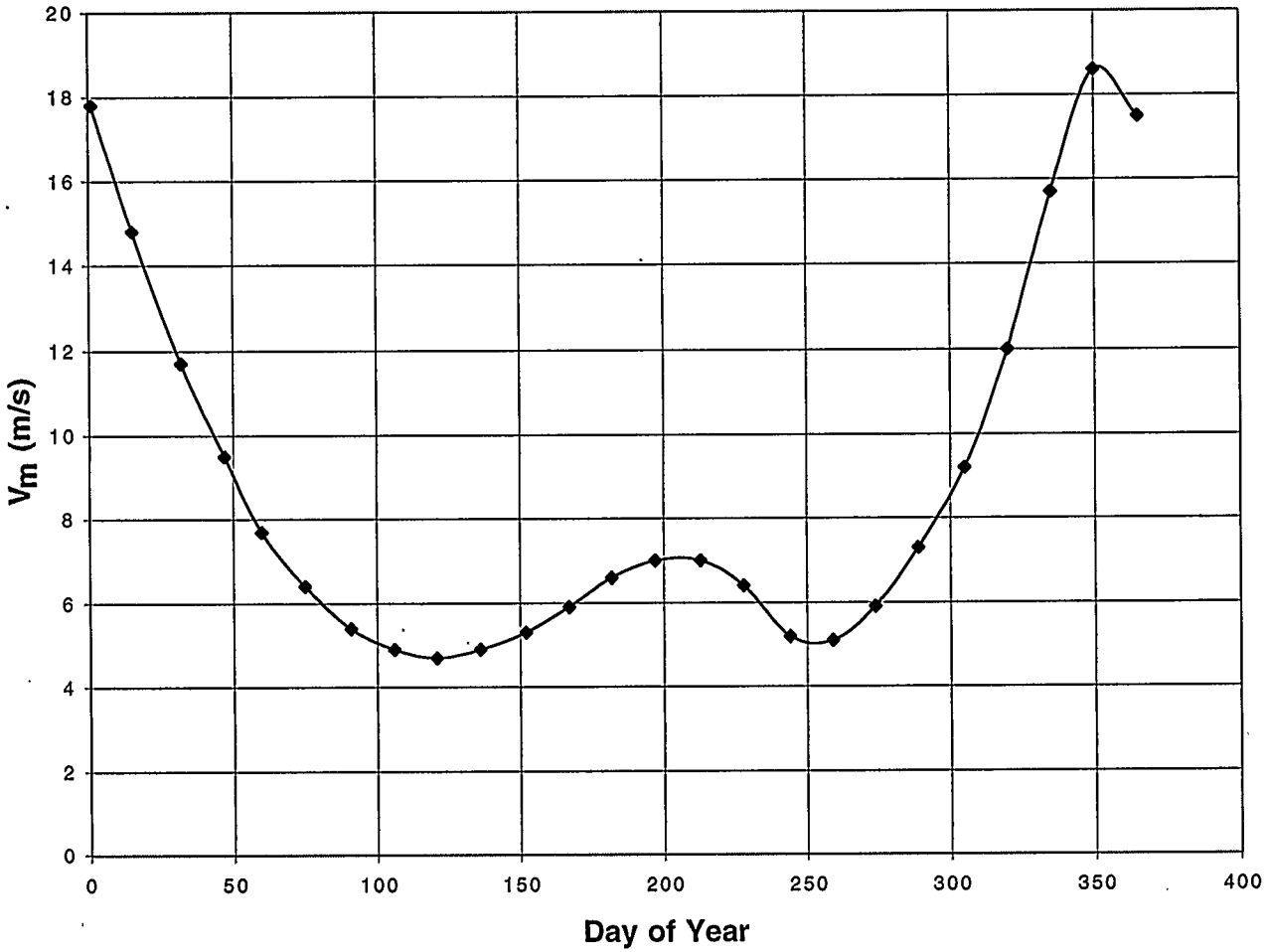

Figure 13. Statistical model for the SCI meridional wind V_m used in the analysis.

VII. ANALYSIS FOR THE EFFECT OF WIND

We analyzed the data from individual stations by a least-squares procedure using Eq. (9); the statistical-model wind data are used in Eq. (10). As examples, Fig. 11 shows the St. George data to be fitted, and Fig. 14 shows the corresponding Bishop data. The Bishop data tend to have less scatter. We have taken the values of n for the yield scaling as 0.429 for W_A values (HOB effect) and 0.456 for W (no HOB effect). The resulting values of k and A_{cs} for each station are given in Table II, together with their unit standard deviations with and without HOB correction. The figures show that the values of k from the two HOB assumptions have very small differences that are within the error limits. Thus, the effect of an HOB correction is negligible. The determination of k becomes very poor for some of the stations (for example, Tonopah, Utah) that have azimuths that make the contribution of the zonal wind very small. This is because the statistical leverage becomes very weak for these cases. For St. George and Bishop, the standard deviation for the fit of $\log A_s$ is about 0.34, in comparison with a value of 0.69 without wind effects normalization. Thus, the normalization allows for significant improvement.

Table II. Stratospheric Signal Analysis

Station	k (W_A) s/m	k (W) s/m	log A_{cs} (W_A)	log A_{cs} (W)
SG	0.0181 ± 0.0014	0.0194 ± 0.0013	1.69 ± 0.046	1.86 ± 0.042
BI	0.0211 ± 0.0016	0.0199 ± 0.0016	1.72 ± 0.048	1.89 ± 0.048
BC	0.0088 ± 0.0017	0.0091 ± 0.0017	1.67 ± 0.033	1.83 ± 0.033
CA	0.0091 ± 0.0032	0.0105 ± 0.0031	1.74 ± 0.102	1.86 ± 0.095
CL	0.0259 ± 0.0023	0.0264 ± 0.0024	1.91 ± 0.052	2.07 ± 0.054
LV	0.0026 ± 0.0015	0.0028 ± 0.0018	1.52 ± 0.027	1.67 ± 0.033
LU	0.0278 ± 0.0052	0.0283 ± 0.0051	1.76 ± 0.061	1.91 ± 0.059
TO	0.0001 ± 0.0021	–0.0001± 0.0021	1.65 ± 0.045	1.81 ± 0.044
GF	0.0047 ± 0.0044	0.0051 ± 0.0039	1.56 ± 0.091	1.68 ± 0.081

Figure 15 shows the values of k versus source distance with corresponding unit standard deviation error bars. It is clear that k is distance dependent within this first-bounce region. This raises two questions: (1) What is the physics that produces this effect? (2) What is the proper value of k to use for longer multibounce distances? An answer to the first question probably will require some modeling with appropriate propagation codes. The second question is addressed in the next section of this report. We adopted a value of 0.0196 s/m for k at the first-bounce location based upon the results for St. George and Bishop, which appear to be most reliable. Examination shows that the value of k has no dependence upon aziumuth except, as previously mentioned, for quality of fit.

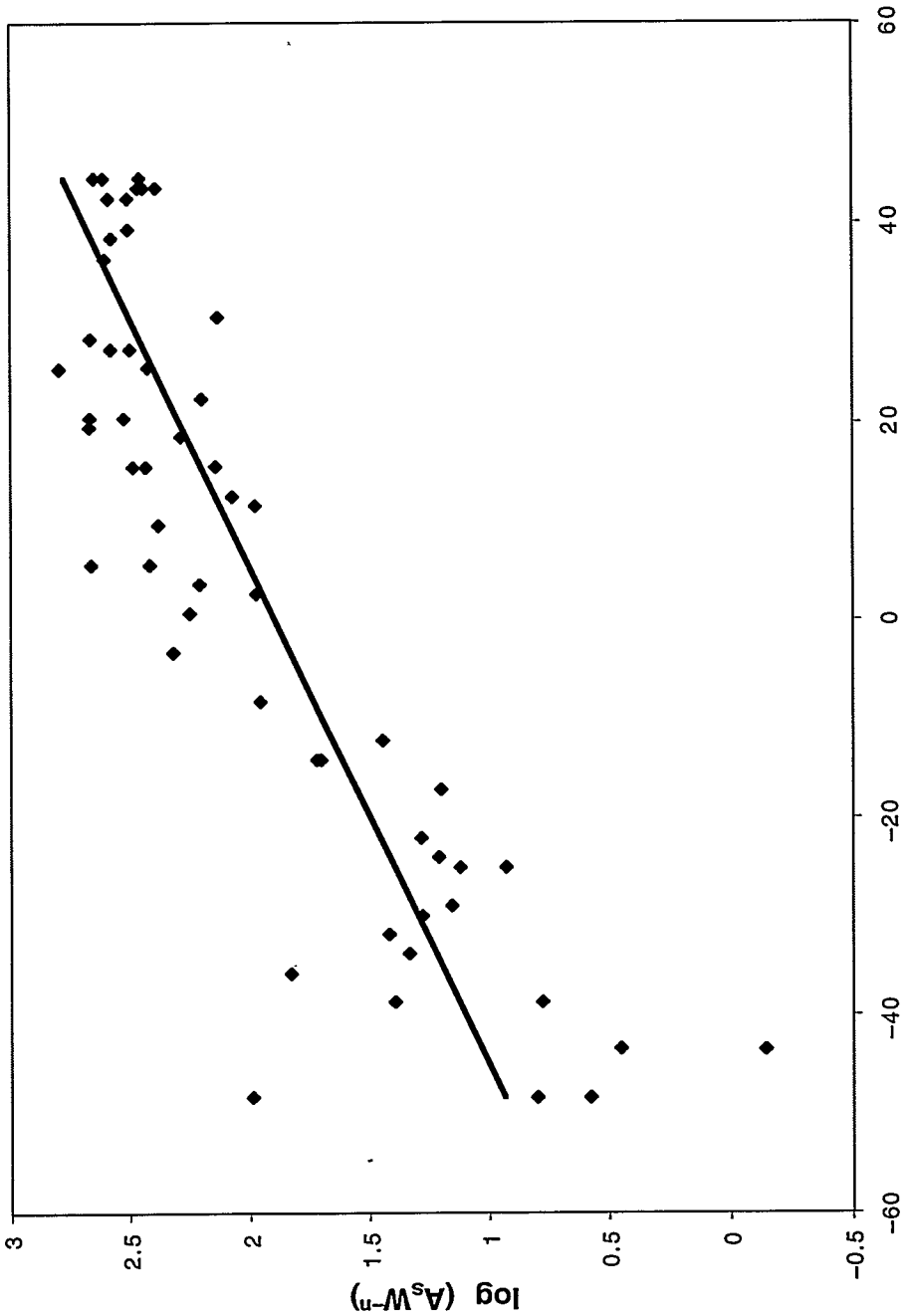

Figure 14. Relation between yield-scaled amplitude and the directed SCI wind V_d for Bishop.

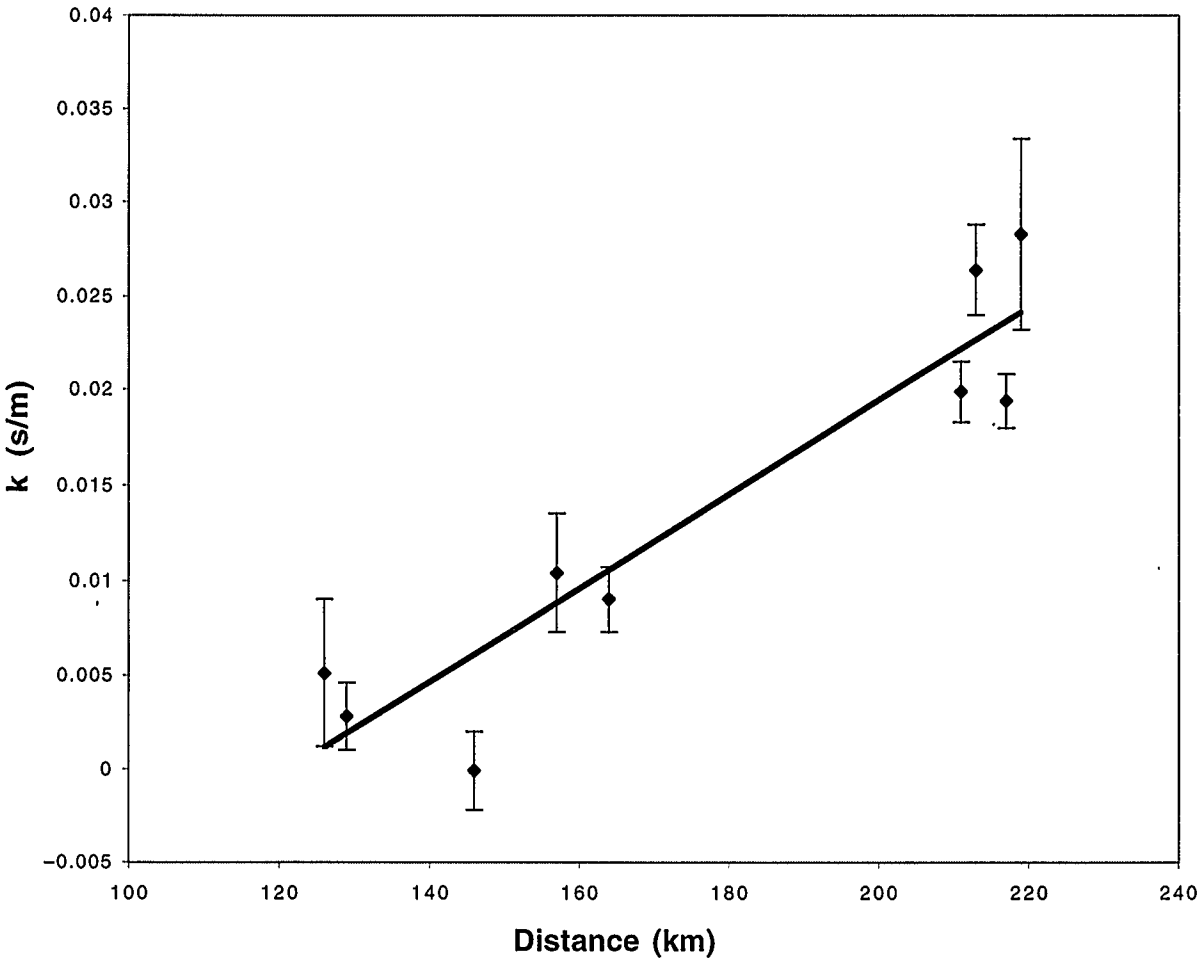

Figure 15. The empirical parameter k for each station versus distance. Unit standard deviation error bars and a least-squares fit are shown.

In Fig. 16 the parameter log A_{cs} is plotted versus distance for the stations. This parameter gives the amplitude for unit yield (1 kt) and zero wind. The values for the non-HOB effect are typically about 45% larger than the HOB values. This distribution of amplitude with distance is referred to as the signal footprint and indicates the variability of signal within a bounce region. Note that the amplitude peaks near 210–220 km, which is a nominal first-bounce distance. It is to be expected that the footprint will vary with time of year and hence with propagation conditions. Because the data used here cover many months and years, the pattern shown in Fig. 16 represents a kind of time-integrated average. Further discussions on footprint effects are given by Mutschlecner (1998) and by Reed (1969B).

An interesting alternative method of determining k relies upon the fact that St. George and Bishop are nearly opposite each other to the east and west and at nearly equal distances from NTS. Under these circumstances we can write Eq. (9) in the forms

$$A_{\mathrm{SG}} = A_{cs} W^{n} 10^{kV_z} \quad (11)$$

and

$$A_{\mathrm{BI}} = A_{cs} W^{n} 10^{-k V_z}, \quad (12)$$

where A_{SG} and A_{BI} are the observed amplitudes at St. George and Bishop, respectively. If pairs of St. George and Bishop observations are used for the same event, one can combine results from Eqs. (11) and (12). Dividing the corresponding sides of Eqs. (11) and (12) and solving for k gives

$$k = \frac{1}{2V_z} \log\left(A_{\mathrm{SG}} / A_{\mathrm{BI}}\right). \quad (13)$$

The advantage of this approach is that there is no dependence on the parameter n or on the HOB assumption. A total of 43 St. George–Bishop pairs are available for use. The result from Eq. (13) is

$$k = 0.0238 \pm 0.0018 \text{ s/m}, \quad (14)$$

which is in fair agreement with the results given in Table II for the two stations. If the corresponding sides of Eqs. (11) and (12) are multiplied and the result solved for A_{cs}, we obtain

$$A_{cs} = \sqrt{A_{\mathrm{SG}} A_{\mathrm{BI}}}\, W^{-n}, \quad (15)$$

which is independent of V_z. The average of the results for the St. George–Bishop pairs is

$$A_{cs} = 84.4 \pm 5.3 \text{ μb}, \quad (16)$$

which can be compared with the Table II values of 72.4 μb and 77.6 μb for St. George and Bishop, respectively.

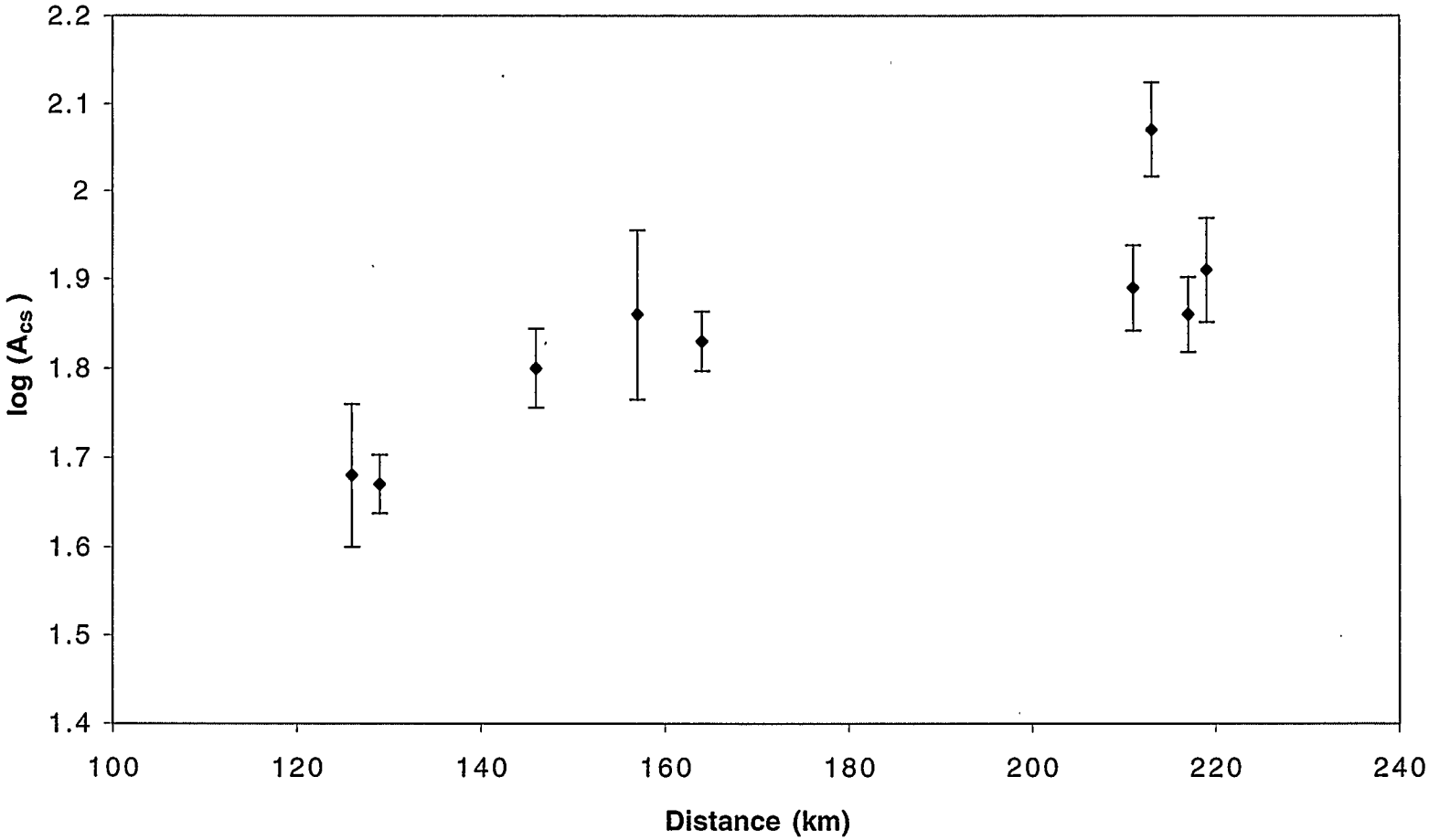

Figure 16. The empirical parameter A_{CS} for each station versus distance. An averaged amplitude footprint over the region is indicated. Unit standard deviation error bars are shown.

VIII. STRATOSPHERIC WIND EFFECTS BEYOND ONE BOUNCE

In the preceding section, we discussed the effects of wind upon stratospheric signal amplitudes. However, the data set allowed analysis only out to about the first-bounce location. We found that the parameter k increased with range. It is of obvious importance to ask what form the effect takes at greater distances. For example, can the value of k at the first-bounce location be employed at much greater distances? Simplistically, it seems likely that the effect continues at large distances because the waves reflected from the first-bounce location in turn produce signals for the later-bounce locations. Thus, we would expect the wind effect to propagate to large distances.

In order to test for the effect at greater distances and perhaps quantify the amplitude normalization procedure, we employed several data sets that allowed us to extend the scope of the analysis. A preliminary discussion of this work is given by Mutschlecner et al. (1998). The first data set includes Los Alamos observations of a series of high-explosive experiments (LAHE) that the Defense Nuclear Agency (now part of the Defense Threat Reduction Agency) carried out at the White Sands Missile Range over several years. These experiments used large volumes of ANFO (ammonium nitrate–fuel oil mix) at or near the surface, so their signals were observable at great distances. Temporary and fixed infrasound arrays were employed to measure the signals. Some further details of the observations are given by Whitaker et al. (1990).

The second data set incorporates observations of NTS atmospheric nuclear events by U.S. Air Force arrays at continental and Pacific locations. The NTS operations included in this data set are Tumbler-Snapper and Upshot-Knothole (TS-UK). Further details of the Tumbler-Snapper data are given by Olmsted (1952); details of Upshot-Knothole are available in Olmsted and Nowak (1954). Some results of an analysis of this and other explosion data are given by Clauter and Blandford (1998).

The third data set contains Los Alamos observations of infrasound signals from earthquakes (EQ) that occurred in the United States and Mexico. Several fixed arrays were used. These data—discussed by Mutschlecner and Whitaker (1990, 1994)—provide the opportunity to study signals from sources with a very wide range of strengths. For these data, seismic magnitude estimates M_b provide indications of the source strength.

Table III provides details of these data sets, including the number of events, number of signals, the range of stations per event, range of distances, range in source size, ratio of maximum source size to minimum source size, and the range in V_d. The range in V_d provides an indication of the variation that can be expected in the stratospheric wind effect. The quantity V_d was defined earlier by Eq. (10). The LAHE explosion data set primarily used observations of stratospheric winds at or near the time of each event. The TS-UK and EQ data sets used statistical winds for their analyses.

Table III. Characterizations of Three Test Data Sets							
Data Set	No. Events	No. Signals	No. Stations	Distances (km)	Source Size	Source Size Max÷Min	V_d Range (m/s)
LAHE	8	25	1 to 7	201 to 5330	0.02 to 4.88 kt (ANFO)	244	–38 to + 38
TS-UK	9	61	3 to 11	217 to 5000	0.2 to 14.9 kt (NUC)	75	–28 to + 33
EQ	22	23	1	267 to 5283	4.4 to 7.0 M_b	400	–32 to + 68

The three data sets provide an excellent test for the effects of stratospheric winds for several reasons: (1) there are a large number of events over a range of dates, (2) distances to over 5000 km are covered, (3) there is a large range in source energy, and (4) the range in V_d is substantial.

The analysis of each data set involved a multivariate least-squares solution of a form of Eq. (1). Note that Eq. (9) could not be used because it does not include a factor for attenuation by distance. We analyzed each data set with and without an assumed stratospheric wind effect in order to judge the long-distance existence of the effect. For the LAHE and TS-UK sets, we used $n = 0.456$ as determined earlier. In the case of the EQ set, the scaling law for seismic magnitude was unknown and therefore was one of the derived quantities.

Table IV gives the results of the analyses for each set, listing (1) the values of the standard deviations of the fit to log-scaled amplitude σ with and without wind correction; (2) the derived values of k; (3) the derived values of p, the distance-scaling parameter, with and without wind correction: and (4) the value of m given by Eq. (5) for the corresponding values of n and p. The values of σ indicate that the inclusion of wind normalization produces a significant improvement in the fits. The values of p seem physically unrealistic without wind normalization for the LAHE and EQ sets, whereas the values are more plausible for all sets with normalization. This gives further evidence for the validity of the normalization procedure. As indicated earlier, the value of m is expected to be about 1/3 in the near field and 1/2 in the far field. The values obtained here for the first two sets seem to be more compatible with near-field expectations.

Table IV. Results from Three Data Sets for Stratospheric Signals						
Data Set	σ [log A_S (with k)]	σ [log A_S (w/o k)]	k (s/m)	p (with k)	p (w/o k)	m
LAHE	0.198	0.276	0.0163 ± 0.0034	—1.18	—0.64	0.386
TS-UK	0.337	0.447	0.018 ± 0.0027	—1.62	—1.51	0.281
EQ	0.145	0.449	0.0162 ± 0.0012	—1.11	—0.83	

The values of k in Table IV indicate values smaller than that at one bounce from the NTS Sandia data analysis: 0.0196 s/m. Because only the LAHE set uses observed wind data, we believe it to be the more reliable evaluation; we adopted a value of 0.016 s/m for the larger ranges beyond one bounce.

Blanc et al. (1997) have presented a result from a combination of atmospheric nuclear and chemical explosion data covering a range of 400–7000 km. They find a k value of 0.0116 s/m, which helps to verify the existence of the wind effect but which is significantly less than our

evaluations. The scatter in their fit is rather large compared with our LAHE set, and they find a value for p of -1.76, which seems very large.

The existence of the wind effect at large distances—out to 5000 or 7000 km—appears to be well established, and we suggest a value for k of 0.016 s/m beyond the first-bounce distance.

IX. ERROR ANALYSIS

As indicated earlier, the standard deviation for the fits to $\log A_s$ for St. George and Bishop is about 0.34. It is useful to examine the sources of uncertainty in the analysis that leads to these values. We modify Eq. (9) as follows:

$$A_s = A_{cs} W^n 10^{kV_d} f(x,t), \tag{17}$$

where the function $f(x,t)$ symbolically represents the effect of short distance (x) or transient temporal (t) effects upon the observed amplitude. For example, in the footprint of the signal region mentioned earlier, there may be irregularities in amplitude over relatively small distances (a few kilometers), and these irregularities may travel along the footprint over short time intervals (minutes to a few hours).

The uncertainty effects can be considered using Eq. (17) to write

$$\sigma^2(\log A_{cs}) = \sigma^2(\log A_s) + k^2\sigma^2(V_d) + \langle V_d^2 \rangle \sigma^2(k)$$

$$+ n^2\sigma^2(\log W) + \langle (\log W)^2 \rangle \sigma^2(n) + \sigma^2(\log f), \tag{18}$$

where the standard deviations σ are denoted for the quantities in parentheses. These error terms contribute, for example, to the scaled amplitude dispersion seen in Figs. 11 and 14. The relation assumes that the error distributions are normal and that the quantities on the right-hand side are independent of each other. The first term on the right represents measurement error. We are able to make estimates for each term based upon analysis of the NTS and other data sets. A more detailed general analysis of infrasound amplitude uncertainty is given by Mutschlecner (1998). The most important contribution is made by the second term on the right, which represents the effect produced by use of the statistical wind. Using observed seasonal values for upper atmospheric wind variance, we estimated a value of 0.13 for this term. We estimated that the other terms together contributed only about 0.016. The spatiotemporal function $f(x,t)$ is poorly known and may be quite variable, depending upon propagation circumstances. Based upon the LAHE data set, we estimated the value for this term to be about 0.006. Certainly it cannot be much larger than this because in the current analysis all terms taken together total 0.15, whereas the left-hand side of Eq. (18) is only 0.12 for St. George and Bishop.

Thus, most of the observed variation in the normalized amplitudes is accounted for by the uncertainty from the use of statistical rather than observed values for V_d. Obviously, the use of

observed, rather than statistical, winds should greatly reduce the scatter; this, in fact, is found for the case of the LAHE data set discussed previously in section VIII.

X. USE OF HIGH-EXPLOSIVE CALIBRATION SHOT DATA

For calibration, HE shots were fired before many of the nuclear explosions. Most of these HE shots consisted of four 0.3-t surplus depth charges fired simultaneously on the surface; a few shots of smaller size were also fired. We have used observations of the 1.2-t HE events to obtain further confirmation of the results from the nuclear events and, more particularly, to look for any evidence of nonlinear effects in propagation. In simple terms, nonlinear effects in propagation might occur when the wave amplitudes are sufficiently large that the medium properties are changed, thereby affecting the propagation. We would expect this to occur for very large sources and close to the source. Thus, some of the nuclear events studied here may be candidates for nonlinear effects. Berthet (1968) has given an analysis of these effects.

We analyzed the data for the HE stratospheric signals taken at St. George and at Bishop by a least-squares procedure in the same manner as for the nuclear data, except that no yield scaling was necessary. Because the amplitudes were much smaller than those for the nuclear events, relatively few observations were available at either location for counterwind conditions. The results for k are given in Table V (see p. 32), together with the corresponding values for the nuclear events. For the HE and nuclear events, the values of k agree within the uncertainty values.

In order to compare the values of A_{cs}, it is necessary to scale the HE values to a standard 1-kt nuclear value; this is done through the relation

$$A_{cs}' = A_{cs}\left[\frac{1\ \text{kt (NE)}}{0.0012\text{kt(HE)}\left(1/F\right)C_h}\right]^n, \tag{19}$$

where A_{cs}' represents the HE parameter converted to nuclear explosive (NE) equivalency. The conversion from NE yield to equivalent HE weight is contained in F, which takes into account the fact that nuclear yield includes both radiative and blast effects. We use the value 0.50 for F from ANSI (1983) in relative energy units from NE to TNT. TNT is believed to be the most appropriate representative explosive for the surplus depth charges. In this equation, C_h is the HOB factor and n the yield-scaling factor for amplitude.

Table V gives the comparison between the A_{cs}' values and the NE values of A_{cs} for St. George and Bishop. Pairs are given first with no HOB correction and then with HOB correction. The pairs show excellent agreement. From the absence of any significant differences in the values of k or of A_{cs} and A_{cs}' between the NE and HE observations, we conclude that there is no nonlinear effect present in the data for HE calibration shots and NE events. Of course, it is well known that there are nonlinear effects from shock waves at close-in ranges.

XI. STRATOSPHERIC SIGNAL AVERAGE VELOCITIES

As indicated earlier, we define an average velocity for a signal as

$$V \equiv R / \Delta t \ , \tag{20}$$

where R is the source-to-receiver distance along the surface and Δt is the travel time of the signal. For the stratospheric signals, we label the average velocity as V_s. Figure 17 shows the values of V_s versus day number for St. George. While there is considerable scatter in the values, there is a suggestion of a systematic seasonal variation. Figure 18 shows the Bishop data, for which there is much less scatter and the seasonal variation is easy to detect. For the other stations, we see similar seasonal effects that tend to mimic the variations in amplitude we have discussed. Using the stations near a first-bounce location, we find average values for V_s as follows:

for $V_d \geq 0$ (downwind) $\qquad \langle V_s \rangle = 294 \pm 2$ m/s; (21)

for $V_d \leq 0$ (counterwind) $\qquad \langle V_s \rangle = 285 \pm 2$ m/s. (22)

Thus, a distinct seasonal effect is seen in these averages.

There are three possible causes of the seasonal variation in V_s. First is the variation in the sound velocity c at any given height during the year. However, at a representative height of 30 km, this variation is only about 2% annually. The second possibility is a variation of the atmospheric path distance with season. This effect happens because the variation in the stratospheric winds in turn causes a variation in the height of the propagation path's turning or "reflection" point. Our ray-trace calculations show that this variation is about 3% during the downwind season. The third possible cause is the variation in the stratospheric wind, which can be as large as 20% annually. This variation adds to or subtracts from the effective signal speed along the path. Thus, while all three causes will contribute, we think that the seasonal variation in the stratospheric wind added to c dominates.

To make the annual variations in V_s clearer, we have fitted stiff spline functions to the data from each station. Figure 19A shows the spline fits versus day number for the stations east of NTS; Fig. 19B shows the corresponding data for the stations west of NTS. The seasonal trends are apparent, as are the maximum values of V_s (during the winter period for the eastern stations and during the summer period for the western stations). Figure 19A shows that for Lund, nearly north of NTS, V_s shows little variation. A comparison of these results with the amplitude variations in Fig. 8 shows the strong likelihood that the stratospheric wind might be used as a predictive parameter.

Table V. Comparison of Stratospheric HE and NE Signal Analysis							
Station	k (HE) s/m	k (NE, W) s/m	log A_{cs} (HE)	log $A_{cs'}$ (HE, HOB)	log A_{cs} (NE, HOB)	log $A_{cs'}$ (HE, no HOB)	log A_{cs} (NE, no HOB)
SG	0.0201 ± 0.0018	0.0194	0.633 ± 0.056	1.63	1.69	1.81	1.86
BI	0.0256 ± 0.0024	0.0199	0.651 ± 0.062	1.65	1.72	1.83	1.89

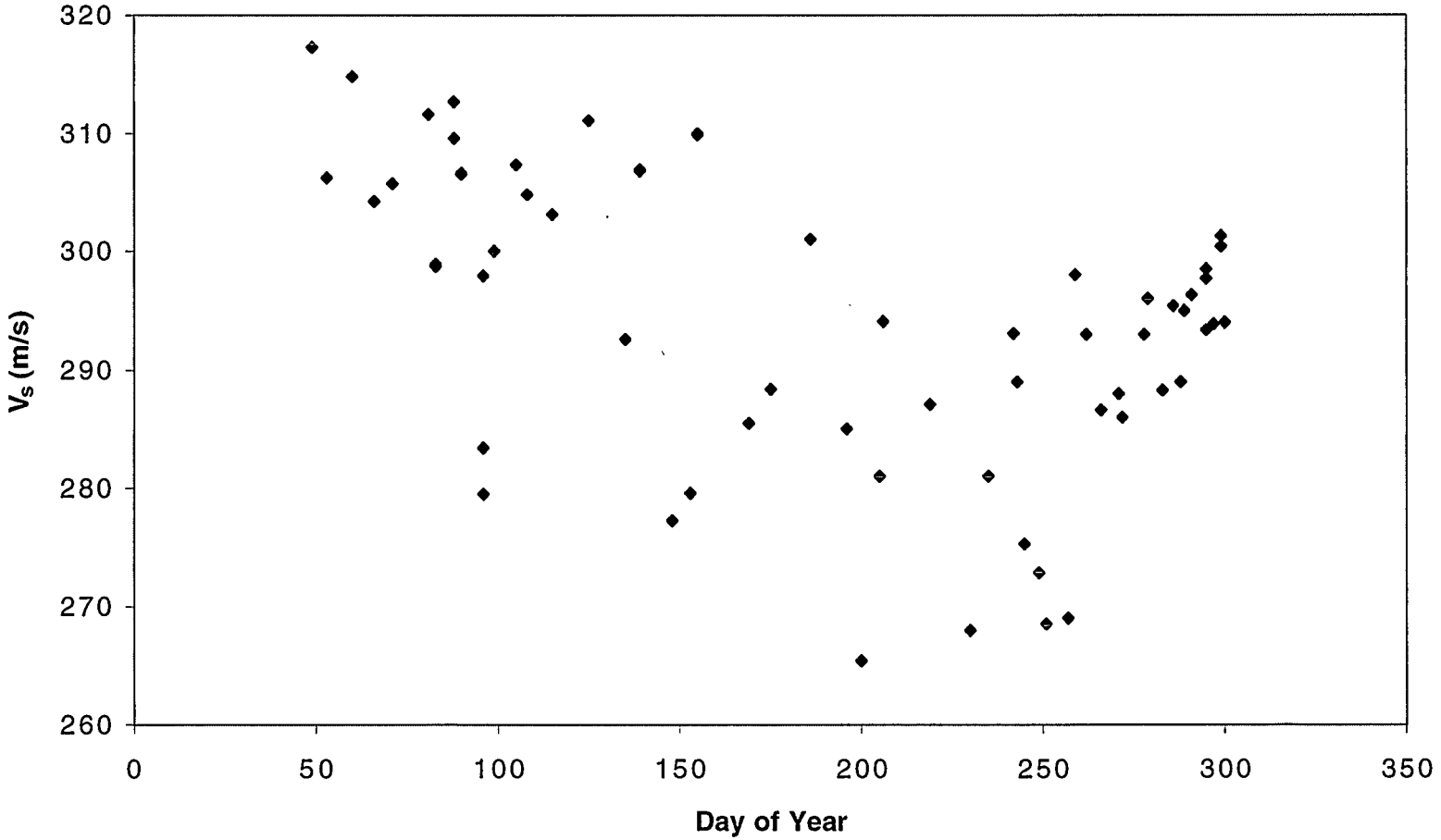

Figure 17. Seasonal variation of the average stratospheric velocity V_S for St. George.

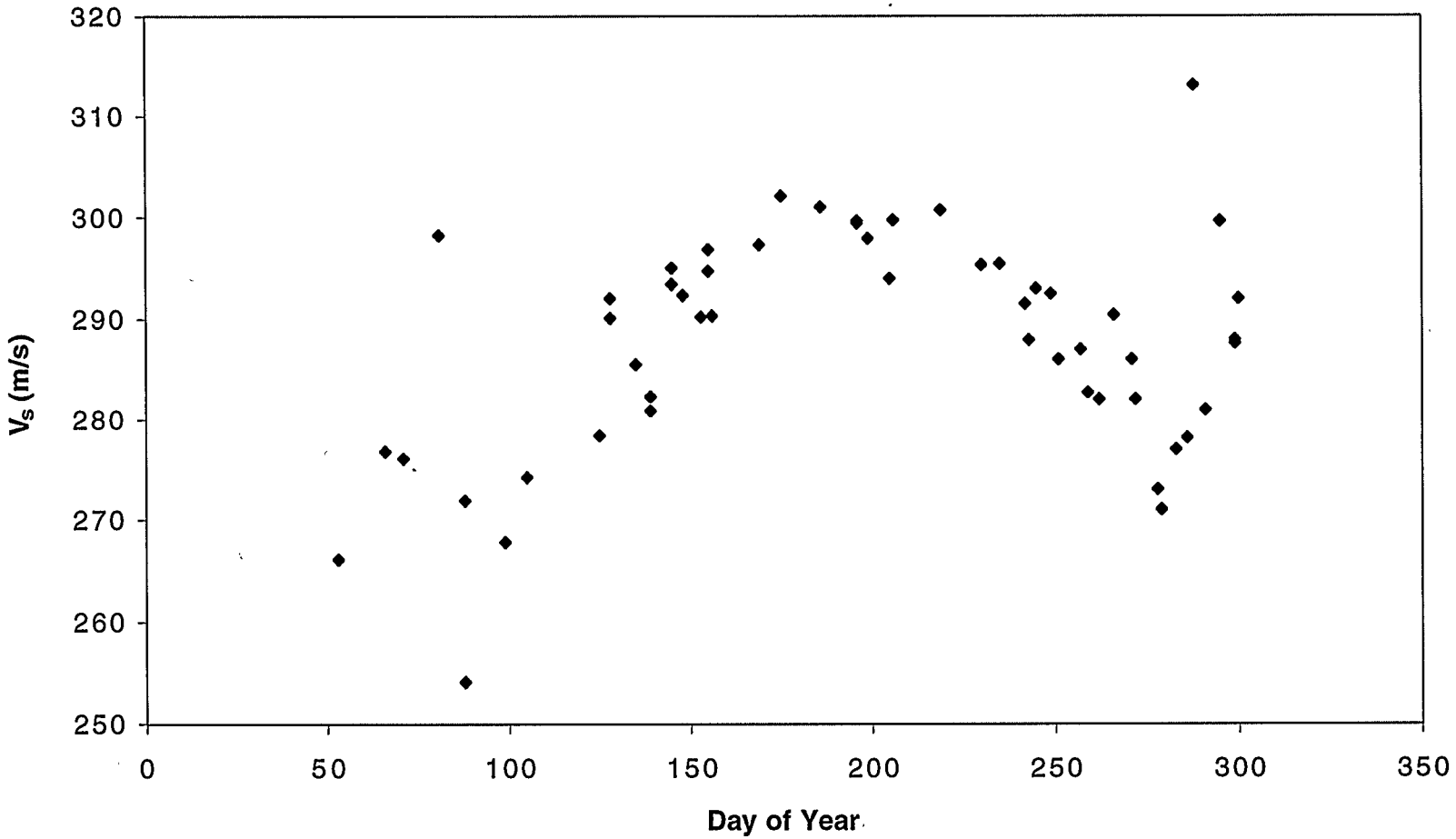

Figure 18. Seasonal variation of the average stratospheric velocity V_S for Bishop.

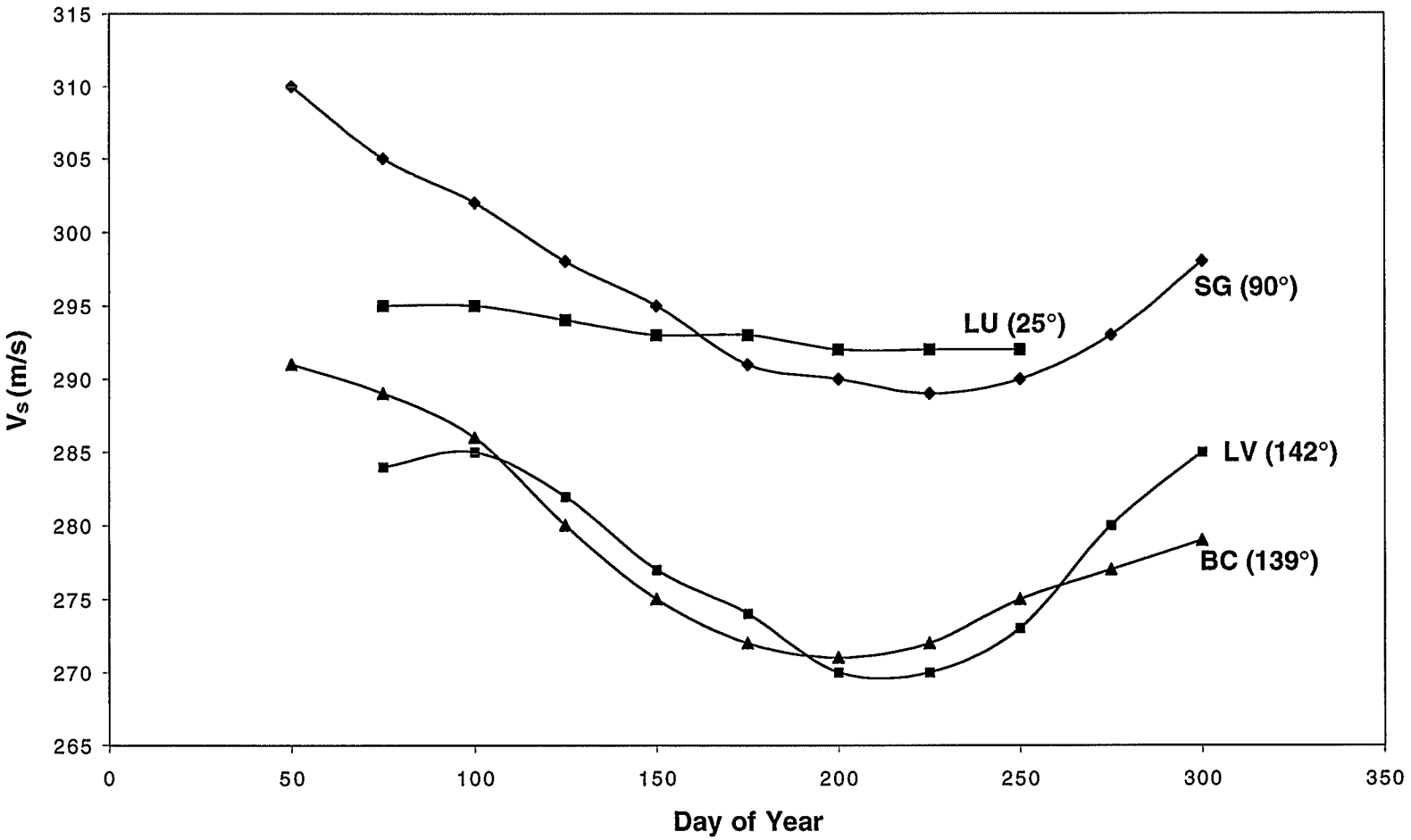

Figure 19A. Spline fits to the seasonal variation of V_S for stations to the east of NTS: Lund (LU), St. George (ST), Las Vegas (LV), and Boulder City (BC).

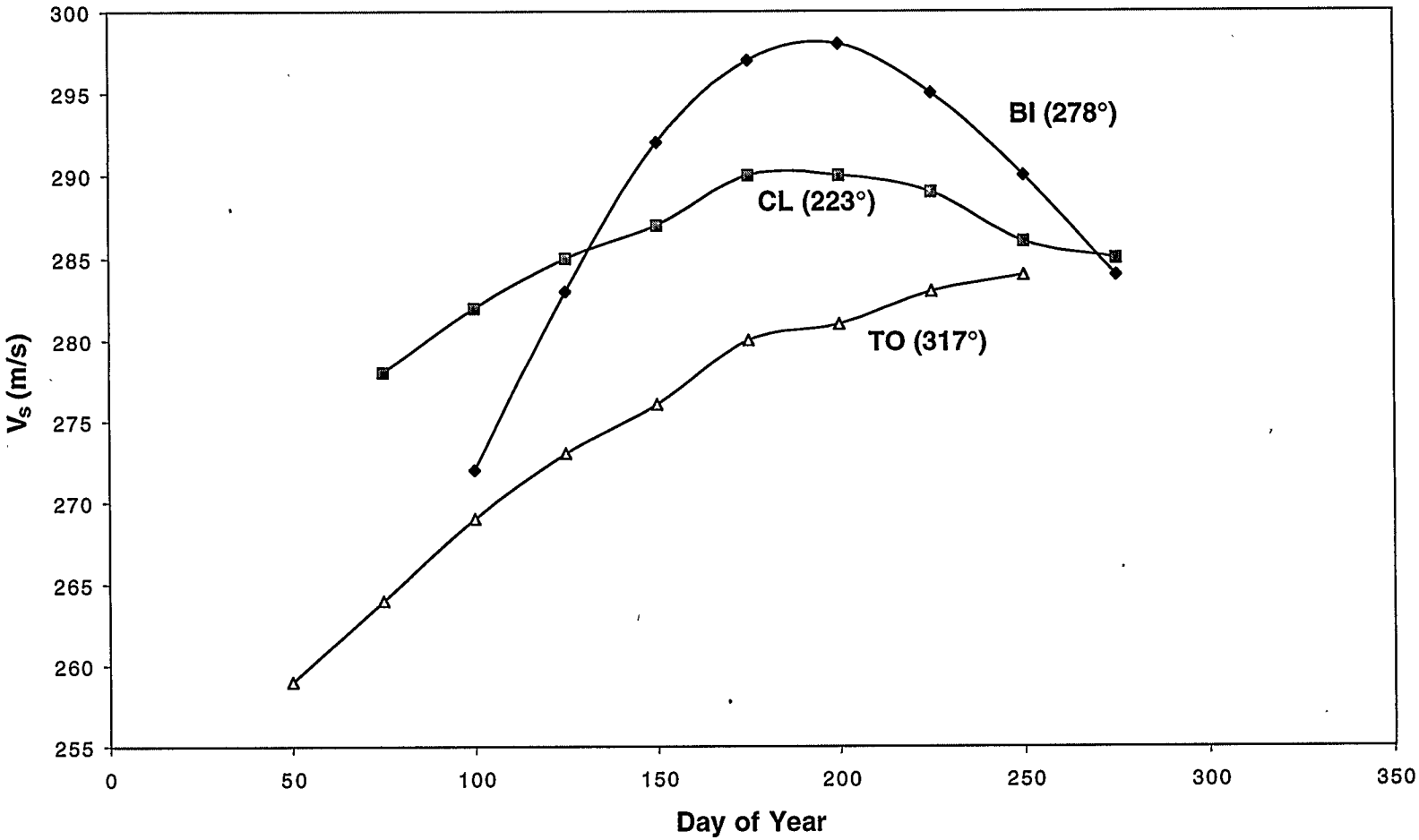

Figure 19B. Spline fits to the seasonal variation of V_S for stations to the west of NTS: Bishop (BI), China Lake (CL), and Tonopah (TO).

For the amplitude variation analysis, we found it appropriate to use winds averaged at 50 km (SCI) because this is near the stratospheric propagation turning point. However, for the analysis of V_s, it is more appropriate to use the winds at some intermediate level that represents an approximate average for the effects of winds upon V_s. We used zonal winds that McCullough and Novlan (1977) recorded for the White Sands Missile Range at heights of 25, 35, and 45 km. We found that the winds at 35 km gave the best overall association with V_s. The spline fits were read at 25-day intervals and these were plotted versus $V_d\,(35)$, the directed component of the zonal wind at 35 km. We ignored the effects of the meridional winds, which were very small. Figure 20 gives the result for Bishop as an example because that result shows reasonably good linearity of the relation. The result varies from station to station, and in several cases there is a tendency for the relation to have a hysteresis type of loop, which is reduced to a minimum by the use of the $V_d\,(35)$ wind data. We made a least-squares fit for each station for the assumed relation

$$V_s = V_o + s\,V_d(35), \tag{23}$$

where V_O and s are empirical constants.

Figure 21 presents the values of V_O for all stations versus source-to-receiver distance. There appears to be an association with distance R, with stations near the first bounce having the largest values of V_O. This effect is probably associated with a variation of ray-path heights with distance. The fitted relation is

$$V_o = 250 + 0.18\,R. \tag{24}$$

The values of s for each station are plotted versus distance in Fig. 22. There is a wide variation in the values of s and no indication of a relation with distance. For this report we adopt a weighted average value of 0.30.

To better understand the stratospheric signal velocities, we used an acoustic ray-trace program originated by Georges and Beasley (1977) to compute propagation paths for each month; we used wind profiles given by McCullough and Novlan (1977) for White Sands Missile Range and computed rays at intervals of 2° in elevation. Figure 23A shows a typical mid-March example east (downwind) of the source; Figure 23B shows an example from the west (counterwind).
In the downwind direction, stratospheric returns are seen, along with several thermospheric returns from the highest-elevation-angle rays. In the counterwind direction, there are thermospheric returns but no stratospheric returns, a condition that exists in the counterwind direction for all months. This lack of predicted stratospheric returns is, of course, in conflict with the observed stratospheric returns for counterwind conditions. ReVelle (1998) has shown that the absence of predicted counterwind stratospheric returns is a result of the lack of acoustic scattering in standard ray-trace calculations. Calculations by Hunter and Whitaker (1998), using a modal approach based upon the code of Pierce and Posey (1970), do predict counterwind stratospheric signals, provided there are irregularities in the assumed atmospheric profiles.

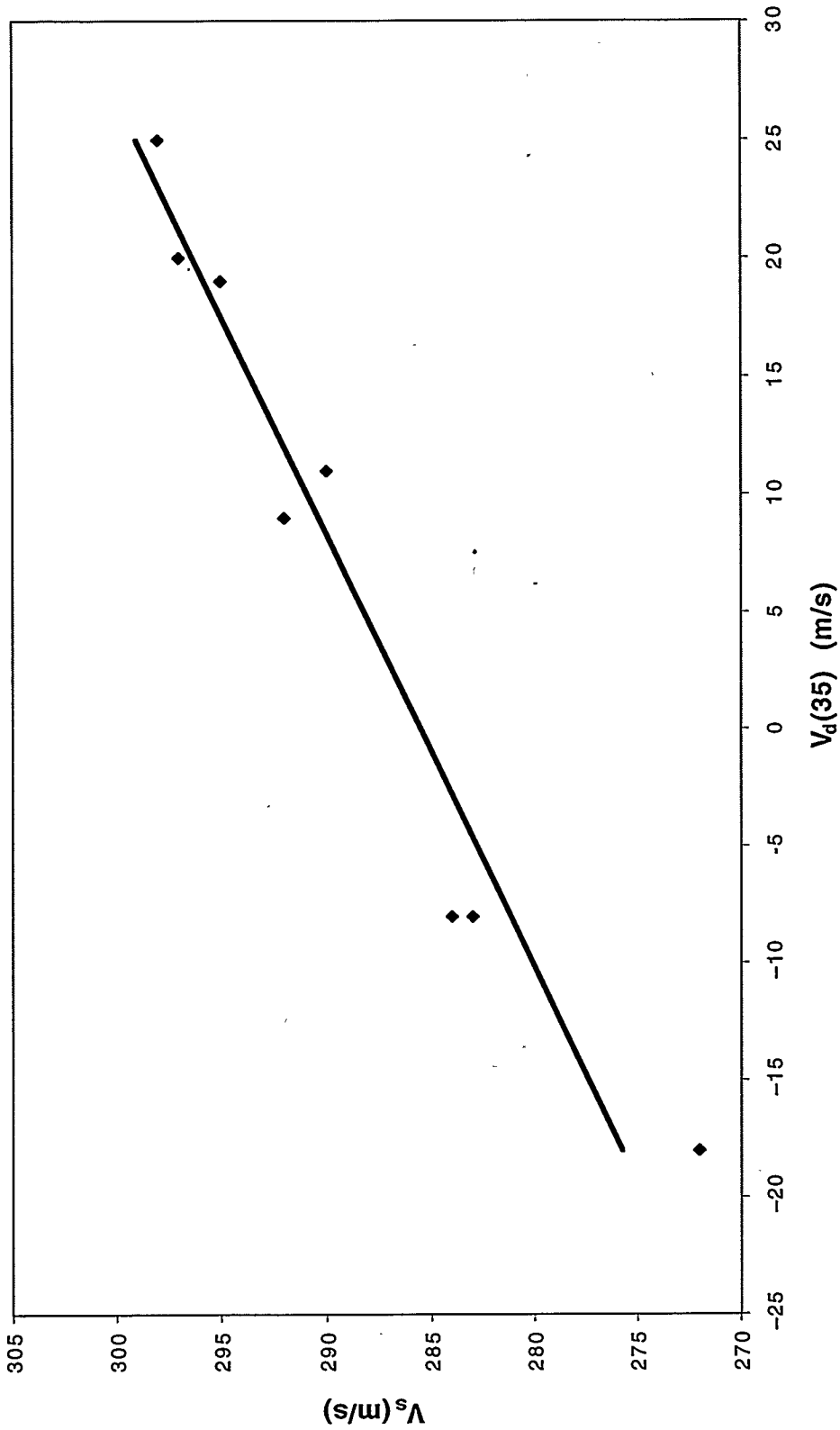

Figure 20. For Bishop, V_s versus the directed wind at a height of 35 km, $V_d(35)$. A least-squares fit line is shown.

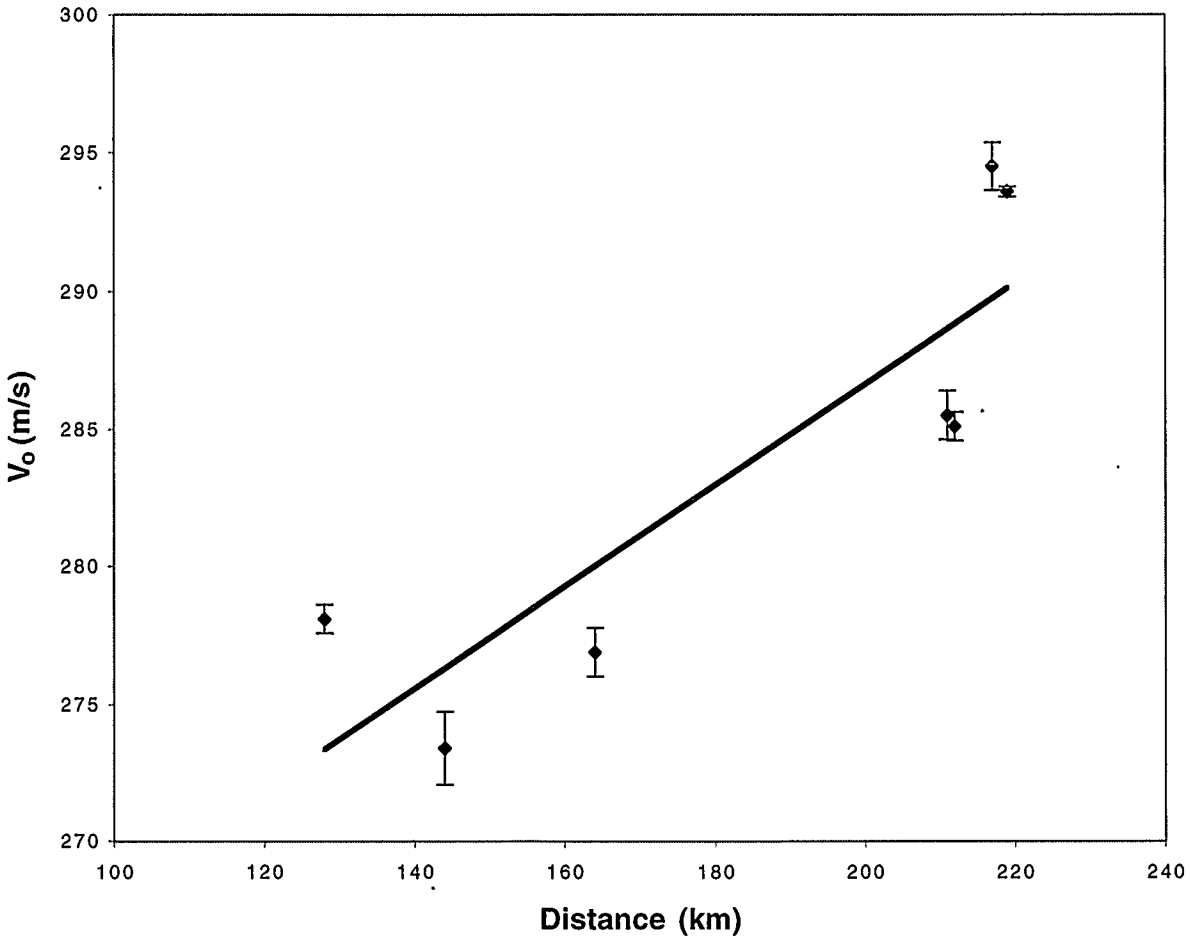

Figure 21. The empirical parameter V_O for each station versus distance. Unit standard deviations and a least-squares fit line are shown.

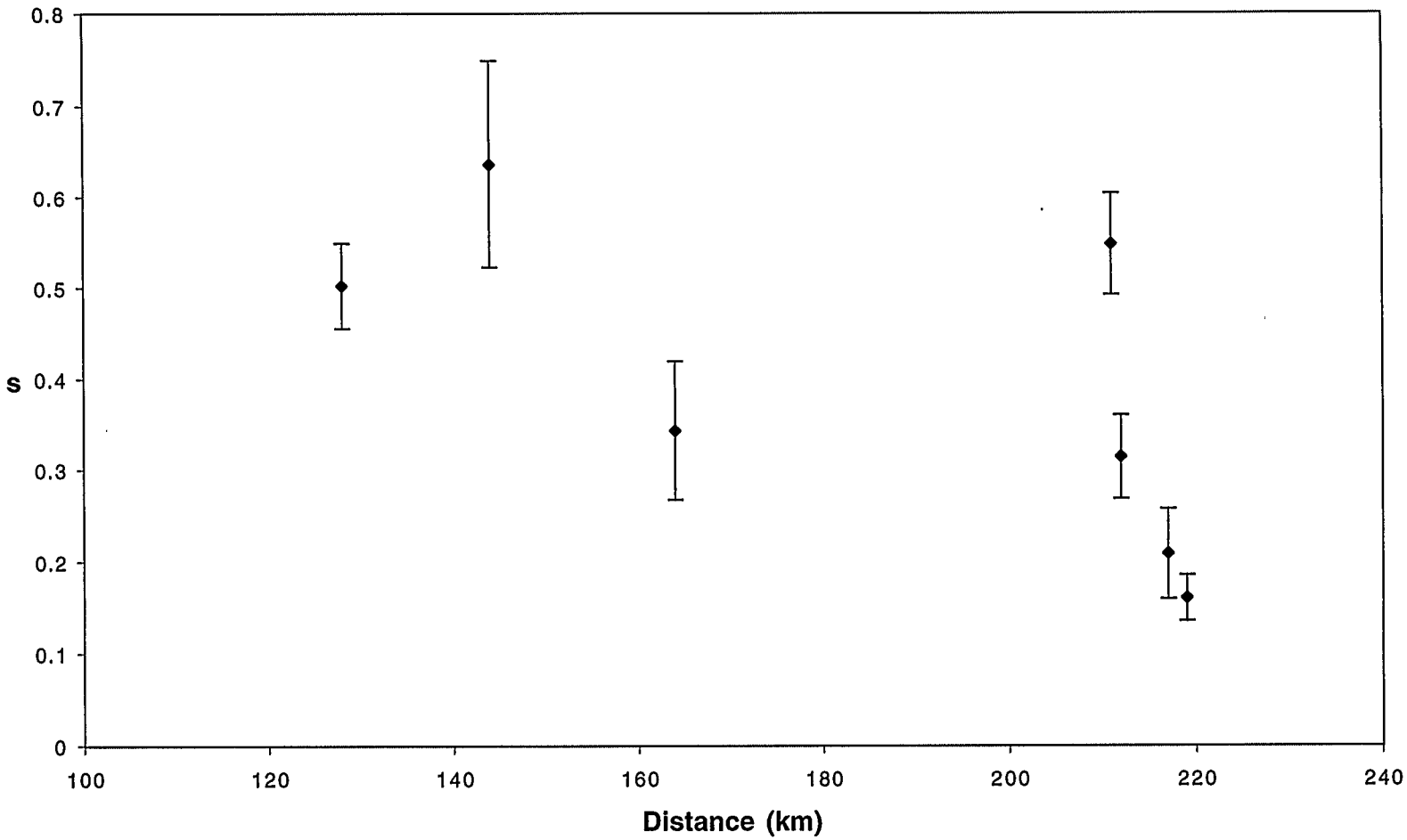

Figure 22. The empirical parameter *s* for each station versus distance. Unit standard deviations are shown.

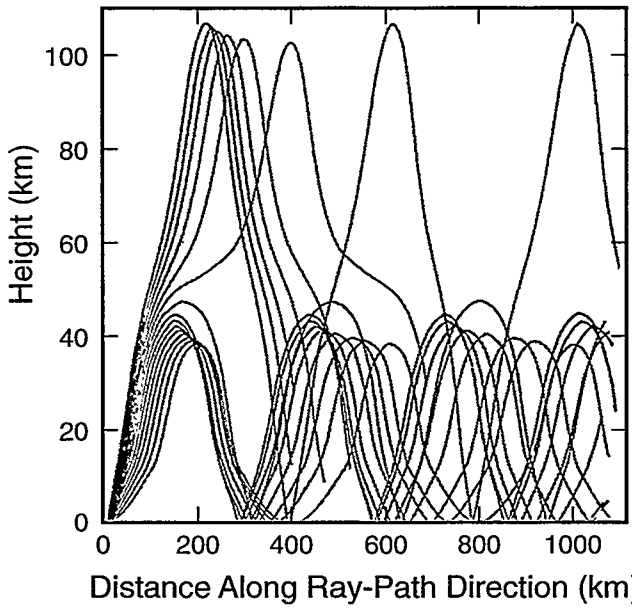

Figure 23A. A ray-trace calculation for downwind propagation in March. Rays are at 2° intervals for elevation angles from 2° to 30°. The source is at 0 km.

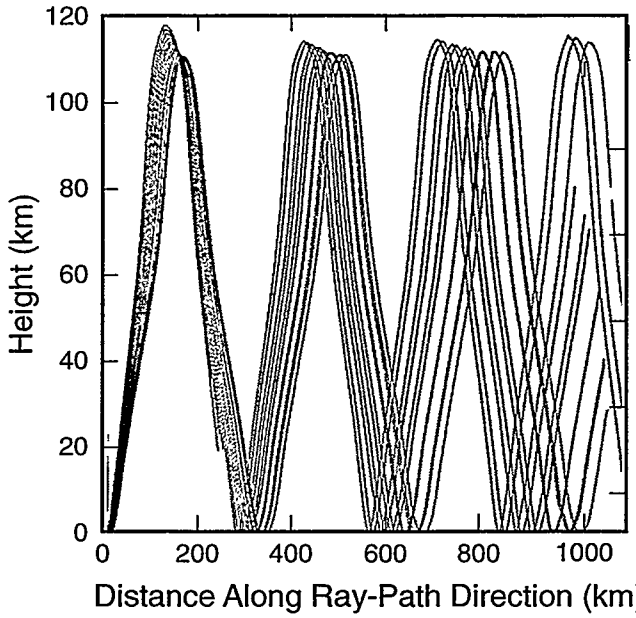

Figure 23B. A ray-trace calculation for counterwind propagation in March. Rays are at 2° intervals for elevation angles from 2° to 30°. The source is at 0 km.

We used the monthly ray-trace results to estimate the values of V_s near the first-bounce locations, and from these, we estimated the corresponding values of s. Of course, counterwind propagation could not be included for the reasons just indicated. We find that $s = 0.64$ at a distance of 220 km and 0.58 at a distance of 250 km. These values are in good accord with the value of 0.55 found for Bishop, but St. George has a value of 0.21 and China Lake 0.31.

Of course, it is important to know if the stratospheric velocity results obtained from this data set apply to greater distances. There is some evidence that the observed velocities at much greater distances—many hundreds to thousands of kilometers—are in general agreement with the values we have discussed. However, we recommend a more comprehensive study of this issue.

XII. THERMOSPHERIC SIGNALS

Infrasonic waves reflected or returned from thermospheric layers are referred to as thermospheric signals. The height for reflection of thermospheric signals is about 100 to 120 km. Figure 24 shows an example of V_t, the average thermospheric signal velocity, that follows the definition given in Eq. (20). This is given versus day number for the Bishop station. Two features are evident. First, the velocities are in the range of about 200 to 250 m/s—much smaller than the stratospheric values. This is to be expected because the height of the reflection region is roughly doubled. Second, there is no obvious trend with time of year.

In Fig. 25 the amplitudes for Bishop, scaled by yield $A_t W^{-n}$, are shown versus day number. Again, no variation with day number is seen, and comparison of this result with Fig. 7 for the stratospheric signals indicates a much smaller thermospheric variation. The absence of any apparent seasonal variation, unlike stratospheric signals, results from the fact that in the thermosphere the strong rise of temperature with height, along with the corresponding rise in sound velocity, provides an effective reflection layer during all seasons. As a result, winds tend to have a secondary effect. In fact, ray-trace calculations show that thermospheric returns are present throughout the year. An effect produced by the winds is present but only changes the height of the reflection region. For example, for propagation to the west in mid-northern latitudes, the height varies from about 114 to 123 km in midwinter to about 100 to 104 km in midsummer. Because there is no obvious annual variation, we calculated mean values of the yield-scaled amplitudes A_{ct} (using $n = 0.456$ for no HOB effect). Table VI contains these values and the corresponding standard deviations. Figure 26 shows the values of $\log A_{ct}$ versus log distance for each station with five or more thermospheric signals. There is an indication of variation with distance, which may be a footprint effect, as in the case of the stratospheric signals. A fitted relation is

$$\log A_{ct} = -2.04 + 1.41 \log R. \tag{25}$$

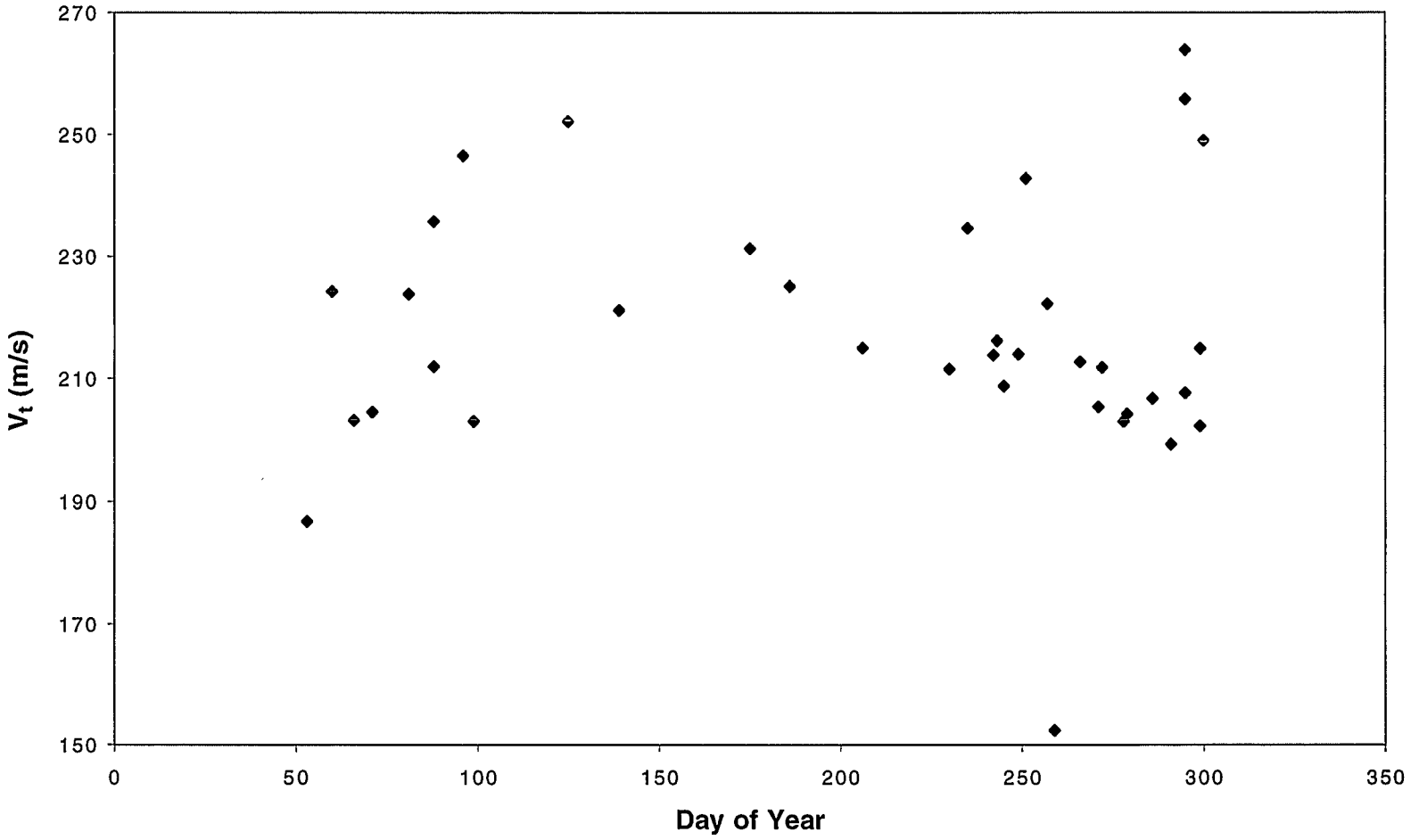

Figure 24. Seasonal distribution of average thermospheric velocity V_t for Bishop.

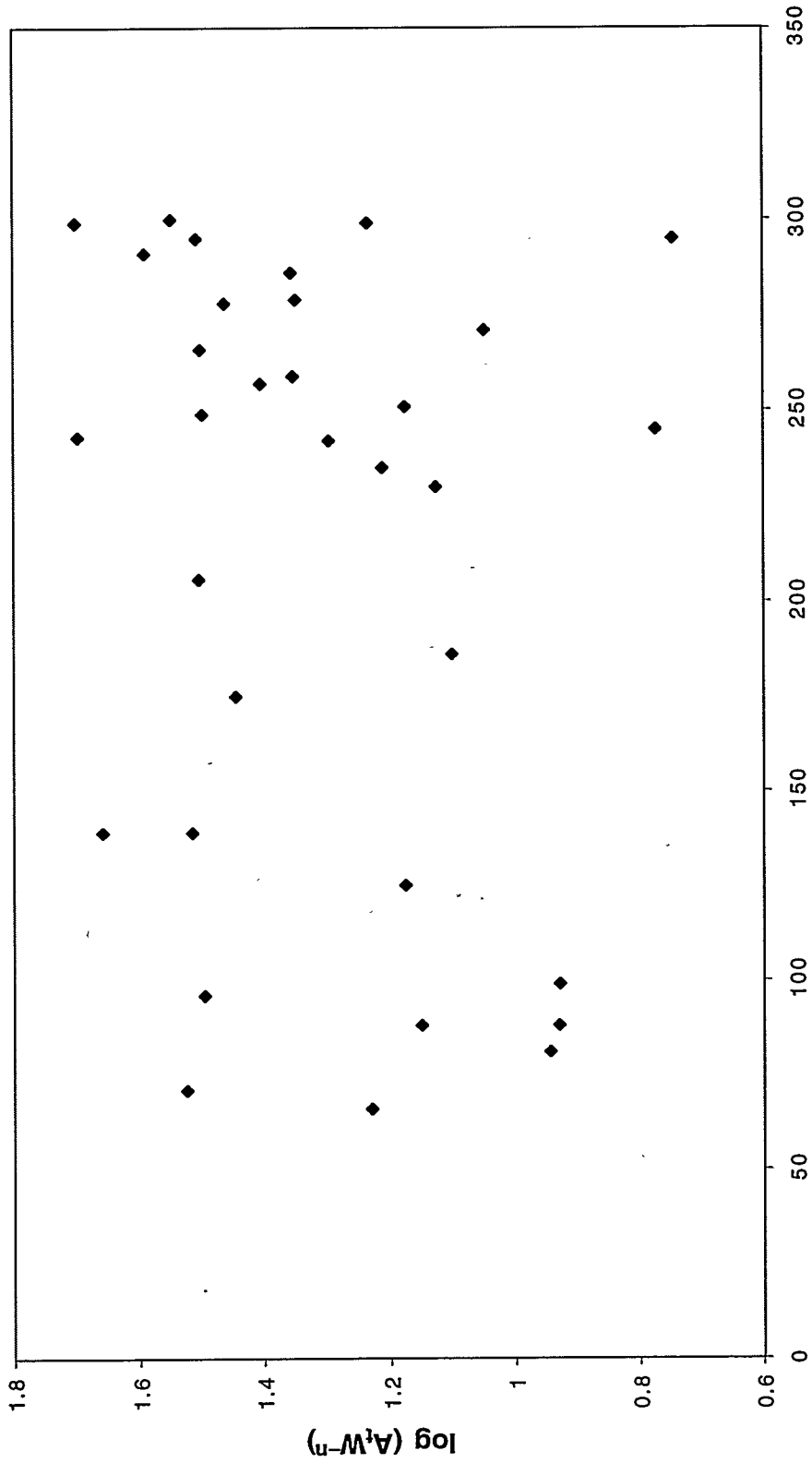

Figure 25. Seasonal distribution of the yield-scaled thermospheric amplitudes for Bishop.

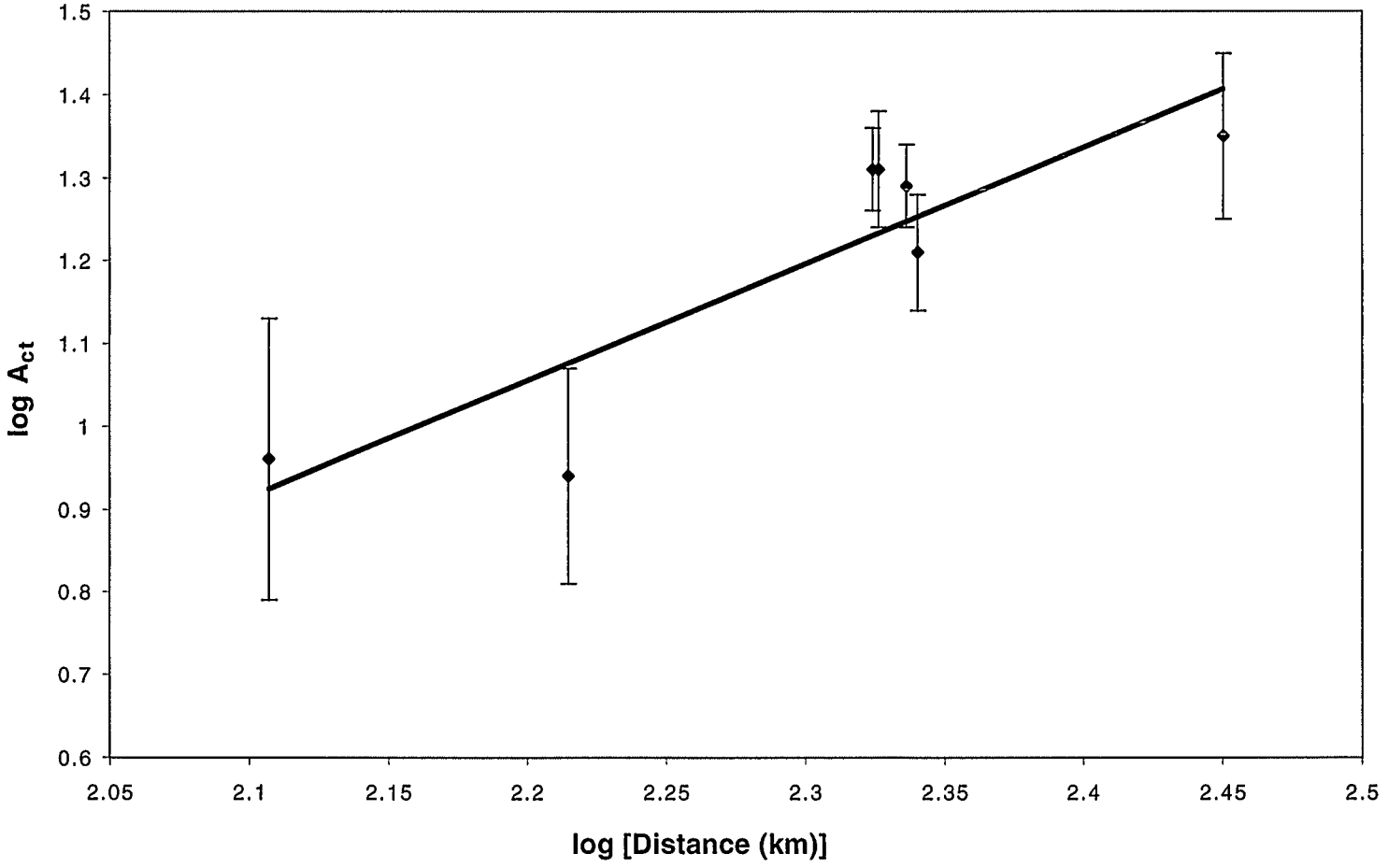

Figure 26. Empirical parameter A_{ct} versus distance for all stations. Unit standard deviations and a least-squares fit are shown.

Only one event, Hood, on July 5, 1957, has a sufficient number of stations with thermospheric signals to give an indication of amplitude variation with distance for a single event. Figure 27 shows the log of the amplitude versus log of distance; again, a possible footprint effect is indicated.

The four stations near the first-bounce location (average distance of 215 km) are very consistent in average amplitude and have a mean value for that position:

$$\langle \log A_{ct} \rangle = 1.29 . \tag{26}$$

Comparing this result with that for stratospheric signals (see Table II) indicates that, with a zero value of V_d, stratospheric amplitudes will be about four times stronger than thermospheric amplitudes. However, under strong counterwind conditions, thermospheric amplitudes can become the larger signal.

We calculated the mean values of the average thermospheric velocities V_t for each station. Those are given in Table VI, along with the standard deviations. Figure 28 shows those values versus distance for the stations. There appears to be no systematic variation with distance, considering the sizes of the standard deviations. However, the observations from Cedar City, Utah, have the greatest velocity at the greatest distance. There may be an east-west difference. A mean value for the four first-bounce stations is

$$\langle V_t \rangle = 219 \text{ m/s} . \tag{27}$$

The seasonal variation for V_t is about 20% for the individual first-bounce stations. This is essentially the variation to be expected from the variation in the propagation-path length caused by the previously mentioned seasonal variation in reflection height.

Table VI. Thermospheric Signal Analysis

Station	No. Observations	log A_{ct}	$\langle V_t \rangle$ m/s
SG	30	1.29 ± 0.05	228 ± 3
BI	33	1.31 ± 0.05	220 ± 3
BC	11	0.94 ± 0.13	208 ± 9
CA	1	1.43	254
CC	5	1.35 ± 0.1	248 ± 1
CL	32	1.31 ± 0.07	211 ± 2
LV	9	0.96 ± 0.17	216 ± 9
LU	15	1.21 ± 0.07	232 ± 3
TO	2	1.67 ± 0.15	259
PS	5	1.35 ± 0.07	252 ± 2

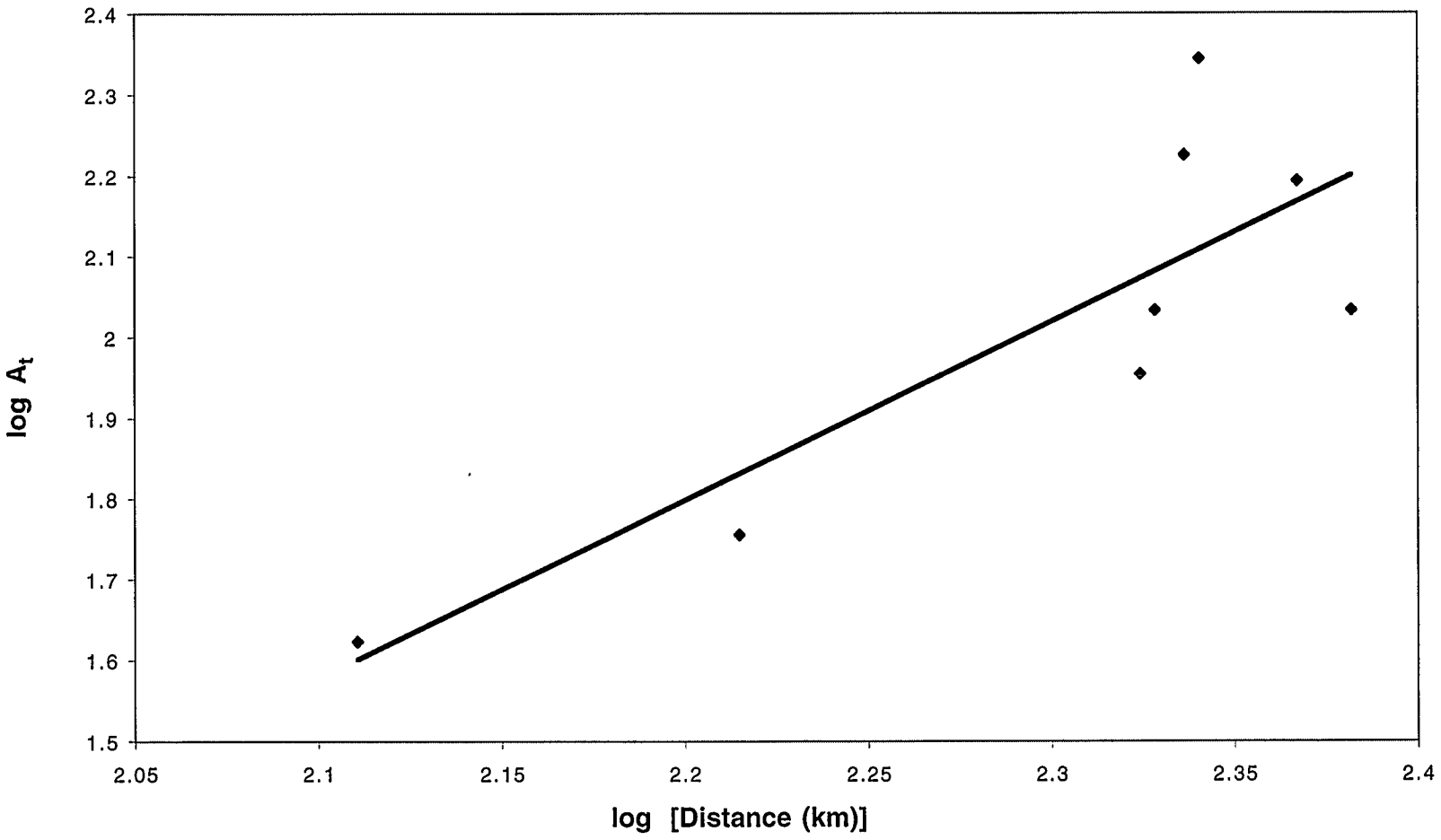

Figure 27. Empirical parameter A_t for the Hood event for all stations versus distance, showing a footprint effect.

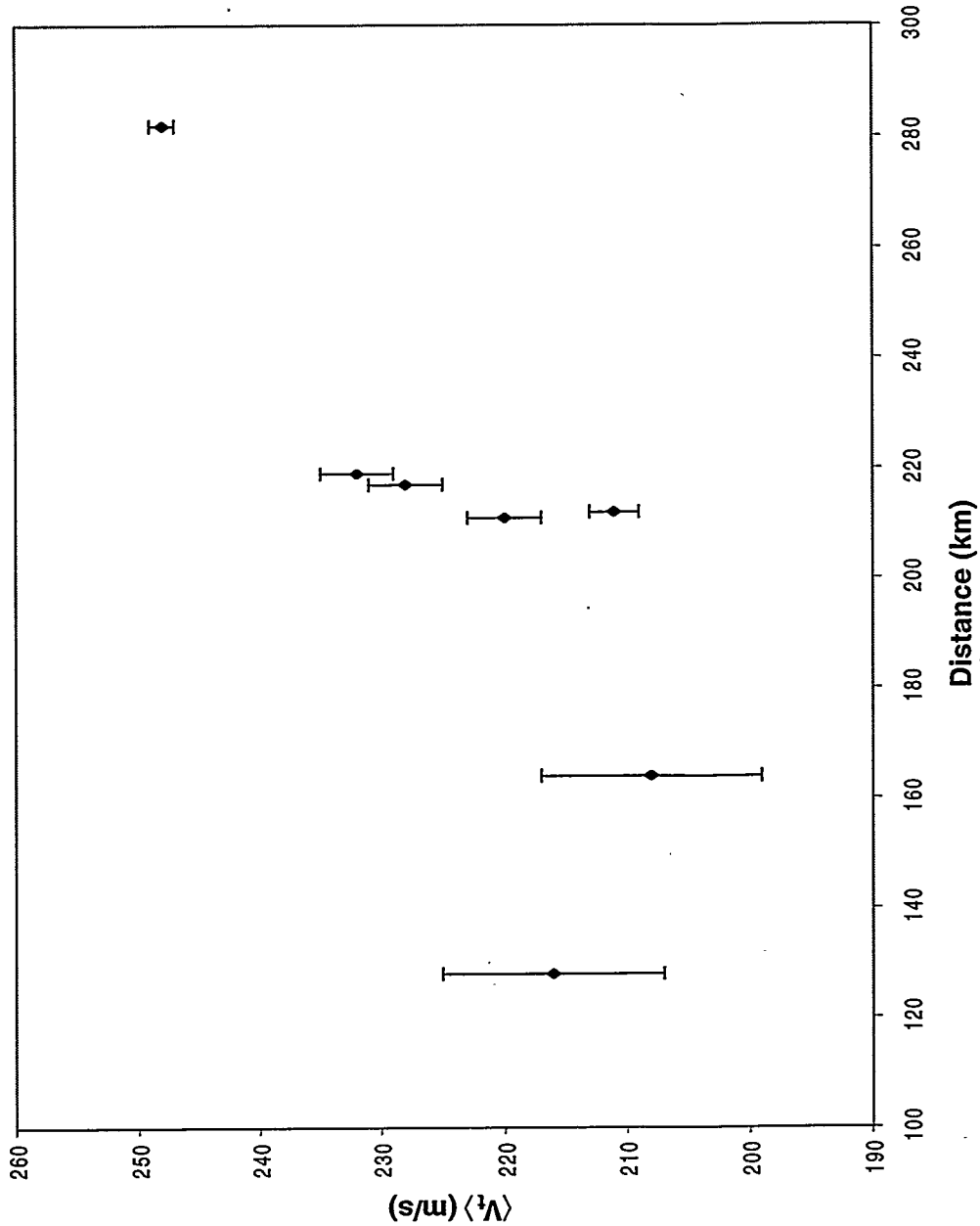

Figure 28. Average velocity of thermospheric signals $\langle V_t \rangle$ for all stations versus distance. Unit standard deviations are shown.

It is useful to ask if the thermospheric results found near the first bounce also apply at longer ranges and for other sources. Table VI shows that at a distance of about 373 km, Pasadena, California, station (PS) has A_{ct} and $\langle V_t \rangle$ in reasonable accord with the first-bounce values. Unfortunately, the Albuquerque station, at a considerably greater distance, has no thermospheric signals; that station was operated for a very restricted time. A White Sands Missile Range test explosion, Miser's Gold, was observed at a number of stations by Los Alamos National Laboratory personnel, and Davidson and Whitaker (1992) reported the results. Miser's Gold was a 2440-t surface explosion of ANFO. Thermospheric signals were detected at Flagstaff, Arizona, (517 km) and at Los Alamos (226 km). The use of Eq. (25) predicts a value of 11.2 μb for Flagstaff compared with the observed value of 12.6 μb. For Los Alamos the predicted value is 30.1 μb compared with the observed value of 37.3 μb. Thus, there is some evidence that the results of this investigation are applicable to other cases.

Because no seasonal variation is apparent in thermospheric amplitudes for the first-bounce location, we can write

$$A_t = A_{ct} W^n, \tag{28}$$

where the value of A_{ct} is taken from Eq. (26). Dividing corresponding sides of Eq. (28) for thermospheric signals and Eq. (9) for stratospheric signals and solving for V_d gives the result

$$V_d = \frac{1}{k}\left[\left(\log A_s - \log A_t\right) - \left(\log A_{cs} - \log A_{ct}\right)\right]. \tag{29}$$

Thus, it is possible to determine values of the effective stratospheric velocity from observations of the stratospheric and thermospheric signals *independent* of distance and yield. In Fig. 29 an example of this determination is given for the signals at Bishop, together with a comparison with the statistical model values of V_d used for Bishop. We see good agreement in general. Unfortunately, we do not know how frequently thermospheric signals are observed at larger ranges and hence how generally applicable this procedure may be.

Average velocities of signals from the closest Nevada stations to record thermospheric signals—Boulder City, Las Vegas, and Caliente—are shown in Fig. 30. Several extremely low velocities, in the range of about 160 to 190 m/s, are evident. These low values are seen only in three cases for stations near the first bounce. It is useful to ask what altitudes in the thermosphere would be required to produce these small values of V_t. We constructed a simple thermospheric propagation model with a triangular approximation for the ray paths. The model shows that, for Caliente and Las Vegas, returns from about 105 to 115 km will produce the observed velocities. However, for Boulder City the required heights are very high, about 130 to 155 km. The required elevation angles for signal launch are about 55° to 60°.

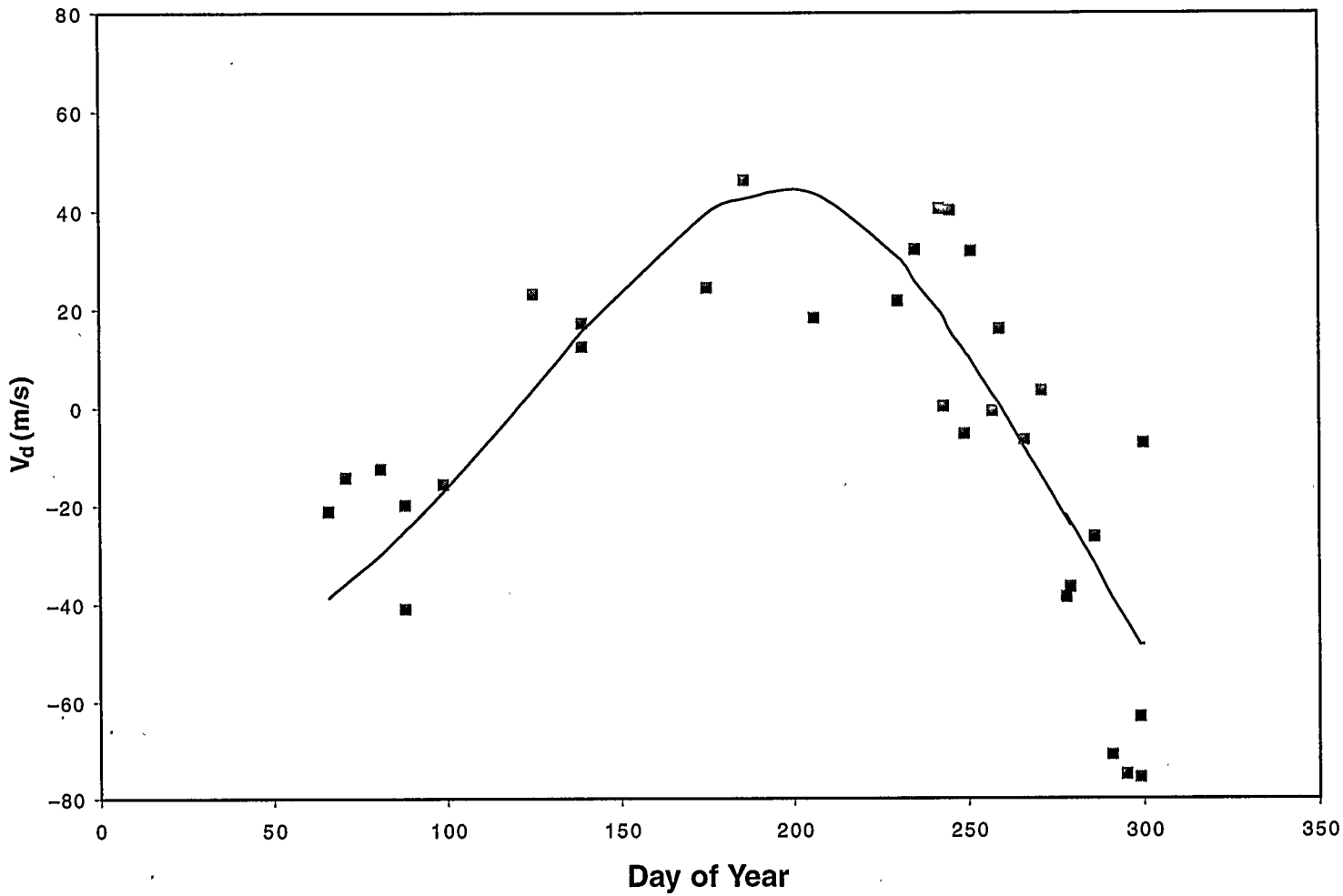

Figure 29. Empirical determination of the SCI values of V_d from stratospheric and thermospheric signal pairs for Bishop (squares). Also shown for comparison is the statistical model V_d (line) for the azimuth of Bishop.

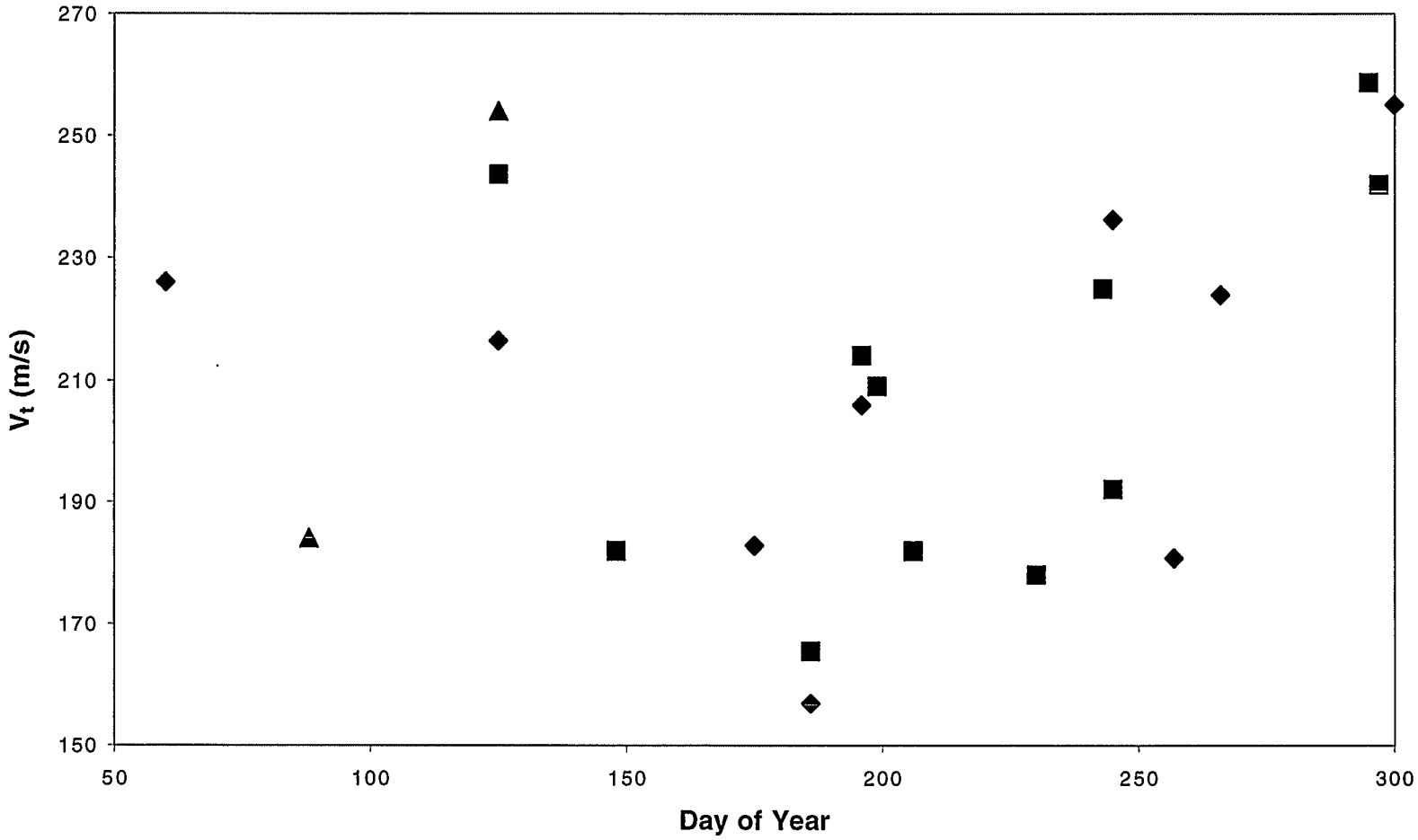

Figure 30. Thermospheric average velocities $\langle V_t \rangle$ for close-in stations versus day of year for Las Vegas (diamonds), Boulder City (squares), and Caliente (triangles).

XIII. TROPOSPHERIC/SURFACE SIGNALS

Many of the signals within the database under study have high average velocities in comparison with the stratospheric or thermospheric values. Reed classifies these signals as tropospheric signals, that is, as signals that are propagated by reflection within a tropospheric duct, possibly the result of a low-level wind-shear layer resulting from a tropospheric jet. On the other hand, it is possible for high-velocity signals to arise from Lamb edge-mode propagation very close to the surface. Lamb wave propagation has been described by ReVelle and Whitaker (1996), ReVelle (1996), and Pierce and Posey (1971). Without waveform details, clearly determining the type of signal may be difficult.

Figure 31 gives an example of the observed high velocities V_h versus day number for St. George. Notice that V_h can reach quite-large values and has a considerable range. The dispersion in V_h is large, but there is an indication of a seasonal variation. A dominant feature of the high-velocity signals is a pronounced asymmetry between eastward and westward propagation. There are many signals east of NTS; for example, about 34% of the signals at St. George are high velocity, whereas at Bishop only about 6% are high velocity. This difference was illustrated in Figs. 3 and 4. The asymmetry no doubt is connected to the prevailing easterly flow in the tropospheric layers. Another possible cause for the asymmetry is the fact that nuclear test activity was largely curtailed when (infrequent) winds to the west were present.

To better characterize the seasonal variation of V_h, we made stiff spline function fits to the data from St. George, Boulder City, and Las Vegas (see Fig. 32). These are the only stations for which we have a fairly complete seasonal history. Reasonably similar variations are seen with a peak in V_h during the summer period. The latter two stations especially have high consistency, as shown in Fig. 33, which presents the velocity for Boulder City versus that for Las Vegas. This suggests that the same type of propagation produced signals at these stations.

We interpolated a seasonal wind variation, $V_z\,(10.5)$, from the longitudinally averaged monthly means of Fleming et al. (1990) for the latitude of NTS at a representative tropospheric height of 10.5 km. That is shown in Fig. 34. Figure 35 shows the average V_h versus $V_z\,(10.5)$ for the three eastern stations. The figure shows that (1) there is a negative correlation between the variables with $V_h \approx 1/V_z(10.5)$ that seems counterintuitive and (2) there is a seasonal loop in the relation. The fitted relation is

$$V_h = 361 - 0.86\,V_z(10.5). \qquad (30)$$

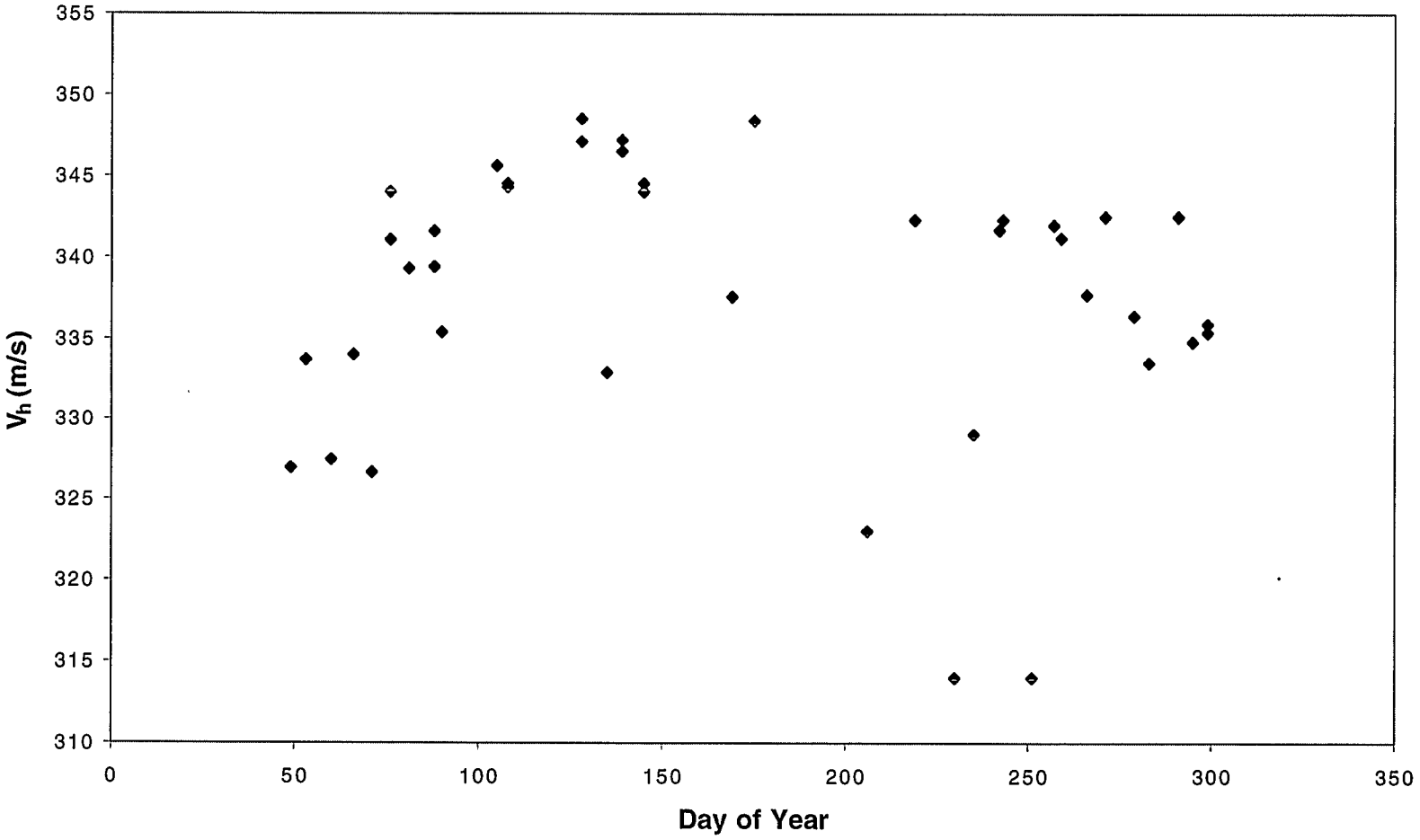

Figure 31. Tropospheric/surface average velocity V_h versus day of year for St. George.

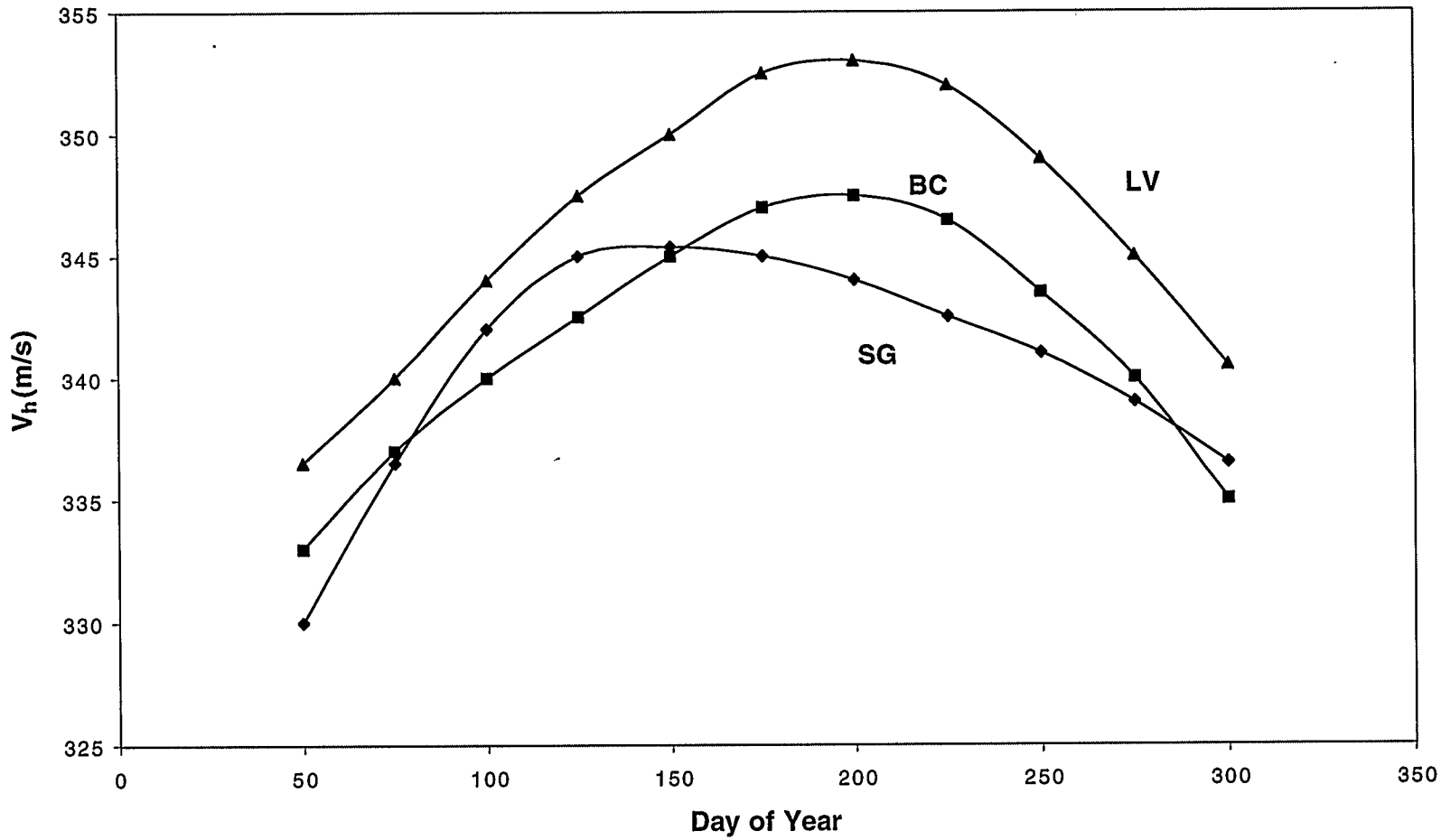

Figure 32. Spline fits of V_h for three stations to the east of NTS. Las Vegas (LV), Boulder City (BC), and St. George (SG).

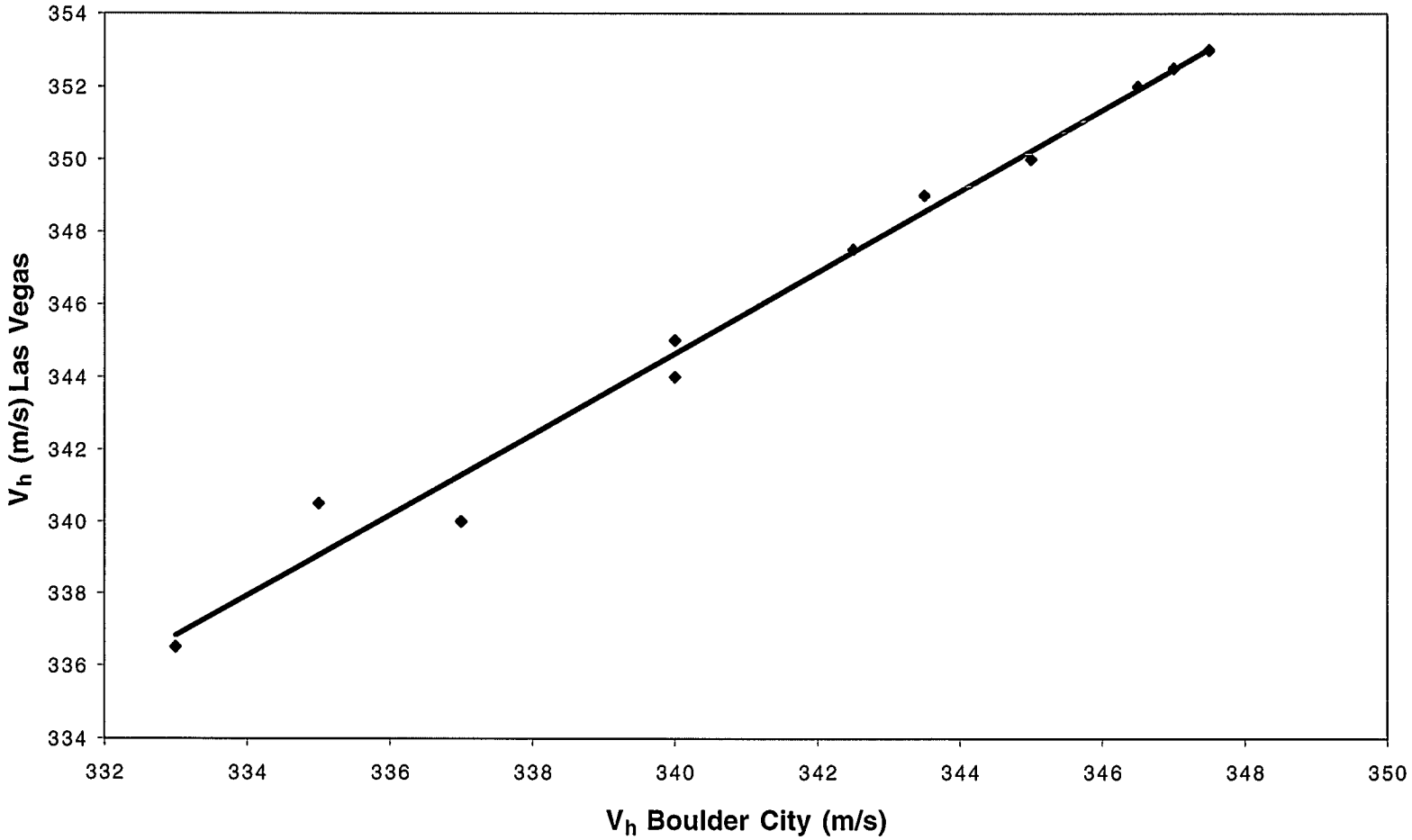

Figure 33. The observed values of V_h for Boulder City versus those for Las Vegas, showing the consistency. A least-squares fit line is shown.

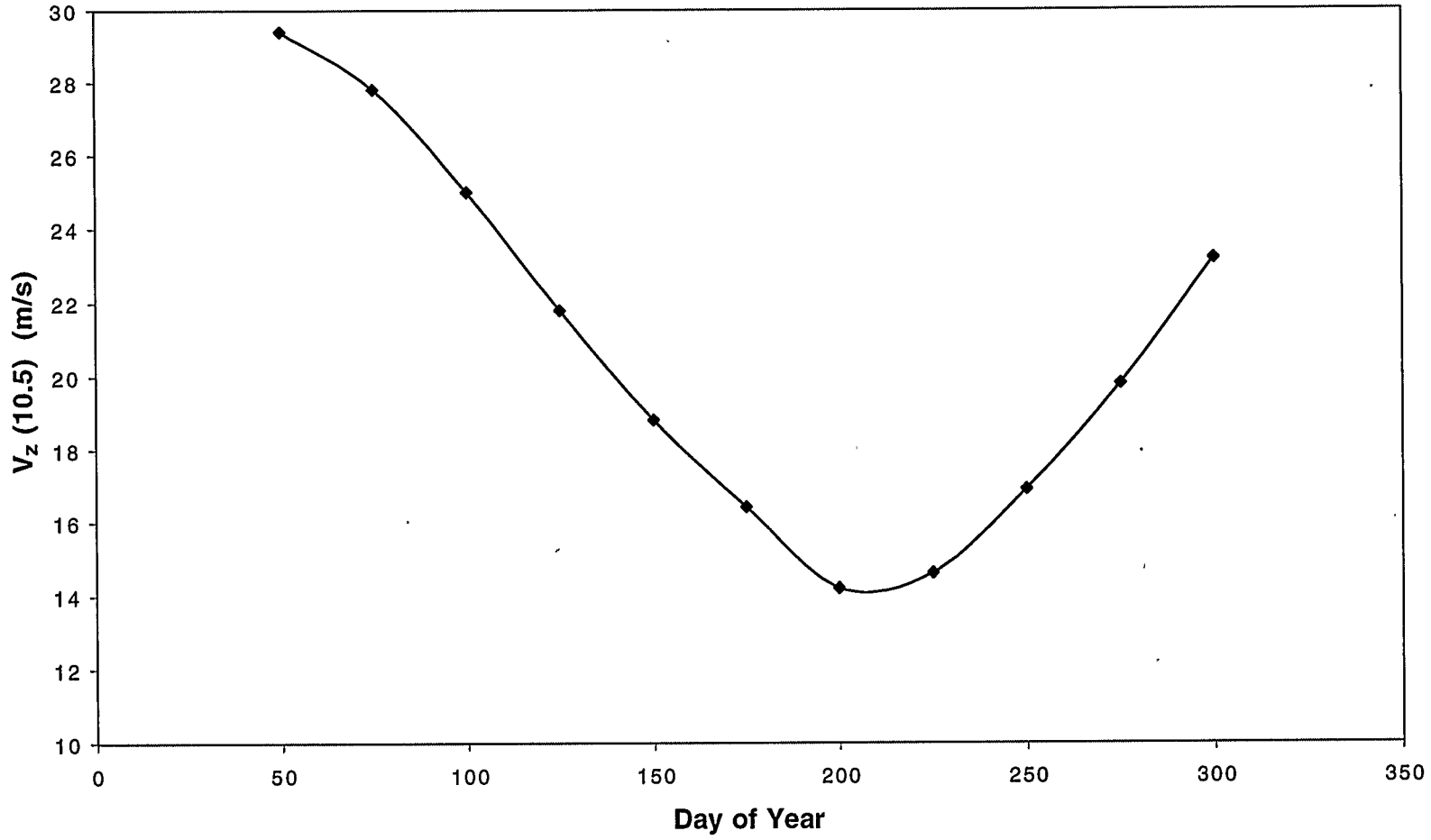

Figure 34. Statistical zonal wind $V_z(10.5)$ at a height of 10.5 km versus day of year. See text for details.

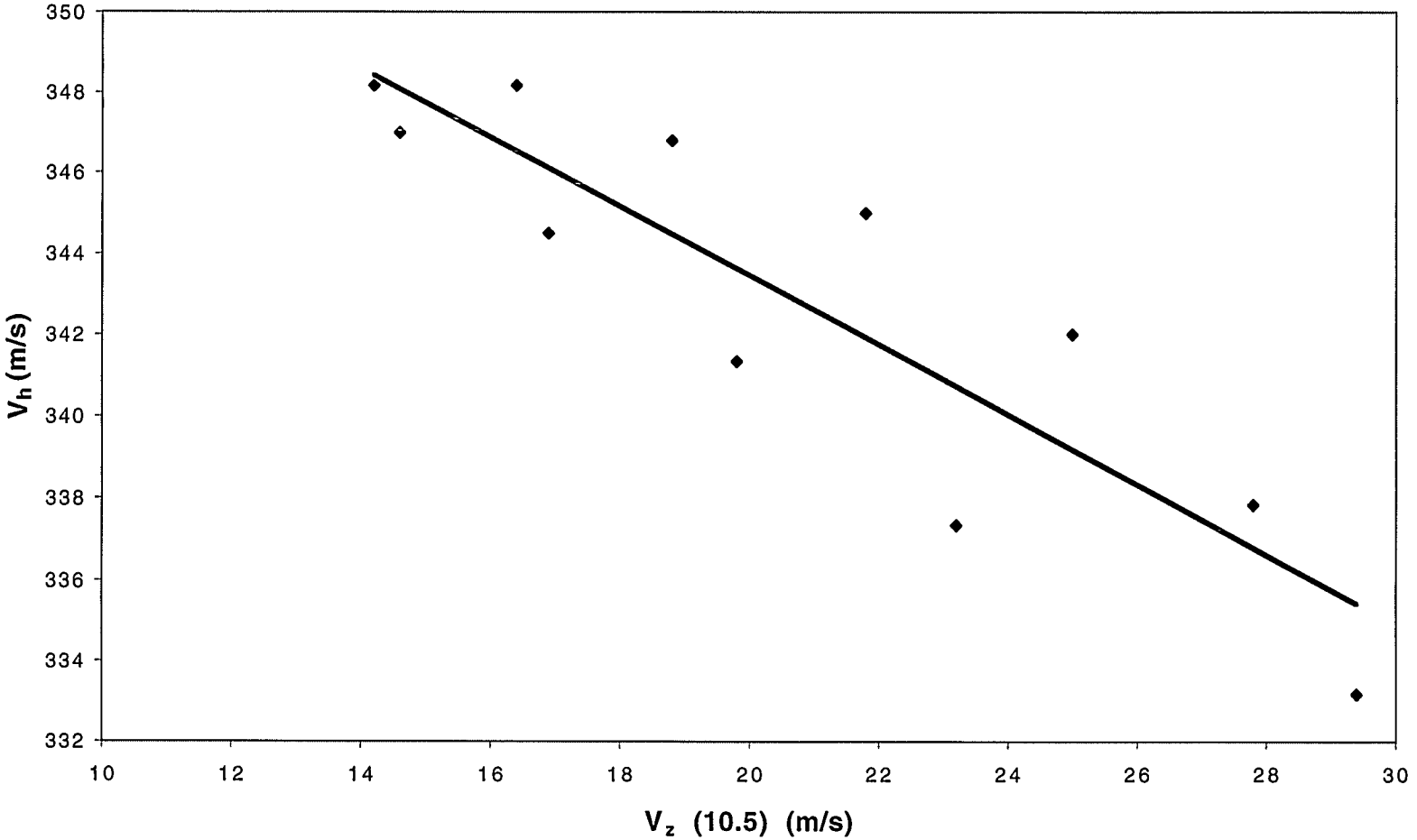

Figure 35. Average easterly V_h for three stations (St. George, Boulder City, and Las Vegas) versus $V_z(10.5)$. A least-squares fit is shown. There is a strong "hysteresis" effect.

It is useful to ask if the high values and the large range in V_h can be supported by the concept of tropospheric propagation. We used the longitudinally averaged values of the temperature structure and the zonal winds from Fleming et al. (1990) near the NTS latitude to make a rough test of this question, assuming that the observed velocity is approximated by

$$V_h \approx c(h) + V_z(h), \tag{31}$$

where $c(h)$ is the sound velocity at height h from the temperature profiles. Figure 36 presents the observed seasonal fit of V_h for St. George and the predicted values from Eq. (31) for heights of 0 and 3.5 km versus day number. The highest values of V_h can be accommodated by surface propagation, but the values outside the summer period require propagation in a higher layer. Of course the shortcoming of this rough analysis is that (1) averaged rather than local values of temperature and $V_z(h)$ have been used and (2) the profiles should be for the generally early morning times of the events. Nevertheless, there is some justification for near-surface propagation as an explanation for the very high velocity observations.

For St. George, Fig. 37 shows high-velocity signal amplitudes A_h scaled by explosive yield versus day number. Again, a seasonal variation is evident, but in contrast with the trend in V_h, the lowest values are seen in the summer period. Figure 38 shows stiff spline function fits of yield-scaled amplitudes versus day number for St. George, Boulder City, and Las Vegas. There is good consistency in the trends among the stations. This occurs in spite of some difference in azimuths and distances between the stations (see Table I).

Because of the consistency among the stations, we took an average of the yield-scaled amplitude for the three stations and in Fig. 39 plotted it versus V_z (10.5 km). The figure suggests a good correlation between the variables with $r^2 = 0.94$; the least-squares fit is

$$A_h W^{-n} = -1.02 + 0.12\, V_z(10.5)\ , \tag{32}$$

where the amplitude is in μb and V_z in m/s; the relation gives an approximation for the distance region of the three stations. Thus, it appears that the scaled amplitudes for high-velocity signals may be predictable in terms of tropospheric velocity.

Some stations in the Reed (1969A) data set were at much closer distances (20 to 70 km) to the explosions than the stations employed in our general analysis. We used data from these close-in stations together with the more-distant stations to investigate the attenuation of amplitude with distance for specific events. Using that method, we examined 13 events distributed over the year. Figure 40 gives an example for one event, Ruth, on day 90 of 1953. The figure shows a good linear fit between the log of the amplitude (μb) and the log of distance (km):

$$\log A_h = 7.10 - 2.44 \log R; \tag{33}$$

that is, there is a power law for attenuation with distance. The value of r^2 is 0.94. The relation covers the distance range of 17 to 269 km and, surprisingly, suggests that propagation conditions producing the high-velocity signals appear to be very uniform over this large distance span.

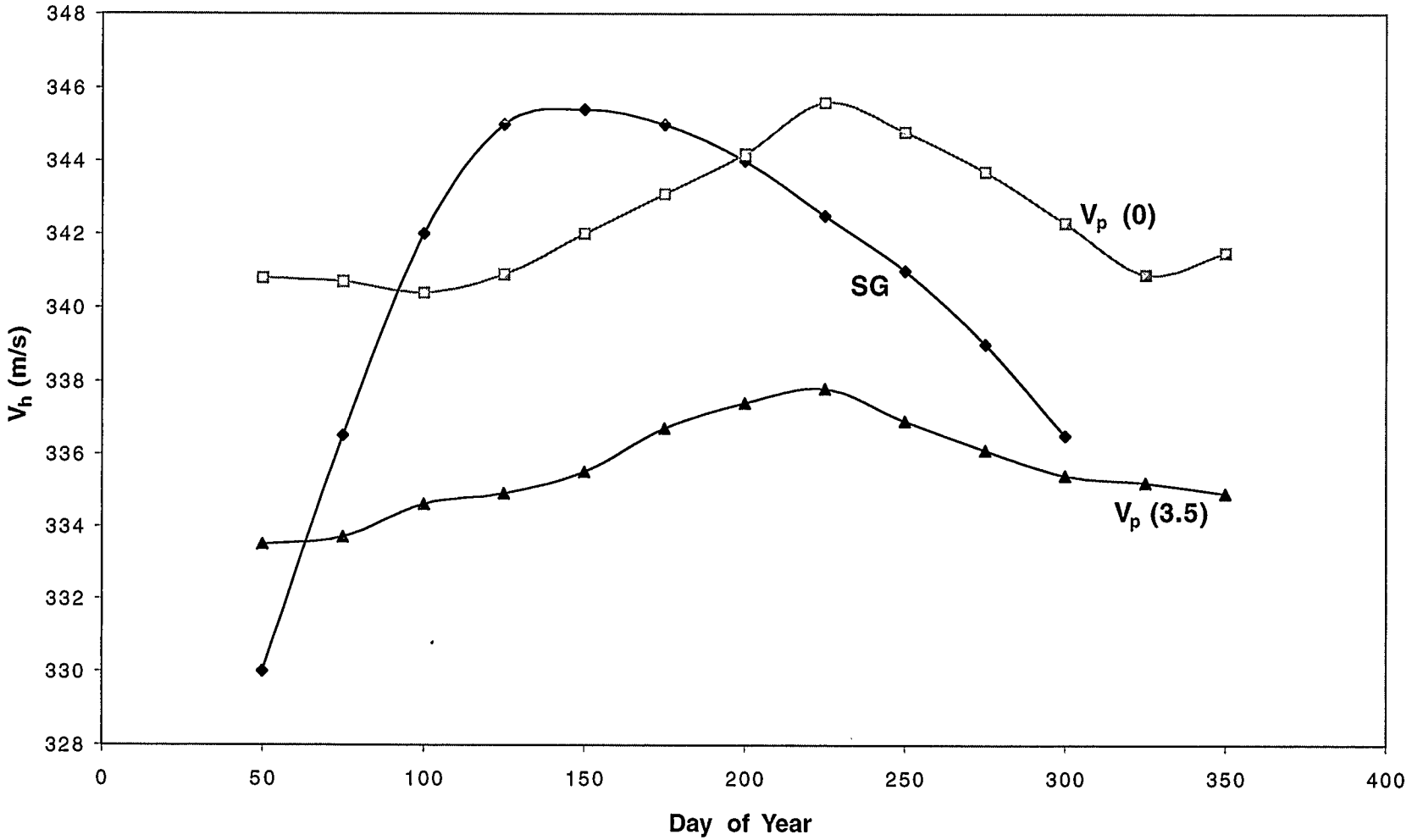

Figure 36. Seasonal variation of V_h for St. George (SG) compared with predicted values at heights of 0 km and 3.5 km using statistical winds. See text for details.

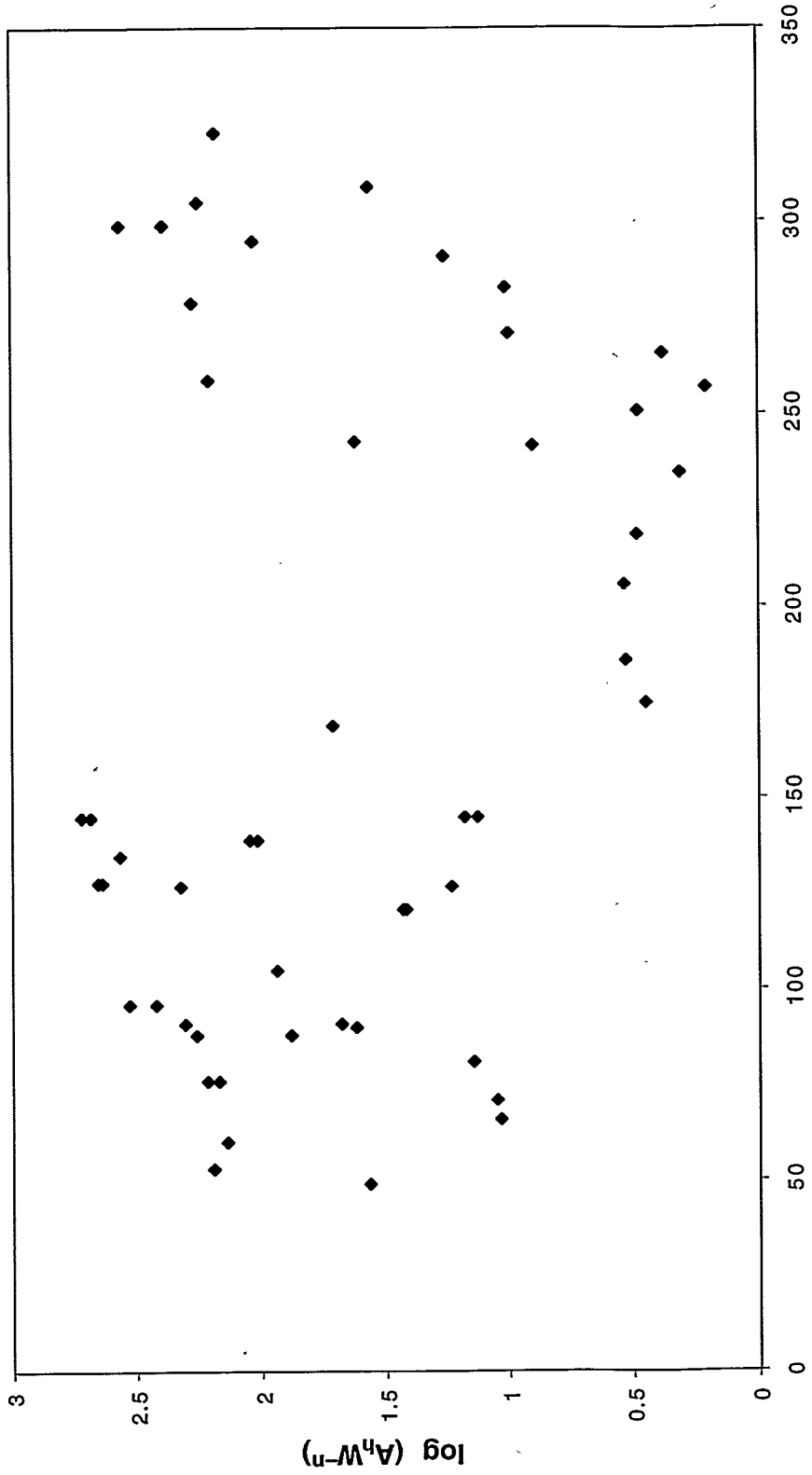

Figure 37. Yield-scaled amplitudes of tropospheric/surface signals for St. George versus day of year.

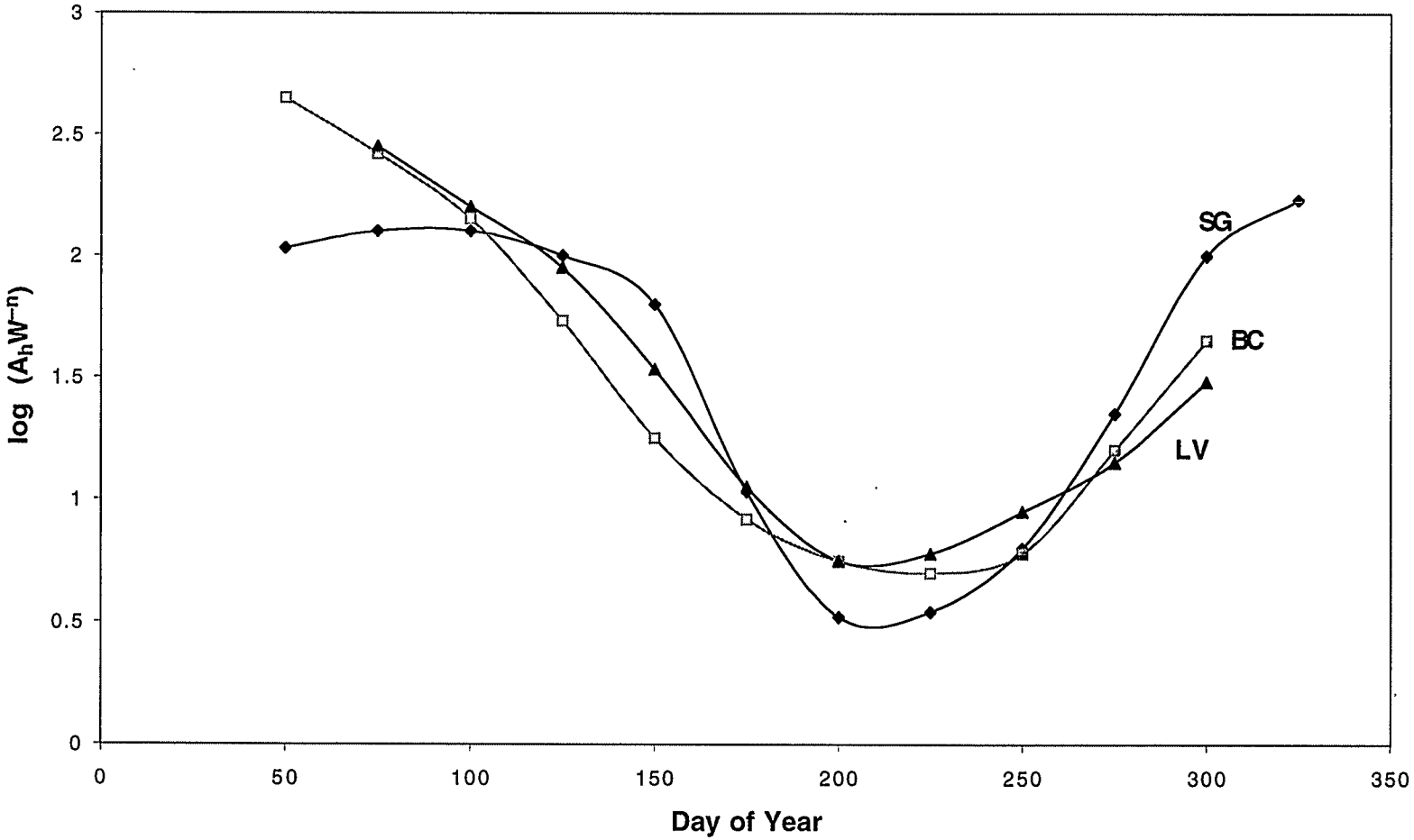

Figure 38. Spline fits to yield-scaled amplitudes of tropospheric/surface signals for three stations: St. George (SG), Boulder City (BC), and Las Vegas (LV).

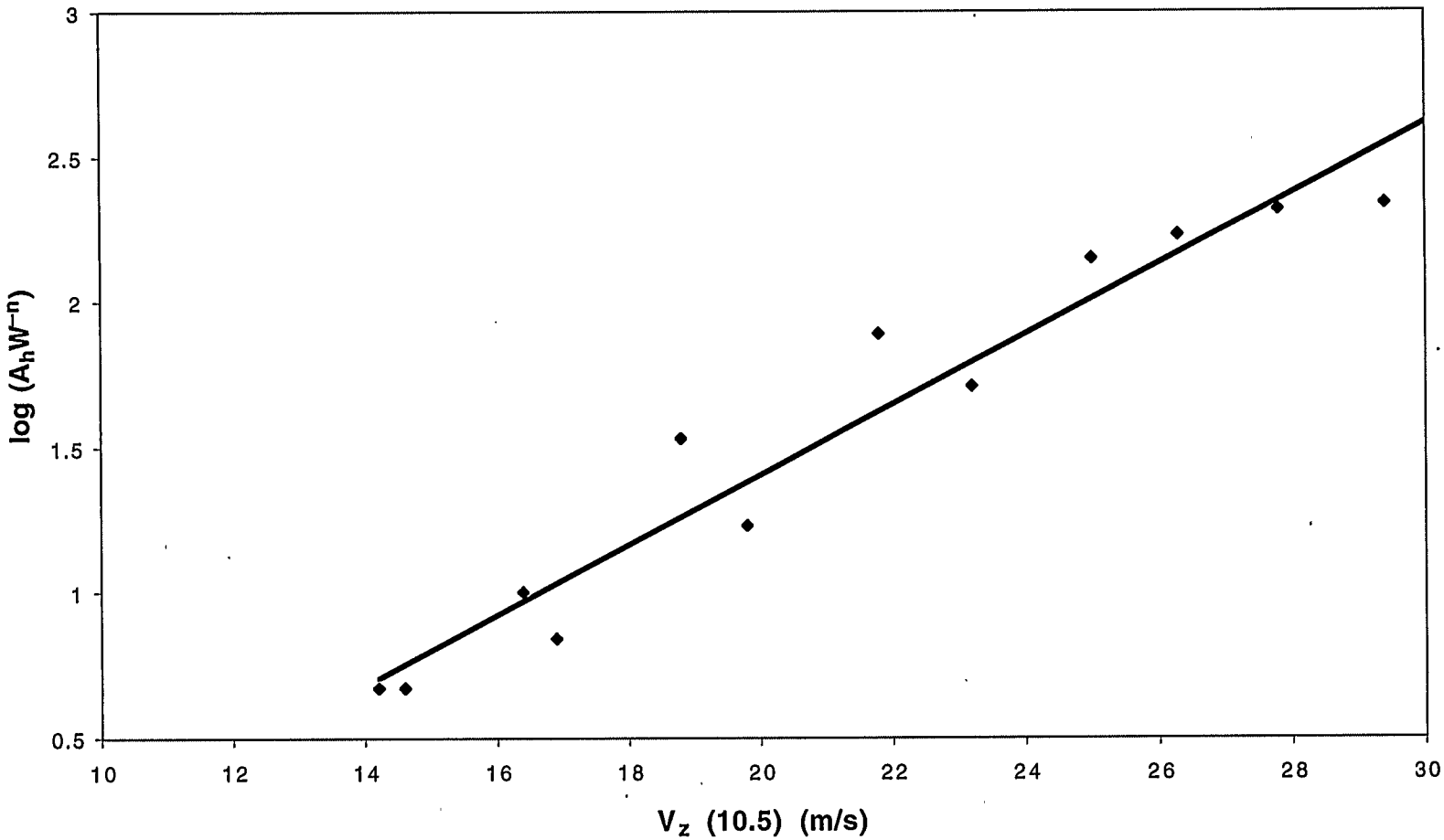

Figure 39. Average values of yield-scaled tropospheric/surface amplitudes for three stations versus $V_Z(10.5)$. A least-squares fit is shown.

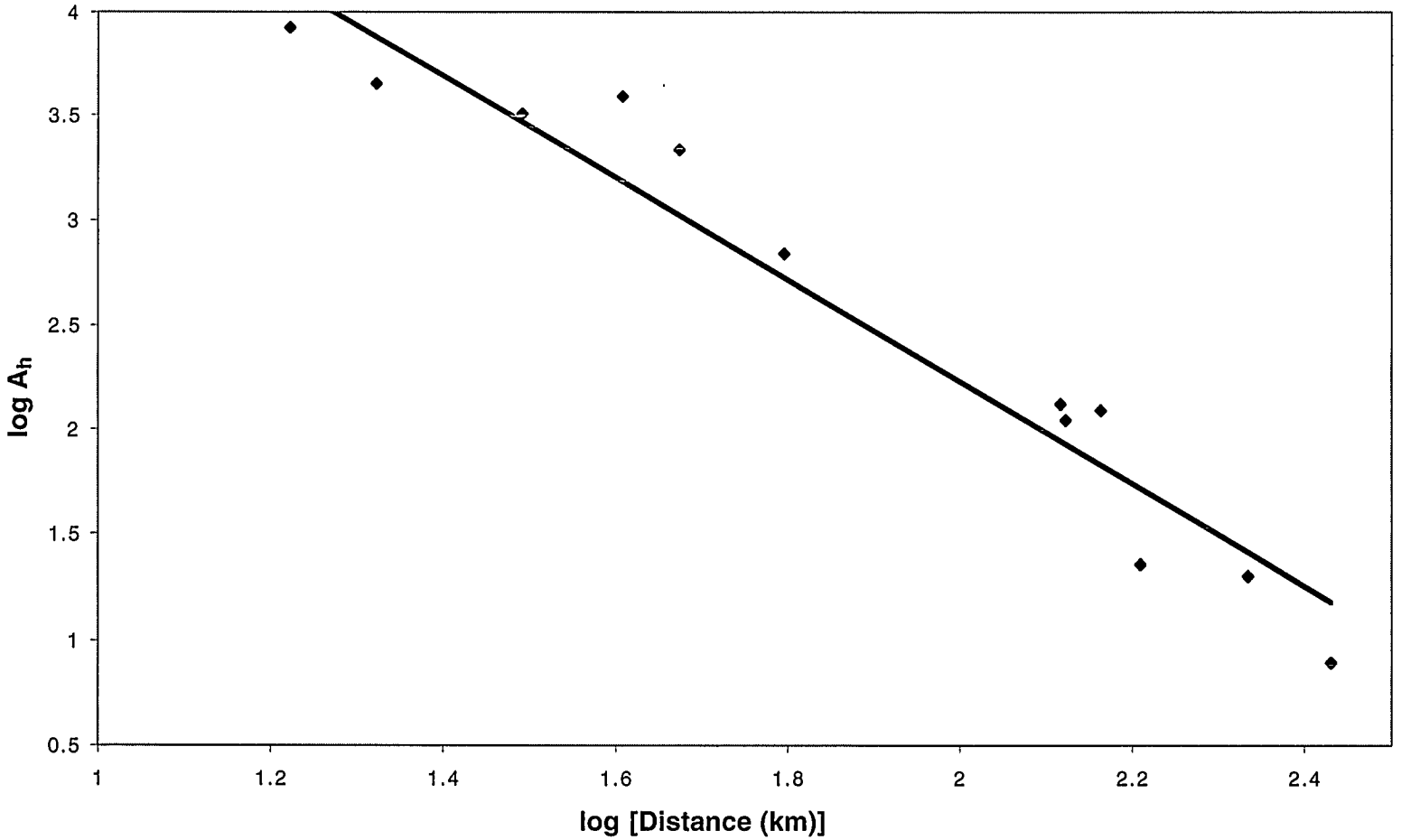

Figure 40. Average yield-scaled tropospheric/surface amplitudes A_h for the event Ruth versus distance. Close-in stations have been added. A least-squares fit is shown.

Not all of the event cases show this quality of fit, but distance–power-law fits like that seen in Eq. (33) are always indicated. Also, the power-law exponents show a substantial range from about –1 to –3; the smaller negative values tend to occur in the spring. At present, the propagation physics responsible for the power-law relations for high-velocity signals, particularly in the cases of exponents from about –2 to –3, is not understood. The relations appear to be relatively insensitive to azimuth.

There is an obvious discrepancy between the results of the analysis for V_h and the analysis for A_h. The former shows a negative correlation with V_z, while the latter indicates a positive correlation. A more detailed analysis of these high-velocity signals is ultimately needed; when possible, that analysis should include (1) examination of the signal forms, (2) the use of the actual wind and temperature profiles appropriate to each event, and (3) modeling of the characteristics for Lamb and tropospheric propagation. We believe, however, that the general consistency of the trends in the data—for example, the distance–power-law relations—suggests that a common class of propagation is responsible for nearly all of the signals.

XIV. SUMMARY

In general, the principal results of our investigation apply to the region within about the first-bounce distance from a source. Some of the results must be considered as tentative and used as suggested relations until future efforts are made. Since this investigation did not consider the effects of distance upon stratospheric signals in a general way, we have provided no definitive results upon that subject. For those who wish to normalize a signal for the effects of distance, we refer to the formulation given in Eq. (1) and the fact that the distance scaling parameter p can be taken as a value between about –1.2 and –1.5. A study by Clauter and Blandford (1998) suggests a value of –1.47 over the distance range of about 200 to 10,000 km. In comparison, the data of this report give a value of –1.2 over a range of about 225 to 900 km but have relatively few longer distance observations. Table IV gives other determinations.

In the following formulas, units are μb for amplitudes, kt for nuclear yield, m/s for velocities, and km for distances. Estimates of the standard deviations for the constants are given following or below each value.

A. Stratospheric Signals

A predictive formula for signals in the region of about 150 to 230 km is

$$A_s = A_{cs} W^n 10^{k V_d} , \tag{34}$$

where

$$\log A_{cs} = 1.87 \pm 0.04, \tag{35}$$

and

$$k = -0.030 + 0.00025\,R \text{ s/m}, \quad (36)$$
$$\pm 0.007 \quad \pm 0.00004$$

or at about the first bounce,

$$k = 0.0196 \pm 0.001 \text{ s/m}, \quad (37)$$

and

$$n = 0.456 \pm 0.05. \quad (38)$$

For ranges greater than about 250 km,

$$k = 0.016 \pm 0.002 \text{ s/m}. \quad (39)$$

To normalize observed amplitudes to unit yield and zero wind,

$$A_{ns} = A_s W^{-n} 10^{-k V_d}. \quad (40)$$

Rough approximations for stratospheric-signal average velocities near the first bounce are

$$V_s \approx 294 \pm 2 \text{ downwind} \quad (41)$$

and

$$V_s \approx 285 \pm 2 \text{ counterwind.} \quad (42)$$

In the region of about 125 to 225 km, a tentative relation is

$$V_s = V_o + s V_d(35), \quad (43)$$

where

$$V_o = 250 + 0.18\,R, \quad (44)$$
$$\pm 9 \quad \pm 0.05$$

$$s = 0.30 \pm 0.20, \quad (45)$$

and $V_d(35)$ is the directed velocity at a height of 35 km.

B. Thermospheric Signals

A predictive formula for thermospheric amplitude is

$$A_t = A_{ct} W^n , \tag{46}$$

where, near the first bounce,

$$\log A_{ct} = 1.29 \pm 0.04 \tag{47}$$

and, for distances of about 125 to 280 km,

$$\begin{aligned} \log A_{ct} &= -2.04 + 1.41 \log R . \\ &\pm 0.76 \quad \pm 0.33 \end{aligned} \tag{48}$$

To normalize amplitude to unit yield and unit distance in the same distance range,

$$A_{nt} = A_t W^{-n} \left[A_{ct}(1) / A_{ct}(R) \right] . \tag{49}$$

An average thermospheric signal velocity is

$$V_t = 219 \pm 9 . \tag{50}$$

There is a possible east-west difference with

$$V_t \approx 228 \text{ to the east} \tag{51}$$

and

$$V_t \approx 214 \text{ to the west.} \tag{52}$$

C. Tropospheric/Surface Signals

A predictive formula for signal amplitude in the region of about 125 to 220 km is

$$A_h = A_{ch} W^n \tag{53}$$

where

$$\log A_{ch} = -1.02 + 0.12 V_z(10.5) \tag{54}$$
$$\pm 0.21 \quad \pm 0.01$$

and where $V_z(10.5)$ is the zonal velocity at a height of 10.5 km. There is a seasonal "hysteresis" effect of up to ± 0.2 in $\log A_{ch}$. Note that these relations apply very poorly to the relatively few signals seen to the west. To normalize amplitudes to unit yield and zero wind,

$$A_{nh} = A_h W^{-n} \left[A_{ch}(0) / A_{ch}(V_z) \right]. \tag{55}$$

A tentative predictive formula for average velocity is

$$V_h = 361 - 0.86 V_z(10.5) \; . \tag{56}$$
$$\pm 3 \quad \pm 0.15$$

There is a seasonal hysteresis effect of about ± 3 m/s.

D. Remaining Problems

This study suggests several problems for future research. Some of these problems may be open to investigation with advanced infrasound propagation modeling codes. Further experimental investigation would be very useful, but the cost of experiments is probably prohibitive and so is likely to be impossible unless existing high-quality data are discovered. The following are suggested problem areas:

1. What produces the distance variation of the parameter k, and does the parameter approach a constant value at large distances such as the value 0.016 s/m discussed in this report?
2. What is the cause of the amplitude footprint observed for both stratospheric and thermospheric signals? In a connected question, how do the footprints change with time of year and for multibounce distances? A possible result based upon preliminary ray-trace calculation is that the footprints tend to flatten with greater distance.
3. What is the cause of the observed variation with distance for the stratospheric average velocity V_S?

4. Can modeling explain the strong asymmetry in the numbers of tropospheric/surface signals seen to the east and to the west based upon the prevailing lower-level winds?
5. Why are the average velocities for tropospheric/surface signals negatively correlated with tropospheric winds while the amplitudes are positively correlated?
6. How well do the relations derived here for stratospheric and thermospheric average velocities at or within first bounce apply at much longer ranges?

ACKNOWLEDGMENTS

We wish to thank Douglas ReVelle, who has been very helpful in discussing this work with us and making useful suggestions. We are especially grateful to Jack W. Reed for the use of his unpublished data and his many helpful discussions; his perseverance in preserving the data used has been vital.

REFERENCES

American National Standards Institute. 1983. "Estimating Airblast Characteristics for Single Point Explosions in Air, with a Guide to Evaluation of Atmospheric Propagation and Effects." ANSI S2.20-1983 (American Institute of Physics).

Berthet, Charles. 1968. *Revue d'Acoustique*, **1** (2), 123.

Blanc, E.; S. Perez; J-P. Issartel; and J-C. Millieres-Lacroix. 1977. *Revue Scientifiique et Technique de la Direction des Applications Militaires*, (17), 23.

Church, Hugh W. 1962. "Height-of-Burst Effects on Long-Range Propagated Blast Pressures," Sandia Laboratories report SC-4687 (RR).

Clauter, Dean, and Robert Blandford. 1998. "Capability Modeling of the Proposed International System 60-Station Infrasonic Network," in "Proceedings of the Infrasound Workshop for CTBT Monitoring," Los Alamos National Laboratory report LA-UR-98-56.

Davidson, Marie, and Rodney W. Whitaker. 1992. "Miser's Gold," Los Alamos National Laboratory report LA-12074-MS.

Donn, William L.; Richard L. Pfeffer; and Maurice Ewing. 1963. *Science*, **139** (3552), 307.

Donn, William L., and Davis M. Shaw. 1967. *Reviews of Geophysics*, **5** (1), 53.

Fleming, Eric L.; Sushil Chandra; J. J. Barnett; and M. Corney. 1990. *Advances in Space Research*, **10** (12), 11.

Georges, T. M., and William H. Beasley. 1977. *Journal of the Acoustical Society of America*, **61** (1), 28.

Gossard, Earl E., and William H. Hooke. 1975. *Waves in the Atmosphere* (Elsevier Scientific Publishing Co., New York).

Hamilton, Kevin. 1982. "Stratospheric Circulation Statistics," National Center for Atmospheric Research Technical Note NCAR/TN-191+STR.

Hunter, James H., and Rodney W. Whitaker. 1998. "Numerical Modeling of Long Range Infrasonic Propagation," Los Alamos National Laboratory report LA-UR-98-56.

McCullough, Darl, and David J. Novlan. 1977. "Atmospheric Structure White Sands Missile Range, New Mexico, Part 6," U.S. Army Electronics Command report DR-942.

Mutschlecner, J. Paul. 1998. "Variation and Uncertainty in Infrasonic Signals," in *Proceedings of the 20th Annual Seismic Research Symposium on Monitoring a Comprehensive Test Ban Treaty (CTBT),* J. Fantroy, D. Heatley, J. Warren, F. Chavez, and C. Meade, Eds. (U.S. Department of Defense and U.S. Department of Energy, Washington, D.C.).

Mutschlecner, J. Paul, and Rodney W. Whitaker. 1990. "The Correction of Infrasonic Signals for Upper Atmospheric Winds," in *Fourth International Symposium on Long-Range Sound Propagation* (NASA Conference Publication 3101).

Mutschlecner, J. Paul, and Rodney W. Whitaker. 1994. "Infrasonic Observations of the Northridge, California, Earthquake," in *Sixth International Symposium on Long-Range Sound Propagation*, D. I. Havelock and M. R. Stinson, Eds. (National Research Council, Institute for Microstructural Sciences, Ottawa, Canada).

Mutschlecner, J. Paul, and Rodney W. Whitaker. 1998. "The Height-of-Burst Effect in Long-Range Infrasonic Signals," in *Proceedings of the 20th Annual Seismic Research Symposium on Monitoring a Comprehensive Test Ban Treaty (CTBT)* (U.S. Department of Defense and U.S. Department of Energy, Washington, D.C.).

Mutschlecner, J. Paul; Rodney W. Whitaker; and Lawrence Auer. 1998. "Effects of Stratospheric Winds on Long-Range Infrasonic Signals," in "Proceedings of the Infrasonic Workshop for CTBT Monitoring," Los Alamos National Laboratory report LA-UR-98-56.

Nastrom, G. D., and A. D. Belmont. 1976. *Journal of Atmospheric Sciences*, **33** (2), 315.

Olmsted, G. B. 1952. "Operation Tumbler-Snapper: Detection of Airborne Low-Frequency Sound from Atomic Explosions (U)," Headquarters U.S. Air Force Office for Atomic Energy, DCS/O, AFOA-1, report WT-539.

Olmsted, G. B., and E. H. Nowak. 1954. "Operation Upshot-Knothole, Detection of Airborne Low-Frequency Sound from Nuclear Explosions (U)," Headquarters U.S. Air Force Office for Atomic Energy, DCS/O, AFOA-1, report WT-763.

Pierce, Allan D. 1981. *Acoustics: An Introduction to Its Physical Principles and Applications* (McGraw-Hill, New York).

Pierce, Allan D., and Joe W. Posey. 1970. "Theoretical Prediction of Acoustic-Gravity Pressure Waveforms Generated by Large Explosions in the Atmosphere," Air Force Cambridge Research Laboratories report AFCRF-70-0134.

Pierce, Allan D., and Joe W. Posey. 1971. *Geophysical Journal of the Royal Astronomical Society*, **26**, 341.

Randel, William J. 1987. "Global Atmospheric Circulation Statistics, 1000-1 mb," National Center for Atmospheric Research Technical Note NCAR/TN-295+STR.

Range Commanders Council. 1983. "Wallops Island, Virginia, Range Reference Atmosphere 0-70 km Altitude," White Sands Missile Range et al. document 364-83.

Reed, Jack W. 1969A. "Climatology of Airblast Propagations from Nevada Test Site Nuclear Airbursts," Sandia Laboratories report SC-RR-69-572.

Reed, Jack W. 1969B. "Operation Prairie Flat, Airburst Project LN-106, Microbarograph Measurements, Final Report: Distribution of Airblast Amplitudes in the Ozonosphere Sound Rings," Sandia Laboratories report SC-M-69-33.

ReVelle, Douglas O. 1988. "Using Modified Mode-Ray Theory to Understand Counter-Wind Propagation Effects from Atmospheric Explosions," in *Eighth International Symposium on Long-Range Sound Propagation* (Applied Research Laboratory, Pennsylvania State University).

ReVelle, Douglas O., and Rodney W. Whitaker. 1996. "Lamb Waves from Airborne Explosion Sources: Viscous Effects and Comparisons to Ducted Acoustic Arrivals," Seventh International Long-Range Sound Propagation Symposium, Ecole Centrale, Lyon, France, July 24–26, 1996, Los Alamos National Laboratory document LA-UR-96-3594.

Webb, Willis L. 1966. *Structure of the Stratosphere and Mesosphere* (Academic Press, New York).

Webb, Willis L. 1969. *Stratospheric Circulation* (Academic Press, New York).

Whitaker, Rodney W.; J. Paul Mutschlecner; Masha B. Davidson; and Susan D. Noel. 1990. "Infrasonic Observations of Large-Scale HE Events," in *Fourth International Symposium on Long-Range Sound Propagation* (NASA Conference Publication 3101).